DIFFRACTION STUDIES
OF
CONCENTRATION VARIATIONS

The Analysis of X-ray Diffraction Line Broadening
and Electron Diffraction Contrast originating
from Specimens with Concentration Variations
Systems studied: Copper-Nickel, Gold-Platinum
and Rubidiumchloride-Potassiumchloride

PROEFSCHRIFT

ter verkrijging van de graad van doctor in de
technische wetenschappen
aan de Technische Hogeschool Delft,
op gezag van de rector magnificus
prof. ir. L. Huisman
voor een commissie aangewezen
door het college van dekanen te verdedigen op
woensdag 22 februari 1978
te 15.00 uur

door

Robert Delhez
scheikundig ingenieur
geboren te Amsterdam

en

Eric Jan Mittemeijer
scheikundig ingenieur
geboren te Haarlem

Dit proefschrift is goedgekeurd door de promotor
PROF. DR. IR. B. OKKERSE

Zoals röntgen hoort bij de diffractie
groeien hoort bij epitaxie
variatie hoort bij concentratie
misfit hoort bij dislocatie
elektron hoort bij mikroskoop
ouders horen bij je levensloop
Metaalkund' hoort bij 't onderzoek

Zó hoort Paula bij dit boek.

From the interference of our minds ....

This work is part of the research programme of the Research group "Metals F.O.M.-T.N.O." of the "Stichting voor Fundamenteel Onderzoek der Materie" (Foundation for Fundamental Research of Matter - F.O.M.) and was also made possible by financial support from the "Nederlandse Organisatie voor Zuiver-Wetenschappelijk Onderzoek" (Netherlands Organisation for pure Research - Z.W.O.).

TO THE READER

A collection of papers - as this thesis - is not easy to read. Therefore the reader is invited to glance through the general introduction, the summary and the epilogue first, because they should offer a survey.

The significance of the investigations reported is their contribution to:

- generally applicable quantitative X-ray diffraction procedures and correction methods for the line profiles measured;
- the knowledge of technologically important systems: thin solid films (electronic devices, coatings) and sintered powder blends (fabrication of special alloys);
- the knowledge of solid state mass transport phenomena and of nucleation, growth and behaviour of layers produced by electrocrystallization or vapour deposition.

We want to emphasize some special aspects of this thesis.

(i) A thesis consisting of a compilation of papers has the following *advantages:*

- the dissemination of information by means of papers is much wider than by means of a "usual" thesis. Publishing the results from a "usual" thesis afterwards implies writing down things twice;
- it conveys in a clear way where others contributed to the investigations;
- a paper is self-contained, making it easier to read only a part of the thesis;
- it diminishes the time needed to edit a thesis.

As *drawbacks* can be mentioned:

- it is difficult to obtain an overall view of the different topics covered;
- it may be necessary to consult other literature, because papers are written on a specialist's level.

(ii) A dual authorship is recommended, because:

- the skills, talents and knowledge of two persons are united - cooperation is a trend in research nowadays;
- it is stimulating to work for the same aim;
- very often it is not very well possible to say who "invented" "it".

TABLE OF CONTENTS

General Introduction 1

I. Methods for the Purification of X-ray Diffraction Line Profiles . 7

1. "Lijnprofielanalyse: de bepaling van deeltjesgrootte en roostervervorming" 9
[Chem. Weekblad, (1977), m 105]

2. "Corrections for the angle dependence of Lorentz, polarization and structure factors in X-ray diffraction line profiles" . 13
[J. Phys. E., 10 (1977) 784]

3. "The X-ray diffraction line broadening due to the diffractometer condition as a function of 2θ" 15
[J. Phys. E., in the press]

4. "An improved α_2-elimination" 29
[J. Appl. Cryst., 8, (1975) 609]

5. "An analysis of errors in the Fourier coefficients of the α_1 line profile" 33
[J. Appl. Cryst., 8 (1975) 612]

6. " A comparison of two computer methods for separation of the $\alpha_1\alpha_2$ doublet" 37
[paper presented at 10th International Congress of Crystallography, Amsterdam, 7-15 August 1975] [Acta Cryst., A31, (1975) Part S3, S202]

7. "The elimination of an approximation in the Warren-Averbach analysis" 45
[J. Appl. Cryst., 9 (1976) 233]

8. "Correction for errors in microstrain values from X-ray diffraction line profiles" 47
[Phil. Mag., 36 (1977) 1261]

9. "The determination of size and strain from the analysis of X-ray diffraction line profiles using a non-ideal standard specimen" 51
[to be published] Zie erratum

II. Analysis of X-ray Diffraction Line Broadening of Specimens with Concentration Variations 65

10. "A note on the kinematical theory of X-ray diffraction from concentration profiles" 67
[J. Appl. Phys., 47 (1976) 1702]

11. "Concentration variations within small crystallites studied by X-ray diffraction line profile analysis" 69
[to be published] Zie erratum

12. "X-ray diffraction line profile analysis of diffusional homogenization in powder blends" 83
[J. Mat. Sci., in the press]

13. "An X-ray diffraction study of diffusional homogenization in RbCl/KCl powder blends" 107
[Phys. Stat. Sol. (a), December 1977]

14. "On the analysis of X-ray diffraction line profiles from small epitaxial binary diffusion couples: determination of concentration profile and influence of TDS" 125
[to be published]

III. Electron Diffraction Investigations of Diffusion-annealed Specimens 145

15. "The effect of interdiffusion on moiré patterns of thin bimetallic films 147
[Thin Solid Films, 41 (1977) 173]
16. "Dislocation wall formation during interdiffusion in thin bimetallic films" 153
[Thin Solid Films, in the press]
17. "Effects of interdiffusion on the misfit dislocation configuration and the moiré patterns of thin bimetallic films" 171
[Proceedings of the International Conference on the Occasion of 50th Anniversary of the Discovery of Electron Diffraction, London, 19-21 September 1977, in the press]
18. "Modification of interfaces in thin epitaxial bimetallic films during interdiffusion" 183
[Thin Solid Films, 50 (1978), in the press]

IV. Epitaxial Growth of Copper Layers onto a Nickel Single Crystal Substrate 193

19. "The initial stages of electrocrystallized copper layers on a 111 nickel surface" 195
[Acta Cryst., A31 (1975) Part S3, S212]
20. "On twinning in crystallized copper layers on a 111 nickel surface" 201
[J. Cryst. Growth, 36 (1976) 249]

V. Notes on phenomenological Diffusion Theory 207

21. "A rapid method for numerical solution of Fick's second law where the diffusion coefficient is concentration dependent . 209
[Scripta Met., 10 (1976) 941]

22. "The determination of concentration dependent diffusion coefficients in semi-infinite media" 213
[Scripta Met., 11 (1977) 113]

Epilogue 217

Summary 221

Samenvatting 227

DIFFRACTION STUDIES
OF
CONCENTRATION VARIATIONS

The Analysis of X-ray Diffraction Line Broadening
and Electron Diffraction Contrast originating
from Specimens with Concentration Variations
Systems studied: Copper-Nickel, Gold-Platinum
and Rubidiumchloride-Potassiumchloride

GENERAL INTRODUCTION

In 1912 Friedrich, Knipping and von Laue[1] discovered the diffraction of X-rays by crystals, whereas Davisson and Germer[2] demonstrated the diffraction of electrons by crystals in 1927. Since then diffraction techniques have been applied extensively to investigate the atomic arrangement in crystals. X-ray diffraction has become the major tool to analyse the "ideal" structure of crystals, although in recent years the application of electron diffraction for structure determination seems to be very promising, especially with the advent of convergent beam techniques[3].

The "ideal" crystal structure determination is not concerned with the imperfections inherent in "real" crystals. Because many technologically interesting properties of crystalline specimens are mainly determined by the structural defects, in the last twenty years the analysis of structural imperfections of crystals has become the subject of a continuously increasing number of diffraction investigations. In this field X-ray and electron diffraction techniques often provide complementary information: In the electron microscope imperfections, such as dislocations, can often be observed individually, whereas X-ray diffractometry yields a description of the imperfect structure as an average over a moderately large diffracting volume.

From a technological point of view the study of concentration variations and their related structural defects is very important, in particular in those cases where the concentration variations occur over small (about 1 μm) and very small (about 10 Å) distances. This is illustrated by the following examples which are closely related to the contents of this thesis:

(i) The numerous applications of micro-electronic devices and metal coatings stimulate the interest in the diffusion-induced concentration variations and the diffusion-generated substructure in thin metal films[4].

(ii) The increasing importance of alloy catalysts necessitates the study of local concentration inhomogeneities occurring in the small catalyst particles[5].

(iii) Several technologically important binary metal alloys are produced by diffusional homogenization of a compacted powder blend of the constituting metal components[6].

From a fundamental point of view "there is an urgent need for high resolution experiments which yield detailed information regarding the fine structure and composition of the diffusion zone"[7].

Recently Gupta[8] discussed critically various existing methods of investigating concentration variations on a small scale, e.g. electrochemical serial sectioning, radioactivity monitoring on the front or back surface of the specimens and microsectioning by argon ion backscattering; Gupta considers the last method to be the most versatile. All of these methods are destructive and/or require rather complicated techniques.

Until now there has been a very limited interest in the application of diffraction methods to study concentration variations, although such techniques are non-destructive *and* make available information on the structural defects. Compilations of literature are given by Carpenter and Tenney[9] for X-ray diffraction and Beers and Mittemeijer[10] for electron diffraction.

Houska and co-workers gave an interpretation of the X-ray diffraction line broadening to determine the concentration profile in a monocrystalline diffusion couple where the diffuson zone was in the range of 1-10 µm[11]. From the width of the rocking-curves information on the mosaic-structure could be obtained[12]. Rudman and Fisher[13,14] proposed an X-ray method to investigate the diffusion process occurring in a powder blend of the components during annealing. In the field of electron diffraction Matthews[15] studied the diffusion-induced behaviour of misfit dislocations originally present in the interface of epitaxial bicrystals. The diffusion-generated substructure was treated theoretically by

Vermaak and van der Merwe[16,17].

This thesis comprises twenty-two recent papers[10,18-38] which contribute to the interpretation of X-ray and electron diffraction phenomena due to concentration variations and to related structural defects. The results and conclusions obtained on the model couples Cu/Ni, RbCl/KCl and Au/Pt often reach beyond the systems employed (Chapters II and III)[18-25].

Within the context of the X-ray diffraction work ample attention had to be paid to the purification of the line profiles recorded. The results on methods of line profile analysis obtained in the course of this study are gathered in Chapter I[26-34].

The application, in both the X-ray and the electron diffraction work, of a model system consisting of a nickel substrate onto which a copper layer was either electrocrystallized or vapour deposited, necessitated a study of the growth process of the copper layer (Chapter IV)[35,36].

Most of the concentration profiles investigated in this thesis are induced by diffusion. Accordingly attention was also paid to the phenomenological diffusion theory (Chapter VI)[37,38]

References

1. W. Friedrich, P. Knipping und M. Laue, Sitzungsberichte der Bayerische Akademie der Wissenschaften, (1912), 303.
2. C.J. Davisson and L.H. Germer, Phys. Rev. 30 (1927) 705.
3. J.M. Cowley, Proc. International Congress on the Occasion of the 50th Anniversary of the Discovery of Electron Diffraction, London (1977), in the press.
4. Thin Solid Films 25 (1975) containing papers presented at the International Conference on Low Temperature Diffusion and Applications to Thin Films; Yorktown Heights; N.Y. U.S.A.; August 12-14, 1974.
5. R.L. Moss, D. Pope and H.R. Gibbens, J. of Catal. 46 (1977) 204.
6. R.W. Heckel and M. Balasubramaniam, Met. Trans. 2 (1971) 379.
7. R.W. Balluffi and J.M. Blakely, Thin Solid Films 25 (1975) 363.
8. D. Gupta, Thin Solid Films 25 (1975) 231.
9. J.A. Carpenter and D.R. Tenney in C.L. Grant, C.S. Barrett, J.B. Newkirk and C.O. Ruud (Eds), Adv. in X-ray Anal, Vol. 17 (1974) 395.
10. A.M. Beers and E.J. Mittemeijer, Thin Solid Films 50 (1978) in the press.
11. D.R. Tenney, J.A. Carpenter and C.R. Houska, J. Appl. Phys. 41 (1970) 4485.
12. J.A. Carpenter, D.R. Tenney and C.R. Houska, J. Appl. Phys. 42 (1971) 4305.
13. P.S. Rudman, Acta Cryst. 13 (1960) 905.
14. B. Fisher and P.S. Rudman, J. Appl. Phys. 32 (1961) 1604.
15. J.W. Matthews, Thin Solid Films 25 (1975) 199.
16. J.S. Vermaak and J.H. van der Merwe, Phil. Mag. 10 (1964) 785.
17. J.S. Vermaak and J.H. van der Merwe, Phil. Mag. 12 (1965) 453.
18. E.J. Mittemeijer and R. Delhez, J. Appl. Phys. 47 (1976) 1702.
19. R. Delhez, E.J. Mittemeijer and E.A. van den Bergen, J. Mat. Sci., in the press.

20. E.A. van den Bergen, R. Delhez and E.J. Mittemeijer, Phys. Stat. Sol (a) 44 (1977) in the press.
21. E.J. Mittemeijer and R. Delhez, to be published.
22. R. Delhez and E.J. Mittemeijer, to be published.
23. T. van Dijk and E.J. Mittemeijer, Thin Solid Films 41 (1977) 173.
24. A.M. Beers and E.J. Mittemeijer, Thin Solid Films, in the press.
25. A.M. Beers, E.J. Mittemeijer and R. Delhez, Proc. International Congress on the Occasion of the 50th Anniversary of the Discovery of Electron Diffraction, London (1977), in the press.
26. R. Delhez and E.J. Mittemeijer, Chemisch Weekblad Magazine (1977) m105.
27. R. Delhez and E.J. Mittemeijer, J. Appl. Cryst. 8 (1975) 609.
28. R. Delhez and E.J. Mittemeijer, J. Appl. Cryst. 8 (1975) 612.
29. R. Delhez and E.J. Mittemeijer, Acta Cryst. A31 (1975) part S3, S202.
30. R. Delhez and E.J. Mittemeijer, J. Appl. Cryst. 9 (1976) 233.
31. R. Delhez, E.J. Mittemeijer, Th.H. de Keijser and H.C.F. Rozendaal, J. of Phys. E. 10 (1977) 784.
32. Th.H. de Keijser and E.J. Mittemeijer, Phil. Mag. 36 (1977) 1261.
33. R. Delhez, Th.H. de Keijser and E.J. Mittemeijer, J. Phys. E., in the press.
34. Th.H. de Keijser and E.J. Mittemeijer, to be published.
35. R. Delhez, E.J. Mittemeijer and W. Smid, Acta Cryst. A31 (1975) part S3, S212.
36. E.J. Mittemeijer, R. Delhez, R. van Rooijen and W. Hoyer, J. Cryst. Growth 36 (1976) 249.
37. E.J. Mittemeijer and H.F.C. Rozendaal, Scripta Met. 10 (1976) 941.
38. E.J. Mittemeijer and Th.H. de Keijser, Scripta Met. 11 (1977) 113.

I

Methods for the Purification of X-ray Diffraction Line Profiles

Normally X-ray diffraction line profiles have to be purified before the determination of physico-chemical data is possible. The purification is usually performed with the aid of one or more of the following procedures:

- correction for (the angle dependence of) the polarization of X-rays and the geometrical (Lorentz) factor;
- correction for (the angle dependence of) the structure factor;
- elimination of the background;
- elimination of the broadening caused by the instrumental conditions (e.g. by deconvolution);
- elimination of the spectral broadening (by α_2 elimination or other approximate correction, or by deconvolution);
- correction for the "hook"-effect appearing in a deconvolution procedure.

R. Delhez en E. J. Mittemeijer

Lijnprofielanalyse: de bepaling van deeltjesgrootte en roostervervorming

Met lijnprofielanalyse van röntgendiffractiepatronen bestudeert men imperfecties in de kristalstructuur van stoffen. Voor een ieder geïnteresseerd in deeltjesgrootten en deeltjesgrootteverdelingen van deeltjes kleiner dan 2000 Å komt röntgendiffractie in aanmerking. Daarnaast levert deze niet-destructieve analysetechniek kwantitatieve informatie betreffende verstoringen in de atomaire rangschikking. Zo wordt in de techniek veelvuldig een spanningsanalyse op basis van röntgendiffractie verricht. Stapelfout- en dislocatiedichtheden en concentratievariaties kunnen eveneens bestudeerd worden.

Sinds de publicatie van Friedrich, Knipping en Von Laue in 1912 bestudeert men met röntgendiffractie de atomaire opbouw van kristallijne materialen. In de afgelopen 60 jaar zijn grote successen behaald met het bepalen van de kristalstructuren. Hierbij worden de intensiteiten van vele reflecties (in veel gevallen ± 2500 reflecties) opgemeten. Uit deze gegevens kan na een 'trial and error'-procedure de 'perfecte kristalstructuur' van een stof bepaald worden.

De laatste 20 jaar is een andere tak van röntgendiffractie sterk opgekomen: Het bestuderen van imperfecties in de kristalstructuur van stoffen. Onder deze imperfecties worden deeltjeskleinheid (bijvoorbeeld van belang voor de katalyse) en afwijkingen van de 'perfecte' atomaire rangschikking veroorzaakt door b.v. dislocaties, spanningen en concentratievariaties (van belang voor onder andere mechanische eigenschappen van materialen en diffusie) verstaan. Deze 'imperfecte kristalstructuur'-bepaling onderscheidt zich van de hierboven genoemde 'perfecte kristalstructuur'-bepaling daarin dat slechts één, of enkele verwante reflecties bestudeerd worden. Deze worden echter minutieus onderzocht: de 'reflectiepiek', hier lijnprofiel genaamd, wordt in kleine stapjes doorlopen (meestal enkele honderden stapjes). De bepaling van imperfecties in de kristalstructuur staat in het nu volgende centraal.

Verbreding in lijnprofielen

Een kristal kan op verschillende wijzen opgebouwd worden gedacht uit een verzameling aan elkaar evenwijdige vlakken van atomen (dit is een vlakkenschaar). Iedere vlakkenschaar wordt gekarakteriseerd door drie kentallen h, k en l en heeft zijn eigen netvlaksafstand de spatie d_{hkl}. Indien een röntgenbundel met golflengte λ op de hkl-vlakkenschaar invalt onder de hoek θ (Fig. 1) treedt alleen een waarneembare gediffracteerde bundel op als geldt, dat $\theta = \theta_B$ waarbij θ_B voldoet aan:

$$n\lambda = 2d \sin\theta_B \quad (n = \text{orde van de reflectie} = 1, 2, 3 \ldots) \qquad (1)$$

Deze formule staat bekend als de wet van Bragg.

De figuur die verkregen wordt door bij variatie van de invalshoek θ de gediffracteerde intensiteit uit te zetten als functie van sinθ wordt het lijnprofiel van de reflectie aan de hkl-vlakkenschaar genoemd; kortweg het hkl-lijnprofiel (Figuur 2). Op grond van het bovenstaande wordt alleen intensiteit verwacht op die waarde van sinθ waarvoor aan *(1)* voldaan is. In de praktijk blijkt echter altijd dat eveneens aanzienlijke intensiteit wordt waargenomen dicht in de buurt van $\sin\theta_B$. Het lijnprofiel is dus verbreed. Hiervoor zijn twee oorzaken aan te wijzen: de instrumentele verbreding en de structurele verbreding.

Instrumentele verbreding is verbreding waarvan de oorzaak niet schuilt in de atomaire opbouw van het preparaat. Een van de belangrijkste bronnen van instrumentele verbreding is bij röntgendiffractie het niet monochromatisch zijn van de gebruikte röntgenstraling. Uit *(1)* volgt immers dat 'buur'-golflengten bij *'buur'-sinθ-waarden diffracteren.* Veelal wordt de karakteristieke Kα-straling toegepast, welke een doubletkarakter bezit: $\alpha_1\alpha_2$-doublet. *Dit betekent dat het totale* lijnprofiel de samengestelde is van twee anderen: het α_1- en het α_2-lijnprofiel (Figuur 2a).

Structurele verbreding vindt zijn oorzaak in de atomaire opbouw van het preparaat:

- Deeltjeskleinheid. Uit de zogeheten kinematische diffractietheorie volgt dat het lijnprofiel van relatief grote kristallen (> 2000Å) niet waarneembaar verbreed is. Naarmate de kristalletjes kleiner zijn, treedt echter een sterk toenemende verbreding op (Figuur 2b).
- Verstoringen in de atomaire rangschikking, zoals spanningen, dislocaties, stapelfouten en concentratievariaties. Deze veroorzaken variaties in de spatie d_{hkl} van de hkl-vlakkenschaar, zodat volgens *(1)* ook diffractie bij afwijkende sinθ-waarden optreedt: lijnverbreding.

Vanzelfsprekend treedt *instrumentele* verbreding altijd op en omdat we juist in de oorzaken van *structurele* verbreding geïnteresseerd zijn, moeten we de instrumentele verbreding na de meting uit het lijnprofiel verwijderen. Met *deconvolutie* is het in principe mogelijk alle instrumentele verbreding te elimineren. In de praktijk is deconvolutie echter niet altijd toepasbaar. Dan resteert de α_2*-eliminatie*: 'achteraf monochromatiseren' van de gebruikte Kα-straling.

Het probleem van de instrumentele verbreding komt in vele gebieden van de

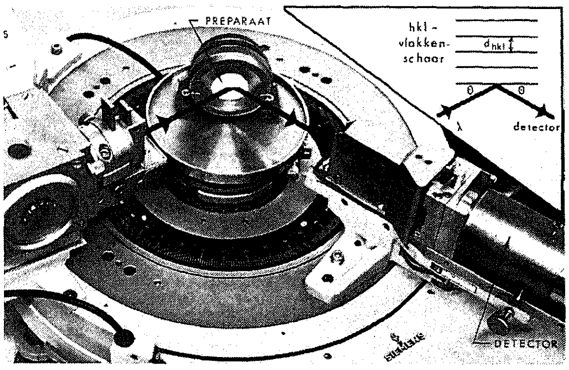

REFLECTIE van röntgenstraling aan de hkl-vlakkenschaar treedt alleen op bij een bepaalde invalshoek θ. Dit wordt geïllustreerd aan een diffractometeropstelling. Met een diffractometer kunnen de lijnprofielen stapsgewijs worden gemeten. (Figuur 1).

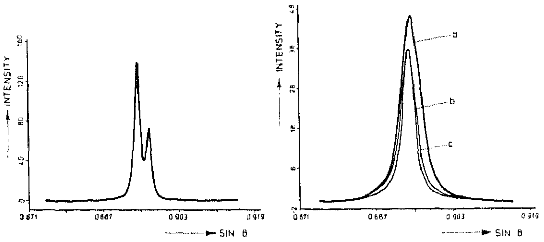

VERBREDING VAN LIJNPROFIELEN. Het 422-lijnprofiel van een MgO-poederpreparaat van 'grote' deeltjes (> 2000 Å), verkregen d.m.v. sinteren is weergegeven in Figuur 2a. Dit lijnprofiel zou, indien met een ideaal instrument gemeten, zeer scherp zijn. Door de niet-ideale instrumentele condities is het echter verbreed. De belangrijkste bron van deze verbreding is het niet monochromatisch zijn van de gebruikte röntgenstraling: duidelijk is het doublet-karakter van de toegepaste CuKα-straling te herkennen. Dit lijnprofiel kan beschouwd worden als het instrumentele *lijnprofiel behorende bij het instrumenteel en structureel verbrede* lijnprofiel van een MgO-poederpreparaat van 'kleine' deeltjes (± 180 Å) Figuur 2b, curve a). Dit laatste lijnprofiel is structureel verbreed door de kleinheid van de deeltjes: het doubletkarakter van de gebruikte röntgenstraling wordt gemaskeerd door deze additionele verbreding. Na *eliminatie van de α_2-component wordt curve b verkregen. Het alleen structureel verbrede* lijnprofiel (curve c) wordt na deconvolutie gevonden. (Figuur 2).

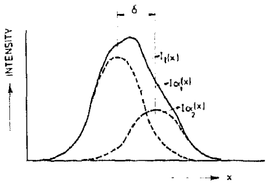

OPBOUW VAN HET Kα-DOUBLET uit de twee componenten: $I_1(x) = I_{\alpha 1}(x) + I_{\alpha 2}(x)$. δ is de doubletscheiding. Indien men aanneemt dat de α_1- en α_2-componenten dezelfde vorm hebben en tevens de verhouding der maxima *van de α_2- en α_1-componenten en de doublet*scheiding δ bekend zijn, dan is $I_{\alpha 1}(x)$ uit $I_1(x)$ te berekenen. (Figuur 3).

natuurwetenschappen voor. Deconvolutietechnieken worden dan ook niet alleen bij röntgendiffractieanalyse toegepast en ontwikkeld. Ook het verwijderen van de spectrale α_2-component heeft wijdere betekenis (zoals in de atoomspectroscopie).

De instrumentele verbreding

Deconvolutie. Een waargenomen structureel en instrumenteel verbreed lijnprofiel heeft zijn vorm gekregen, doordat het structureel verbrede lijnprofiel door het waarnemingsinstrument wordt uitgesmeerd. Deze instrumentele factoren blijken belichaamd te zijn in het instrumentele lijnprofiel: dit is het lijnprofiel dat onder identieke omstandigheden als het structureel en instrumenteel verbrede lijnprofiel wordt gemeten aan dezelfde stof, maar bij afwezigheid van die verschijnselen die de te bestuderen structurele verbreding veroorzaken. Voor het lijnprofiel van het MgO-poeder in Figuur 2b (curve a) betekent dit dat het onder identieke omstandigheden gemeten lijnprofiel van een MgO-poeder van grote deeltjes (Figuur 2a) het bijbehorende instrumentele lijnprofiel is.

Immers de structurele verbreding wordt verondersteld veroorzaakt te zijn door de deeltjeskleinheid.

Wiskundig is de uitsmering van het structureel verbrede lijnprofiel door de instrumentele factoren te beschrijven als een 'convolutie' van het structureel verbrede lijnprofiel met het instrumenteel verbrede lijnprofiel. Daarom heet het verwijderen uit het instrumenteel en structureel verbrede de lijnprofiel van de uitsmering veroorzaakt door de instrumentele factoren: 'deconvolutie'. De bekendste methode voor deconvolutie is gebaseerd op het ontwikkelen in Fourierreeksen van het instrumenteel verbrede lijnprofiel en het instrumenteel en structureel verbrede lijnprofiel. In de röntgendiffractie draagt deze methode de naam van Stokes (1). Voor het genoemde MgO-poeder is het resultaat weergegeven met curve c in Figuur 2b.

α_2-eliminatie. Vaak is het onmogelijk het alleen instrumenteel verbrede lijnprofiel te bepalen, bijvoorbeeld omdat daarvoor geen geschikt preparaat te maken is. Zoals *vermeld, draagt het niet monochromatisch* zijn van de gebruikte röntgenstraling veelal het sterkst bij tot de instrumentele verbreding. Dan wordt achteraf het α_2-lijnprofiel uit het gemeten lijnprofiel verwijderd (2, 3, 4). (Zie Figuur 3). Voor ons MgO-poeder van Figuur 2b is het resultaat van α_2-eliminatie weergegeven met curve b. Het blijkt, dat α_2-eliminatie inderdaad het belangrijkste gedeelte van de instrumentele verbreding verwijdert. Vergelijking van curven b en c toont, dat alleen deconvolutie voor een algehele eliminatie van de instrumentele verbreding zorgt.

De structurele verbreding

Nadat uit het lijnprofiel de instrumentele verbreding verwijderd is, kan de structurele verbreding bestudeerd worden.

We moeten ons realiseren, dat we bij röntgendiffractie altijd informatie verzamelen over zogenaamde *coherent verstrooiende gebiedjes.* Een coherent verstrooiend gebiedje wordt daardoor gekarakteriseerd dat daarin slechts zeer geringe afwijkingen van de regelmatige kristalstructuur voorkomen. Een kristalgrens, bijvoorbeeld, is een grote onregelmatigheid en vormt daarom een scheiding tussen coherent verstrooiende gebiedjes. Daarom kan ieder coherent verstrooiend gebiedje identiek zijn met een poederdeeltje, maar dit hoeft niet.

Deeltjesgrootte. Naarmate de deeltjes kleiner worden, neemt de breedte van het lijnprofiel toe. Bij afwezigheid van roosterfouten geldt voor de breedte β van het lijnprofiel op sinθ-as de Scherrer-vergelijking:

$$\beta = \lambda K/2D \qquad (2)$$

Voor β wordt vaak de breedte op halve hoogte genomen. De constante K (ca. 1) wordt bepaald door de – veronderstelde – vorm van de deeltjes en door de gekozen maat voor β. D is de gemiddelde deeltjesgrootte.

Variaties in de netvlaksafstand. Stel dat een preparaat plaatselijk zo gedeformeerd is dat de netvlaksafstand d met een bedrag Δd verandert. Door uitgebreidheid van de gebruikte röntgenbundel bevat het waargenomen lijnprofiel informatie over de veranderingen in netvlaksafstand in een groot gebied, zodat de locale variaties niet afzonderlijk worden waargenomen. Voor de breedte β van het lijnprofiel op sinθ-as kan met behulp van vergelijking *(1)* de volgende benadering geschreven worden:

$$\beta = \Delta(\sin\theta) = <\Delta d/d> \sin\theta \qquad \mathit{(3)}$$

De breedte β is hier – in tegenstelling tot de verbreding door deeltjesgrootte – afhankelijk van sinθ.

Een andere methode om variaties in de netvlaksafstand te bepalen is de '$\sin^2\Psi$-methode' (5). (Wegens ruimtegebrek niet besproken).

De rek <e> en de spanning <σ> kunnen uit *(3)* berekend worden vervolgens $<e> = <\Delta d/d> = <\sigma>/E$ waarin E de modulus van Young is.

Scheiden van invloeden

Indien de structurele verbreding bepaald wordt door deeltjeskleinheid én roosterfouten falen de methoden die hiervoor aangestipt zijn. In eerste instantie zou men kunnen denken dat de totale breedte van het lijnprofiel geschreven kan worden als de som van de formules *(2)* en *(3):*

$$\beta = \lambda K/2D + <\Delta d/d> \sin\theta \qquad \mathit{(4)}$$

Na bepaling van β voor meer reflecties en uitzetten van de resultaten tegen sinθ volgt uit *(4)* dat een rechte lijn verkregen wordt (de 'Hall-plot'). Uit het afgesneden stuk

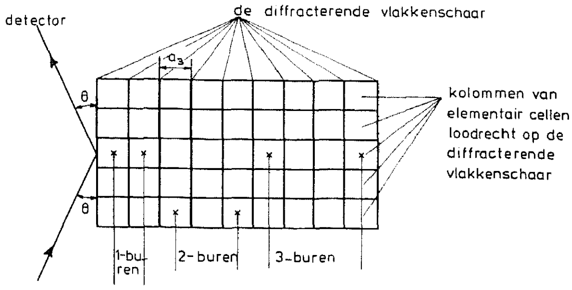

EEN POEDERPREPARAAT bestaat uit een verzameling coherent verstrooiende gebiedjes (Een poederdeeltje kan één of meer van deze gebiedjes bevatten). Een coherent verstrooiend gebiedje kan worden opgebouwd uit kolommen elementair cellen loodrecht op de diffracterende vlakkenschaar. In een kolom van elementair cellen kan men zgn. 'n-buren' onderscheiden. Voorbeelden zijn aangegeven. (Figuur 4)

van de verticale as volgt de deeltjesgrootte en uit de helling <Δd/d>. Deze formulering wordt als grove indicatie nog wel toegepast, maar zij is alleen maar juist voor een bepaalde vorm van het lijnprofiel.

Een fundamentele methode om bij gelijktijdige aanwezigheid van deeltjeskleinheid en roosterfouten het lijnprofiel te bestuderen is de *Warren-Averbach-analyse* (6, 7). Om redenen van eenvoud wordt in het volgende aangenomen, dat stapelfouten en concentratiefluctuaties afwezig zijn.

Volgens een model van Bertaut wordt ieder coherent verstrooiend gebiedje (zie de inleiding bij deze paragraaf) opgebouwd gedacht uit kolommen elementair cellen loodrecht op de diffracterende vlakkenschaar (Figuur 4). In zo'n kolom kunnen 'n-buren' onderscheiden worden: n-buren zijn elementair cellen in een kolom die n elementair cellen van elkaar verwijderd zijn. Voorbeelden zijn in Figuur 4 gegeven. Ten gevolge van spanningen kan er rek zijn opgetreden in de richting van a_3. Dan is de afstand tussen n-buren niet meer $L(=na_3)$ maar $L + \Delta L$. De component van de rek in de richting van a_3 gemiddeld over de lengte L is dan: $e_L = \Delta L/L$.

Het totale lijnprofiel kan opgebouwd worden gedacht uit een deeltjesgroottelijnprofiel (bevat alleen verbreding veroorzaakt door de deeltjeskleinheid) en een roosterdeformatielijnprofiel (bevat alleen verbreding veroorzaakt door netvlaksafstandsvariaties). Essentieel hierbij is dat het deeltjesgroottelijnprofiel geen functie is van de orden van de reflectie maar het roosterdeformatielijnprofiel wél. Op grond hiervan vindt de scheiding van beide effecten plaats (8).

Voorbeelden van resultaten van dergelijke berekeningen zijn weergegeven in Figuur 5. Voor het MgO-poederpreparaat van Figuur 2b werd een gemiddelde lengte van ± 180Å bepaald.

De gemiddelde kolomlengte is niet synoniem met wat men onder de 'deeltjesgrootte' verstaat, de deeltjes kunnen ieder voor zich uit meer dan een coherent verstrooiend gebiedje bestaan (zie inleiding van deze paragraaf). Bijvoorbeeld in het geval van bolvormige deeltjes bedraagt de gemiddelde kolomlengte slechts 2/3 deel van de boldiameter.

Onder het voorbehoud van de hierboven vermelde restricties is het ook mogelijk 'deeltjesgrootte'-verdelingen te bepalen.

Toepassing

Onderzoekingen op basis van de hierboven geschetste analyse zijn legio. Bedenk echter dat het succes van dergelijke methodes voor een groot deel bepaald wordt door de nauwkeurigheid waarmee de Fouriercoëfficiënten van het alleen structureel verbrede lijnprofiel bekend zijn (9).

De in dit artikel aangegeven analysetechnieken kunnen op vele plaatsen in de natuurwetenschappen toegepast worden. De voorbeelden gegeven in dit artikel illustreren dit.

Tenslotte: Wij willen graag in contact komen met onderzoekers die werk op dit gebied verrichten of overwegen.

1. Stokes, A. R. (1948). Proc. Roy. Soc. *61*, 382.
2. Rachinger, W. A. (1948). J. Sci. Instrum. *25* 254.
3. DuMond, J. W. M. & Kirkpatric, H. A. (1931). Phys. Rev. *37*, 154.
4. Delhez, R. & Mittemeijer, E. J. (1975). J. Appl. Cryst. *8*, 609.
5. Klug, H. P. & Alexander, L. E. (1974). X-ray Diffraction Procedures, pp. 755-790, New York: John Wiley and Sons.
6. Warren B. E. & Averbach, B. L. (1950). J. Appl. Phys. *21*, 595.
7. Warren, B. E. (1969). X-ray Diffraction, pp. 262-275, Reading: Addison-Wesley.
8. Delhez, R. & Mittemeijer, E. J. (1976), J. Appl. Cryst. *9*, 233.
9. Delhez, R. & Mittemeijer, E. J. (1975). J. Appl. Cryst. *8*, 611.

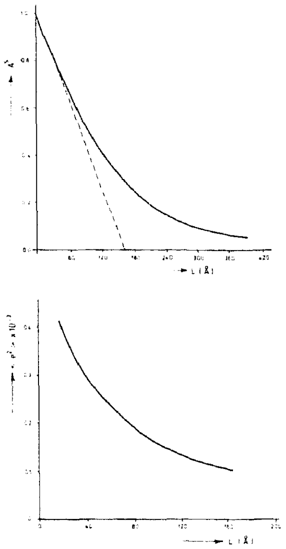

WARREN-AVERBACH-ANALYSE. Voorbeelden van het scheiden van de invloeden van deeltjesgrootte en van netvlaksafstandsvariaties. De resultaten worden gewoonlijk uitgedrukt in de cosinus-Fouriercoëfficiënt van het deeltjesgroottelijnprofiel $A^S(L)$ en het gemiddelde van het kwadraat van de rek $<e^2(L)>$. L stelt een afstand loodrecht op de diffracterende vlakkenschaar voor ($L = na_3$, waarbij n en a_3 respectievelijk het harmonische getal en de roosterparameter uit Figuur 4 zijn). Figuur a: de deeltjesgrootte Fouriercoëfficiënt $A^S(L)$ van een AuPt-poeder (9 at% Pt) bereid voor katalysedoeleinden door F. Kuyers (Universiteit van Leiden). Het deel dat van de abscis wordt afgesneden door de raaklijn voor L → 0 (stippellijn) stelt de gemiddelde kolomlengte voor: ± 160 Å. Figuur b: het gemiddelde van het kwadraat van de rek $<e^2(L)>$ van een door R. van Rooijen (Technische Hogeschool Delft) d.m.v. elektrokristallisatie bereid Cr-poeder. Het bij de elektrokristallisatie gevormde waterstof wordt ervan verdacht de aanleiding te zijn tot spanningen in het metaalrooster. De hierbij optredende verstoring van de atomaire rangschikking is aanzienlijk. Gewoonlijk ligt $<e^2(L)>$ in het gebied 10^{-6}-10^{-4}. (Figuur 5)

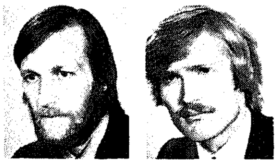

Rob Delhez (36) (links) en Eric Mittemeijer (27) (rechts) studeerden in 1968 resp. 1972 af aan de Technische Hogeschool Delft. Zij hopen dit jaar te promoveren. Beiden zijn werkzaam in de groep van prof. dr. ir. B. Okkerse , sectie Fysische Chemie van de Vaste Stof, op het laboratorium voor Metaalkunde van de T.H. Delft.

Corrections for the angle dependence of Lorentz, polarization and structure factors in x-ray diffraction line profiles

R Delhez, E J Mittemeijer, Th H de Keijser and H C F Rozendaal
Laboratory of Metallurgy, Delft University of Technology, Rotterdamseweg 137, Delft, The Netherlands

Received 24 January 1977, in final form 12 April 1977

Abstract In accurate line profile analysis, corrections have to be made for the angle dependence of the Lorentz and polarization factors. These corrections should be performed before the deconvolution procedure if the spectral broadening dominates in the instrumental line profile, but after the deconvolution procedure if instrumental factors dominate the instrumental line profile. The different formulae to be applied for the Lorentz–polarization factor are indicated. The correction for the angle dependence of the structure factor should always be performed after the deconvolution procedure.

1 Introduction

In the interpretation of the broadening of x-ray diffraction line profiles it should be recognized that the Lorentz (L), polarization (P) and structure factors are angle dependent *within a given profile*. Normally corrections for the angle dependence of these factors are ignored. However if accurate line profile analysis is demanded such corrections should be applied. In this paper rules are given which, in our opinion, should be followed when correcting for the angle dependence of the L, P and structure factors (§§3, 4). Further, the different formulae to be applied for the LP factor are indicated (§2).

2 Formulae for the Lorentz–polarization factor

In textbooks normally the LP factor is given for the integrated intensity of a reflection. However, in structurally broadened line profiles the LP factor relevant to the distribution of the intensity over 2θ has to be considered. Warren and Averbach (1950) have calculated this LP factor for a powder specimen:

$$LP = (1 + \cos^2 2\theta)/\sin^2 \theta.$$

Following the same procedure one can calculate the LP factor relevant to the distribution of the intensity over 2θ for a single crystal:

$$LP = (1 + \cos^2 2\theta)/4 \sin \theta.$$

It can be useful to perform line profile analysis on a $\sin \theta$ scale (Delhez and Mittemeijer 1975). Then all LP factors mentioned should be divided by $\cos \theta$.

3 The correction for the angle dependence of the Lorentz and polarization factors

In x-ray diffraction the measured line profile h can be considered as the outcome of the folding $f * g$ (Jones 1938) where f is the pure, only structurally broadened, line profile and g is the line profile which is only broadened by the instrumental factors and the x-ray spectrum used. The f profile is obtained after a deconvolution procedure (Stokes 1948).

Two cases can be considered in practice.

(i) *The broadening due to instrumental factors is dominant in the g profile*
This occurs at the smaller 2θ values. If we assume that the wavelength distribution is a delta function, each f value is diffracted at a sharply defined diffraction angle; however, the intensity is recorded over a range of measured 2θ values for which the L and P factors are determined by that one sharply defined diffraction angle. Therefore both the g and the h profile should not be corrected for the angle dependence of the L and P factors. *After* the deconvolution procedure the f profile should be corrected for the angle dependence of the L and P factors. Then the LP factor relevant to the distribution of the intensity over 2θ has to be used.

(ii) *The spectral broadening dominates in the g profile*
This occurs at the larger 2θ values. With only spectral broadening present, each f value is diffracted by the whole wavelength distribution, leading to recorded intensities over a range of measured 2θ values. The recorded intensity at each 2θ value is dependent upon the L and P factors for that 2θ value. Therefore both the g and the h profile should be corrected for the angle dependence of the L and P factors *before* performing a deconvolution procedure. In this case the g profile should be corrected using the LP factor for the integrated intensity (but with a variable θ) (see also Ladell 1961). If the h profile is dominated by the structural broadening (which is usually the case) it should be corrected by applying the LP factor relevant to the distribution of the intensity over 2θ. If the spectral broadening dominates the h profile, the LP factor for the integrated intensity should be used.

4 The correction for the angle dependence of the structure factor

Within the g profile taken from an ideal standard specimen (no structural broadening) the structure factor is not angle dependent at all. It is clear that a correction for the angle dependence of the structure factor should be performed *after* the deconvolution procedure.

In most cases this correction is performed sufficiently if the angle dependence of the atomic scattering factors is taken into account (an exception has been dealt with by Bley and Fayard 1976).

Acknowledgment
Financial support of the Stichting voor Fundamenteel Onderzoek der Materie (FOM) is gratefully acknowledged.

References

Bley F and Fayard M 1976 *J. Appl. Cryst.* 9 126
Delhez R and Mittemeijer E J 1975 *J. Appl. Cryst.* 8 609
Jones F W 1938 *Proc. R. Soc.* A 166 16
Ladell J 1961 *Acta Cryst.* 14 47
Stokes A R 1948 *Proc. Phys. Soc.* 61 382
Warren B E and Averbach B L 1950 *J. Appl. Phys.* 21 595

Journal of Physics E: Scientific Instruments 1977 Volume 10
Printed in Great Britain

THE X-RAY DIFFRACTION LINE BROADENING DUE TO THE DIFFRACTOMETER CONDITION AS A FUNCTION OF 2θ

by

R. Delhez, Th.H. de Keijser and E.J. Mittemeijer

Laboratory of Metallurgy, Delft University of Technology
Rotterdamseweg 137, Delft, The Netherlands

Accepted for publication in Journal of Physics E.

I.3

Abstract

Up to now theoretical work did not arrive at a full description of the X-ray diffraction line broadening due to the instrumental conditions in the absence of spectral broadening. Therefore in this paper an experimental approach was chosen. The line profile due to the instrumental conditions, was obtained from the measured line profile of a standard specimen by elimination of the spectral broadening, applying a model for the wavelength distribution. Employing common experimental conditions, it was found that for $2\theta > 50^{o}$ the spectral broadening is dominant in the line profile and that for the larger 2θ values and for small values of the harmonic number the Fourier coefficients corresponding to the broadening by the instrumental conditions may be assumed to be independent of 2θ. Therefore, if one is obliged to use in size-strain analysis a standard specimen that diffracts in a 2θ-range different from that of the line profile to be investigated, corrections for the difference in broadening due to the instrumental conditions between the profiles of approximate and ideal standard specimen are unnecessary. Hence only corrections for the difference in spectral broadening should be made. In addition a method is proposed to determine the ratio $R = I_{\alpha_2}(\max)/I_{\alpha_1}(\max)$.

1. Introduction

Apart from the structural broadening, X-ray diffraction line profiles are broadened by

(i) the instrumental factors of the diffractometer used, and

(ii) the wavelength distribution applied.

A knowledge of these two types of broadening, which interfere with the structural broadening, is desired.

In the literature there have been moderately successful attempts to describe the line broadening caused by the instrumental conditions from a theoretical point of view. According to Klug & Alexander (1974) the difference between theory and practice is due to alignment errors. In view of the large discrepancies found it may be concluded that an experimental treatment of these broadening phenomena is useful.

The purpose of this paper is to investigate the X-ray diffraction line broadening due to the diffractometer condition as a function of 2θ. To this end the broadening caused by the X-ray spectrum used is eliminated from experimentally determined line profiles of a so-called standard specimen, using an analytical description of the $K\alpha$ doublet. The treatment is restricted to the Fourier coefficients of the profiles since these are widely used in deconvolution procedures (Stokes 1948) and in size-strain analysis (Warren 1969).

2. Experimental procedure

From a standard silicon powder sample [Nat.Bur. of Standards SRM 640] the line profiles of the (111), (220), (311), (331), (511)/(333), (531) and (533) reflections were recorded applying the $CuK\alpha$ doublet. The profiles were stepscanned according to the preset-time method on a Siemens ω diffractometer equipped with an X-ray tube operating at 45 kV.

(HKL)	2θ range	step size ($^o2\theta$)	counting time per step (s)	mean background at low angle side (counts)	mean background at high angle side (counts)	peak maximum (counts)
(111)	26.5-30.4	0.010	10	75	70	41511
(220)	45.5-49.1	0.010	10	70	70	16008
(311)	53.5-58.5	0.010	10	55	50	8888
(331)	73.5-79.5	0.010	20	75	80	8611
(511)/(333)	92.0-98.5	0.015	30	130	120	9730
(531)	110.5-118.0	0.015	30	135	125	8608
(533)	133.0-141.5	0.015	90	390	420	11316

Table 1.
The number of counts measured at the background and at the peak maximum and the 2θ ranges, the step sizes and the counting times per step employed in recording the line profiles of the standard silicon powder sample [NBS SRM640].

A graphite monochromator was mounted between the spinning sample and the scintillation counter. Divergence and receiving slits were 0.5° and 0.05 mm respectively. Soller slits with 4° divergence were used. Pulse-height discrimination was employed. In table 1 the 2θ ranges, the step sizes, the counting times per step, and the numbers of counts measured at the background and the peak maximum are gathered.

The line profiles were corrected for the background by linear interpolation. According to Delhez c.s. (1977) all profiles, except the (111) profile, were corrected for the angle dependency of the Lorentz and polarization factors. The Fourier analysis was performed on a $\sin\theta$-scale. The origin was placed at the centroids of the line profiles. The period a used for the calculation of the Fourier coefficients runs from -0.0433 to +0.0433 for all reflections.

3. Mathematical basis

Structural broadening by the standard specimen used, can be considered negligible. The measured instrumental line profile g_m, which comprises the broadening due to the X-ray spectrum applied and the instrumental factors of the diffractometer used, is taken as the sum of the profiles of the K_{α_1} and K_{α_2} components. The broadening due to the instrumental factors is very nearly the same for both components (c.f. section 4); the spectral broadening differs somewhat (Edwards and Langford 1971; Compton and Allison 1935). From the combined effect of both types of broadening it may be assumed that both components have the same shape. This shape is put equal to that of an instrumental profile g_c intermediate between that of the α_1 and α_2 components.

The centroid of the intermediate wavelength distribution is chosen such that $<\lambda_c> = (<\lambda_1> + R<\lambda_2>)/(1 + R)$ where R is the ratio of the maxima of the α_2 and α_1 profiles and $<\lambda_1>$ and $<\lambda_2>$ are the centroids of the α_1 and α_2 wavelength distributions. With x defined on a sinθ-scale (advantages discussed by Delhez and Mittemeijer 1975a), the Fourier coefficients $G_m(n)$ of the instrumental profile $g_m(x)$ are given by

$$G_m(n) = G_c(n)\ [\exp - inR\alpha + R\exp in\alpha] \qquad (1)$$

where, d being the spacing of the reflecting planes, $\alpha = \pi(<\lambda_2> - <\lambda_1>)/d(1+R)a$ and $G_c(n)$ is the n-th Fourier coefficient of $g_c(x)$.

The instrumental profile g_c can be considered as the convolution of the spectral profile g_c^s of the intermediate wavelength distribution and the profile g_c^i due to the broadening caused by the instrumental conditions. Expressing this in terms of Fourier coefficients one obtains

$$G_c(n)/G_c(o) = G_c^i(n).G_c^s(n) \qquad (2)$$

where $G_c^i(n)$ and $G_c^s(n)$ are the Fourier coefficients of g_c^i and g_c^s respectively, normalized such that $G_c^i(o) = G_c^s(o) = 1$.

It is generally accepted that the wavelength distribution can be given by (e.g. Klug and Alexander 1974)

$$g_c^s(\lambda) = \{1 + 4(\lambda - <\lambda_c>)^2/w^2\}^{-1} \qquad (3)$$

where w is the width at half height.

Combination of eqs. (1), (2) and (3) yields

$$\frac{G_m(n)}{G_m(o)} = G_c^i(n)\ \frac{1}{1+R}\ [\exp - inR\alpha + R\exp in\alpha]\exp - \frac{\pi nw}{2da} \qquad (4)$$

Further we define

$$\frac{G_m(n)}{G_m(o)} = A_m(n) + iB_m(n) \text{ and } G_c^i(n) = A_c^i(n) + iB_c^i(n) \qquad (5)$$

The unknown $A_c^i(n)$ and $B_c^i(n)$ can be calculated from eqs. (4) and (5): $A_m(n)$ and $B_m(n)$ follow from the measured line profiles. $<\lambda_1>$, $<\lambda_2>$ and w follow from the literature (Edwards and Langford 1971; Compton and Allison 1935). R should in principle be determined for each line profile separately (Kidron and Cohen 1973). In this paper R has been determined for each line profile according to a method described in the appendix.

4. Results and discussion

In practice the Fourier coefficients should be given as a function of the distance $L = n\lambda/2a$, perpendicular to the reflecting planes.

In Figs. 1a, b and c $A_m(L)$, $A_c^i(L)$, $B_m(L)$ and $B_c^i(L)$ are plotted for the (111), (331) and (533) profiles respectively. In eliminating the spectral broadening the noise from counting statistics produces periodic ripples on the Fourier coefficients (Delhez and Mittemeijer 1975b). The factor exp $-\pi nw/2da$ implies an increasing amplitude of the ripple with increasing L and sinθ. This is seen in the $A_c^i(L)$ abd $B_c^i(L)$ curves of Figs. 1a, b and c.

The ratio of the width of the $A_c^i(L)$ curve to the width of the $A_m(L)$ curve, at $A_c^i(L) = A_m(L) = 0.5$, is shown in Fig. 2 as a function of sinθ. It can be seen from Fig. 2 that at small angles the broadening by the instrumental factors dominates [c.f. Fig. 1a], while at larger angles [c.f. Fig. 1c] the spectral broadening is dominant. In fact it was found that for $2\theta > 50^o$ over half of the line broadening is due to the spectrum used. This stresses the usefulness of corrections for spectral broadening

1.3

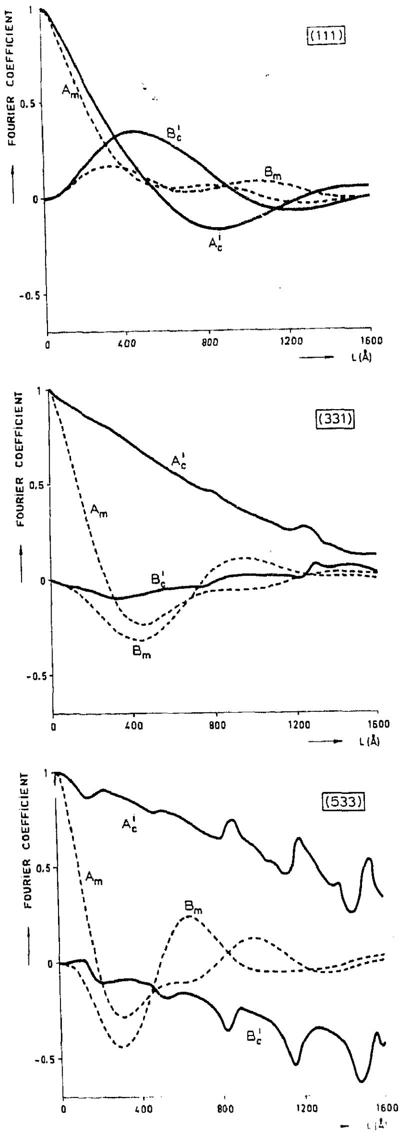

Fig. 1. The cosine and sine Fourier coefficients of the measured line profile, $A_m(L)$ and $B_m(L)$ respectively, and of the profile solely due to the instrumental conditions, $A_c^i(L)$ and $B_c^i(L)$ respectively, for the (111) reflection (Fig. 1a), the (331) reflection (Fig. 1b) and the (533) reflection (Fig. 1c).

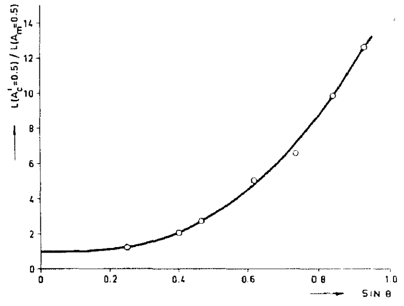

Fig. 2. The ratio of the width of the $A_c^i(L)$ *curve to the width of the* $A_m(L)$ *curve at* $A_c^i(L) = A_m(L) = 0.5$ *as a function of* $\sin\theta$.

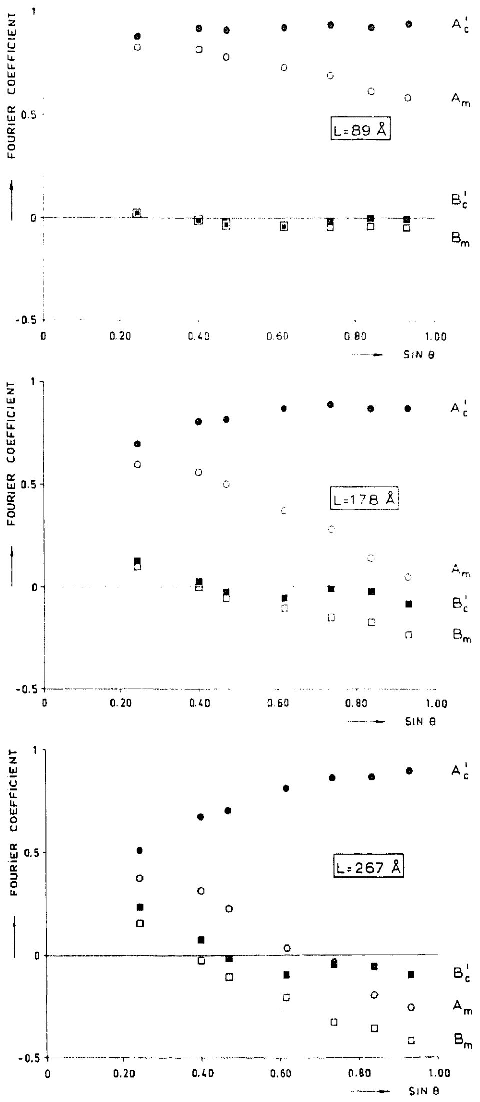

Fig. 3. The cosine and sine Fourier coefficients of the measured line profile, A_m *and* B_m *respectively, and of the line profile solely due to the instrumental conditions,* A_c^i *and* B_c^i *respectively, as a function of* sinθ *for* L = 89 Å *(Fig. 3a),* L = 178 Å *(Fig. 3b) and* L = 267 Å *(Fig. 3c).*

(Delhez and Mittemeijer 1975a; de Keijser and Mittemeijer 1977).

Figs. 3a, b and c show A_m, A_c^i, B_m and B_c^i as a function of sinθ for L equals 89 Å, 178 Å and 267 Å respectively.

In line profile analysis it is often unavoidable to use an approximate standard line profile in the deconvolution procedure (de Keijser and Mittemeijer 1977). In case the spacings of the reflecting planes of ideal and approximate standard specimen are different the approximate and ideal standard line profiles are centered around different sinθ values. More or less correct values for the Fourier coefficients of the ideal standard line profile can be obtained from an interpolation at the correct sinθ value of the A_m and B_m curves as shown in Figs. 3a, b and c*. However this has to be done at every value of L. Furthermore every change in the instrumental conditions and in the wavelength distribution and in composition of the specimen under investigation obliges to start over again the measurements of the standard line profiles. Therefore this may be considered as an impracticable method.

In many practical situations an alternative procedure is possible: Figs. 3a, b and c show that at larger sinθ values G_c^i is approximately constant and that with larger values of L this constancy is attained at larger values of sinθ [the scatter at large sinθ values is primarily

---

* In the profile fitting method (Taupin 1973; Huang and Parrish 1975), which was applied succesfully to unravel clusters of peaks in complex powder patterns, the parameters for the Lorentzians used to describe the profile, are obtained analoguously. When Fourier series are used in size-strain analysis (Warren 1969) a direct description in terms of Fourier coefficients is preferable.

due to counting statistics]*. With a view to size-strain analysis only the smaller values of L are of interest (c.f. Fig. 1 in the paper by Delhez and Mittemeijer 1976). If the centroids of the line profiles of the approximate and the ideal standard specimen differ less than 0.025 [this implies a difference in spacing of 5% at $\sin\theta = 0.5$] it follows from Figs. 3a, b and c that for the L values of interest and for the whole $\sin\theta$ range investigated $0.96 < G^i_c/G^i_{c,m} < 1.04$, where $G^i_{c,m}$ and G^i_c denote the Fourier coefficients corresponding to the approximate and ideal standard specimen. It should be noted that this range is an overestimate obtained from Fig. 3c. Assuming $G^i_c/G^i_{c,m} = 1$ results in negligible errors in size-strain analysis: as can be easily shown the error in the particle size calculated is nil while the error in the mean square strain calculated $< 1.10^{-7}$. Hence only corrections for the difference in spectral broadening between ideal and approximate standard line profile should be made by use of eq. (4).

Acknowledgements

The authors wish to thank Mr. H.D.F. Meijer for assistance with the numerical calculations.

Financial support of the Stichting voor Fundamenteel Onderzoek der Materie (F.O.M.) is gratefully acknowledged.

---

* This result may be interpreted as follows: with increasing $\sin\theta$ values the changes in the profile due to the instrumental conditions diminish. Higher Fourier coefficients yield information about details of the profile. Therefore with larger values of L the constancy mentioned is obtained at larger values of $\sin\theta$.

Appendix

THE DETERMINATION OF R = $I_{\alpha_2}(\max)/I_{\alpha_1}(\max)$

According to Gangulee (1970) the true value of R is settled if the minimal value is obtained for the residue

$$\mathrm{Res}(R) = \sum_x |I_{\alpha_1}(x)| - I_{\alpha_1}(x)$$

where the α_1 intensities $I_{\alpha_1}(x)$ are obtained by elimination of the α_2 intensities $I_{\alpha_2}(x)$.

According to Kidron and Cohen (1973) and our own experience this procedure does not always give satisfactory results. Therefore a modified procedure is applied. The minimum of the residue

$$\mathrm{Res}(R) = \sum_x |I_{\alpha_1}(x)| + |I_{\alpha_2}(x)| - I_{\alpha_1}(x) - I_{\alpha_2}(x)$$

is used as the criterion for the true value of R.* The α_1 intensities are found by the method of Delhez and Mittemeijer (1975a). Up to now satisfactory results have been obtained.

---

* In principle the residue may also be used to optimize the doublet separation.

1.3

References

Compton A H and Allison S K 1935 X-rays in Theory and Experiment, p. 734, London: MacMillan

Delhez R and Mittemeijer E J 1975a J.Appl.Cryst. 8 609

Delhez R and Mittemeijer E J 1975b J.Appl.Cryst. 8 612

Delhez R and Mittemeijer E J 1976 J.Appl.Cryst. 9 233

Delhez R, Mittemeijer E J, Keijser Th H de and Rozendaal H C F 1977 J.Phys.E: Sci.Instrum. 10 784

Edwards H J and Langford J I 1971 J.Appl.Cryst. 4 43

Gangulee A 1970 J.Appl.Cryst. 3 272

Huang T C and Parrish W 1975 Appl.Phys. Letters 27 123

Keijser Th H de and Mittemeijer E J 1977 Phil.Mag. 36 1261

Kidron A and Cohen J B 1973 J.Appl.Cryst. 6 8

Klug H P and Alexander L E 1974 X-ray Diffraction Procedures, p. 297, New York: John Wiley & Sons

Stokes A R 1948 Proc.Phys.Soc. London. 61 382

Taupin D 1973 J.Appl.Cryst. 6 266

Warren B E 1969 X-ray Diffraction, pp 264-275, Reading Mass.: Addison-Wesley

I.4

Reprinted from *J. of Appl. Crystallography*, Vol. 8, Part 6, December 1975

PRINTED IN DENMARK

J. Appl. Cryst. (1975). **8**, 609

An Improved α_2 Elimination

By R. Delhez and E. J. Mittemeijer

Laboratory of Metallurgy, Delft University of Technology, Rotterdamseweg 137, Delft, The Netherlands

(*Received* 14 *April* 1975; *accepted* 15 *July* 1975)

It is shown that it is necessary to use an angle-dependent doublet separation within a given profile when performing an α_2 elimination in X-ray diffraction line profiles. Two formulations for the doublet separation are suggested, which give better results than the doublet separation as obtained from a differentiation of Bragg's law. One formulation has the important advantage of being a constant on a sin θ scale; the other formulation may serve as the basis for a computerized monochromator.

1. Introduction

In line-profile analysis it is often impossible to obtain a satisfactory correction for the instrumental broadening by a deconvolution method. In such cases separation of the α_1–α_2 doublet is still possible. Two methods for α_2 elimination are commonly employed: the substitution correction (usually referred to as the Rachinger correction) (DuMond & Kirkpatrick, 1931; Rachinger, 1948) and the Fourier correction (Gangulee, 1970). The basic assumptions of both methods are (i) that the two components have the same shape, (ii) that the intensity ratio is known and (iii) that the doublet separation is also known.

In practice both methods are usually applied on a 2θ scale with a constant doublet separation – within a given profile – which is obtained by differentiating Bragg's law (*e.g.* Wagner, 1966).

The main purpose of this paper is to show the necessity of using an angle-dependent doublet separation *within a given profile*, but it will also be emphasized that the doublet separation has to be calculated properly.

2. Formulae for the doublet separation

For both α_2-elimination methods the basic assumption involved in the analysis is the shape identity. This can be formulated as: an intensity I_{α_2} of the α_2 distribution at any position x is accompanied by a *corresponding* intensity I_{α_1} of the α_1 distribution at x-Δx, the doublet separation Δx being a constant. Thus

$$I_{\alpha_2}(x)=K\,.\,I_{\alpha_1}(x\text{-}\Delta x), \qquad (1)$$

where K is a constant.

Usually x is identified with 2θ, so the doublet separation $\Delta 2\theta$ is assumed constant, although it is well known that the doublet separation on a 2θ scale increases with increasing values of 2θ. It is more realistic to identify x either with the wavelength or with the frequency (Compton & Allison, 1935).

Identifying x with wavelength λ – so that $\Delta\lambda=\lambda_2-\lambda_1$ is a constant – the doublet separation δ_λ on a 2θ scale can be calculated. Using the Bragg law for λ_1 and λ_2, one obtains

$$\delta_\lambda=2\theta_2-2\theta_1=2\arcsin(\sin\theta_1+\Delta\lambda/2d)-2\theta_1, \qquad (2)$$

in which θ_1 and θ_2 are the angles at which the corresponding wavelengths λ_1 and λ_2 of the α_1 and α_2 distributions diffract and d is the interplanar lattice spacing.

If x is identified with the frequency ν the doublet separation δ_ν on a 2θ scale can be calculated in a similar way.

It can be shown that δ_λ and δ_ν may be approximated very accurately by

$$\delta_R=2\arcsin(R\sin\theta_1)-2\theta_1 \qquad (3)$$

in which $R=\lambda_2/\lambda_1$ is a constant.

By differentiation of the Bragg law the doublet separation δ_B is obtained:

$$\delta_B=2\tan\theta\,.\,\Delta\lambda/\langle\lambda\rangle, \qquad (4)$$

where $\langle\lambda\rangle$ is the centroid wavelength of the doublet. The doublet separation δ_B is angle dependent with θ between θ_1 and θ_2. In the literature usually a constant doublet separation is applied, calculated from (4) using a fixed value of θ for the profile.

The constants $\Delta\lambda$ in (2) and (4) and $R=\lambda_2/\lambda_1$ in (3) can be determined from spectroscopic data for the peak values of the α_1 and α_2 wavelength distributions.

The interplanar lattice spacing d can be obtained from the centroid of the line profile and the centroid wavelength (Delf, 1963).

3. Discussion

Calculations showed that the differences between δ_λ, δ_ν and δ_R are very small. Since only δ_R can be determined without knowledge of the interplanar spacing and since the differences between δ_R and δ_B are much larger than those between δ_R, δ_λ and δ_ν, only the differences between δ_R and δ_B are given here.

Fig. 1(*a*) shows δ_R as a function of 2θ for different characteristic $K\alpha$ radiations. For small values of 2θ the angle dependency of the doublet separation is of minor interest. But at larger values of 2θ it is observed

1.4

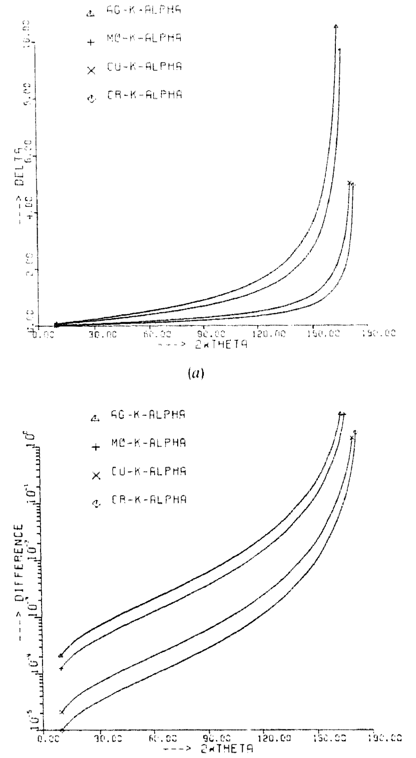

Fig. 1. (*a*) The doublet separation δ_R as a function of 2θ. (*b*) The difference of the doublet separations $\delta_R - \delta_B$ as a function of 2θ.

that a considerable error will be made if this angle dependency is neglected.

In Fig. 1(*b*) $\delta_R - \delta_B$ is given as a function of 2θ for the same characteristic wavelengths. It is clear that δ_B is systematically less than δ_R and this difference increases sharply at higher 2θ values.

We performed α_2 eliminations according to the substitution correction on a number of experimentally determined line profiles. After smoothing and subtraction of the background, the line profile was corrected for the angular dependence of the Lorentz, polarization, structure and Debye–Waller factors. Typical results of the α_2 elimination for constant doublet separation and for angle-dependent separation according to (4) and (2) are shown in Figs. 2 and 3. The oscillations on the high-angle side in Fig. 3 curve *a* are caused by the invalid assumption of a constant doublet separation. We believe that these are 'the oscillations on the high-angle side' reported frequently in the literature as inherent in the substitution correction.

However, as can be seen from curves *b* and *c*, the oscillations are diminished by the use of an angle-dependent doublet separation. The remaining inaccuracies are most probably caused by the fact that even on a wavelength scale there is no perfect shape identity of the α_1 and α_2 distributions.

The line profile of curve *b* obtained with the doublet separation δ_λ, should be compared with curve *c*, based on (4). (The results obtained with δ_R and δ_v were identical to that obtained with δ_λ.) The decrease of intensity in curve *b* has a more realistic appearance than the rather angular character of curve *c*, as is illustrated by the dashed curves. We remark that the angle of incidence for the profile of Figs. 2 and 3 was not very high in terms of the scale of Fig. 1. The difference $\delta_R - \delta_B$ was only 0·003° 2θ. Nevertheless the differences between curves *b* and *c* are quite clear. At higher angles of incidence and/or with shorter characteristic wavelengths these differences are still more pronounced.

If the α_2 eliminations are performed with the Fourier correction instead of the substitution correction the same results are obtained (see also Delhez & Mittemeijer, 1975).

Line-profile analysis is usually done on a $\sin\theta$ scale. Therefore it is efficient to use a doublet separation which is a constant on such a scale. Only δ_λ has

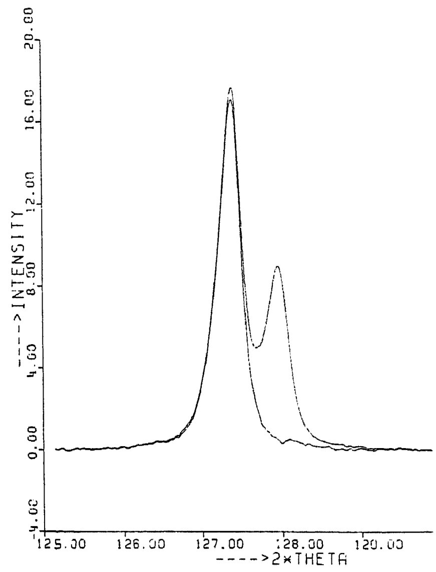

Fig. 2. The substitution correction applied to the 422 line profile of an MgO powder specimen using the doublet separation δ_λ. The measured total profile and the computed α_1 line profile are shown.

1.4

this convenient property, because for a fixed value of d the $\sin\theta$ scale is proportional to the λ scale.

Thus it is concluded that the use of an angle-dependent doublet separation within a given profile according to (2) is strongly recommended when an α_2 elimination is performed. Formulation (3) is of particular interest when it is impossible to determine the interplanar spacing. If an α_2 elimination is needed over a large range of θ values containing more than one line profile, formulation (3) serves as the basis for a computerized monochromator.

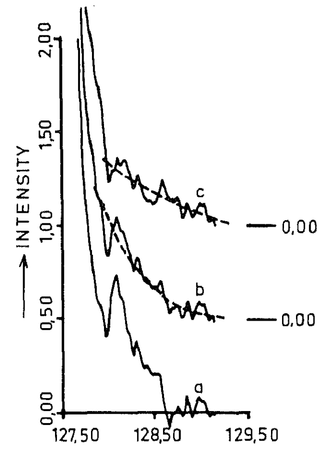

Fig. 3. Parts of the high-angle side of the α_1 line profiles obtained with the substitution correction from the total 422 line profile of Fig. 2. Curve *a*: with a constant doublet separation; curve *b*: with δ_λ; curve *c*: with δ_B.

The authors are greatly indebted to Professor B. Okkerse, Dr F. W. Schapink and Mr T. v. Dijk for stimulating discussions. They also read the manuscript carefully.

Part of this work was carried out under the research programme of the Stichting voor Fundamenteel Onderzoek der Materie (F.O.M.), with financial support from the organisation Z.W.O. and the Metaalinstituut TNO.

References

Compton, A. H. & Allison, S. K. (1935). *X-rays in Theory and Experiment*. London: Macmillan.
Delf, B. W. (1963). *Brit. J. Appl. Phys.* **14**, 345–350.
Delhez, R. & Mittemeijer, E. J. (1975). *J. Appl. Cryst.* **8**, 612–614.
DuMond, J. W. M. & Kirkpatrick, H. A. (1931). *Phys. Rev.* **37**, 154–156.
Gangulee, A. (1970). *J. Appl. Cryst.* **3**, 272–277.
Rachinger, W. A. (1948). *J. Sci. Instrum.* **25**, 254–255.
Wagner, C. N. J. (1966). *Local Atomic Arrangements Studied by X-ray Diffraction*. Edited by J. M. Cohen and J. E. Hilliard, pp. 234–235. New York: Gordon and Breach.

Reprinted from *J. of Appl. Crystallography*, Vol. 8, Part 6, December 1975

PRINTED IN DENMARK

J. Appl. Cryst. (1975). 8, 612

An Analysis of Errors in the Fourier Coefficients of the α_1 Line Profile

BY R. DELHEZ AND E. J. MITTEMEIJER

Laboratory of Metallurgy, Delft University of Technology, Rotterdamseweg 137, *Delft, The Netherlands*

(*Received* 14 *April* 1975; *accepted* 15 *July* 1975)

The errors in the Fourier coefficients of the α_1 component obtained by α_2 elimination are investigated analytically. The effects of counting statistics, of an incorrect intensity ratio of the α_1 and α_2 components and of an incorrect doublet separation are calculated. The mean-square error in the Fourier coefficient caused by counting statistics is a periodic function of the harmonic number, while errors in the intensity ratio and in the doublet separation primarily affect the first Fourier coefficients. The results are confirmed by computer simulations and by computations with experimental line profiles. The α_2 elimination methods assume a perfect shape identity of the α_1 and α_2 components, but this assumption is not completely justified. Deviations might be interpreted as local errors in the doublet separation and the intensity ratio.

1. Introduction

The Fourier coefficients of a line profile are very often used, for example in the well known Warren–Averbach analysis (Warren, 1969).

Different sources of errors occurring in the Fourier coefficients have been considered in the literature. The errors caused by sampling and truncation of the profile have been treated fully by Brigham (1974). The errors in the Fourier coefficients caused by an inaccurate choice of background have been treated by Young, Gerdes & Wilson (1966), while Wilson (1967, 1968, 1969) considered the influence of counting statistics. This paper considers the errors in the Fourier coefficients of the α_1 line profile obtained by elimination of the α_2 component from the $K\alpha$ doublet. As mentioned earlier (Delhez & Mittemeijer, 1975) two methods for α_2 elimination are commonly employed: the substitution correction and the Fourier correction.

2. Brief formulation of the two α_2 elimination methods

Let $I_t(x)$, $I_1(x)$ and $I_2(x)$ be respectively the total, the $K\alpha_1$ and the $K\alpha_2$ line profiles. Then

$$I_t(x)=I_1(x)+I_2(x). \tag{2.1}$$

Introducing the three basic assumptions (Delhez & Mittemeijer, 1975), we obtain:

$$I_1(x)=I_t(x)-RI_1(x-\delta), \tag{2.2}$$

where $R=I_2(\max)/I_2(\max)$ and δ is the doublet separation.

(i) *The substitution correction*

When the expression for $I_1(x-\delta)$ obtained by replacing x by $x-\delta$ in (2.2) is substituted in (2.2) and the substitution is made repeatedly, one obtains:

$$I_1(x)=\sum_{m=0}^{M}(-R)^m I_t(x-m\delta). \tag{2.3}$$

If there are $2N$ equidistant data points the Fourier coefficients $A_S(n)$ are defined by:

$$A_S(n)=\frac{1}{2N}\sum_{x=0}^{2N-1} I_1(x)\exp\{-2\pi inx/2N\}. \tag{2.4}$$

These coefficients are obtained by fast Fourier transformation (*e.g.* Brigham, 1974). The error of the machine algorithm for this transform procedure is negligible compared to the experimental errors considered in this paper.

(ii) *The Fourier correction*

The Fourier coefficients of the total and the α_1 line profiles are defined by $T(n)$ and $A_F(n)$ respectively [$A_F(n)$ is analogous to $A_S(n)$ in (2.4)]. After substitution of the Fourier series for $I_t(x)$ and $I_1(x)$ in (2.2) it is found that

$$A_F(n)=T(n)/P(n), \tag{2.5}$$

in which:

$$P(n)=1+R\exp\{-2\pi in\delta/2N\}. \tag{2.6}$$

In recent literature the Fourier correction is favoured (Gangulee, 1970; Kidron & De Angelis, 1971) although the two methods are mathematically equivalent; from (2.3) and (2.4) follows that

$$\begin{aligned} A_S(n) &= \frac{1}{2N}\sum_m(-R)^m\exp\{-2\pi imn\delta/2N\} \\ &\quad\times\sum_x I_t(x-m\delta)\exp\{-2\pi in(x-m\delta)/2N\} \\ &= T(n)/P(n)=A_F(n)=A(n). \end{aligned} \tag{2.7}$$

Because computation time for the Fourier correction is considerably larger than for the 'old' substitution correction, we prefer the latter.

3. The influence of counting statistics

The mean-square error in the Fourier coefficient of the total line profile is given by:

1.5

$$\overline{|\Delta T(n)|^2} = \frac{1}{(2N)^2} \sum_{x1} \sum_{x2} \overline{\Delta I_t(x_1)\Delta I_t(x_2)} \times \exp\{-2\pi i n(x_1 - x_2)\}. \quad (3.1)$$

We assume 'white noise', *i.e.* there exists a relation between the errors caused by counting statistics only if $x_1 \equiv x_2 \equiv x$. Hence

$$\overline{|\Delta T(n)|^2} = \frac{1}{(2N)^2} \sum_x \overline{|\Delta I_t(x)|^2}. \quad (3.2)$$

When (2.6), (2.7) and (3.2) are combined,

$$\overline{|\Delta A(n)|^2} = \frac{1}{(2N)^2} \frac{\sum_x \overline{|\Delta I_t(x)|^2}}{(1 + 2R\cos 2\pi n\delta/2N + R^2)}. \quad (3.3)$$

If $I_t(x)$ represents the actual number of counts:

$$\sum_x \overline{|\Delta I_t(x)|^2} = \sum_x I_t(x). \quad (3.4)$$

The result (3.3) is supported by a computer simulation. For this purpose we used α_1 and α_2 line profiles of the asymmetric Gaussian type, with an index of asymmetry of 1·5. The ratio R was taken as 0·5. The total profile is given by:

$$I_t(x) = C_1 \exp\{-c_1^2(x+\delta)^2\} + C_2 \exp\{-c_2^2 x^2\}, \quad (3.5)$$

in which $C_1 = 10; C_2 = 5; c_1 = 1{\cdot}5$ for $x < -1{\cdot}2, c_1 = 1$ for $x > -1{\cdot}2; c_2 = 1{\cdot}5$ for $x < 0, c_2 = 1$ for $x > 0$; and $\delta = 1{\cdot}2$. The spacing of the 128 data points used was 0·1 [so $\delta/2N = (1{\cdot}2/0{\cdot}1)/128$]. Scatter was generated using subroutines to calculate random numbers according to the normal distribution for a given mean and a given standard deviation. The given mean is the intensity calculated from (3.5) and the standard deviation σ was taken as $\sigma(x) = \sqrt{I_t(x)}$, which means that the preset-time method of measurement was simulated. Each simulation consisted of the generation of a profile with counting statistics superimposed and subsequent α_2 elimination.

From the Fourier transforms of α_1 profiles obtained from 50 simulated profiles and the transform of the pure α_1 profile the $\overline{|\Delta A(n)|^2}$ values were obtained. The result of the simulations is shown in Fig. 1 and agrees fairly well with (3.3). This implies that the relative mean-square error of the Fourier coefficients $A(n)$ increases rapidly with $|n|$, because $A(n)$ has only large values for small values of $|n|$.

4. The influence of an error in R and in δ

From (2.7) one obtains:

$$|\Delta A(n)|^2 = \left|\frac{-T(n)\Delta P(n)}{P^2(n)}\right|^2. \quad (4.1)$$

From (2.6) and (4.1) it is derived in the case of an error ΔR in the intensity ratio R that

$$|\Delta A(n)|^2 = \frac{|\Delta R|^2 T^2(n)}{(1 + 2R\cos 2\pi n\delta/2N + R^2)^2} \quad (4.2)$$

and in the case of an error $\Delta\delta$ in the doublet separation δ:

$$|\Delta A(n)|^2 = \left(\frac{2\pi R\Delta\delta}{2N}\right)^2 \frac{n^2 T^2(n)}{(1 + 2R\cos 2\pi n\delta/2N + R^2)^2}. \quad (4.3)$$

The results (4.2) and (4.3) are supported by computer simulations, using the procedure as described in § 3. The influence of counting statistics is combined with an error $\Delta R = -0{\cdot}05$ and an error $\Delta\delta = +\delta/9$.

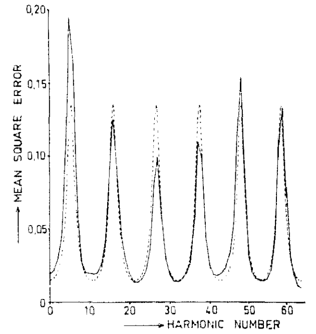

Fig. 1. Mean-square error in the Fourier coefficients of an α_1 line profile caused by counting statistics. Full line: obtained from 50 simulated doublets. (Straight line segments have been drawn between the calculated points.) Dashed line: theoretical curve; equation (3.3).

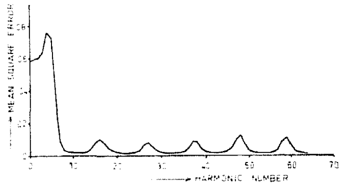

Fig. 2. Mean-square error in the Fourier coefficients of an α_1 line profile caused by an inaccurate R value (0·45) and counting statistics. Fifty simulated doublets with $R = 0{\cdot}5$ were used.

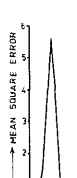

Fig. 3. Mean-square error in the Fourier coefficients of an α_1 line profile caused by an inaccurate δ ($= 1{\cdot}2 * 10/9$) and counting statistics. Fifty simulated doublets with $\delta = 1{\cdot}2$ were used.

The results are shown in Figs. 2 and 3. It follows that the influences of errors in R and δ are restricted to the smaller values of $|n|$, which are the most important ones (*e.g.* for a Warren–Averbach analysis). The periodic mean-square error caused by counting statistics predominates at larger values of $|n|$ (§ 3). Furthermore it follows from a comparison of Figs. 2 and 3 that the α_1 Fourier coefficients are more sensitive to an error in the doublet separation than to an error in the intensity ratio. If the influence of an error in the intensity ratio is neglected – which is usually justified except for the first Fourier coefficients – it follows from (3.3) and (4.3) that the error in the doublet separation is only important if

$$\sum_x \overline{|\Delta I_t(x)|^2}/T^2(n) \lesssim (\Delta\delta)^2(2\pi nR)^2/(1+2R\cos 2\pi n\delta/2N+R^2). \quad (4.4)$$

This inequality supplies a criterion to decide whether a further improvement in the counting procedure is useful compared to the inaccuracy in the doublet separation from spectroscopic data.

5. α_2 elimination in experimental line profiles

The 533 line profile of a standard silicon powder sample was recorded 31 times with Cu $K\alpha$ radiation. After subtraction of the background, the profiles were corrected for the angular dependence of the Lorentz factor, the polarization factor, the structure factor and the Debye–Waller factor. The α_2 eliminations were performed on a sin θ scale and the doublet separation was calculated according to Delhez & Mittemeijer (1975). Since the transform of the true α_1 profile is not known, we assume the mean of the 31 transforms of the α_1 component obtained after α_2 elimination to be the true transform. Therefore the variance for each n of $A(n)$ may be considered as the mean-square error. In Fig. 4 the variance is plotted. For larger values of $|n|$ the periodic behaviour, as predicted by (3.3) as a consequence of counting statistics, is observed. For the smaller values of $|n|$ the variances are large. This may be explained in the following way: The α_2 elimination method assumes the shapes of the α_1 and α_2 components to be identical. In practice this is not true, since there are systematic deviations in shape (Compton & Allison, 1935) – but these are not detectable by a variance calculation – and statistical fluctuations in shape (for example originating from counting statistics). Deviations from perfect shape identity can be considered as local errors in δ and/or R. Therefore in our opinion the first large variances in Fig. 4 could be due to imperfect shape identity in each experimental line profile.

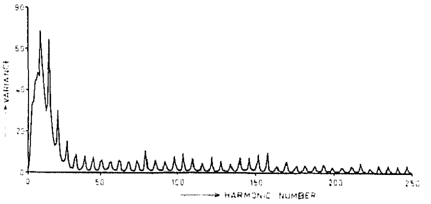

Fig. 4. Variance in the Fourier coefficients of the α_1 line profile obtained by α_2 elimination from 31 recordings of the 533 line profile of a standard silicon powder specimen.

The authors are greatly indebted to Professor B. Okkerse, Dr F. W. Schapink and Mr T. v. Dijk for stimulating discussions. They also read the manuscript carefully.

Part of this work was carried out under the research programme of the Stichting voor Fundamenteel Onderzoek der Materie (F.O.M.).

References

BRIGHAM, E. O. (1974). *The Fast Fourier Transform*, pp. 91–109. Englewood Cliffs, New Jersey: Prentice Hall.
COMPTON, A. H. & ALLISON, S. K. (1935). *X-rays in Theory and Experiment*, p. 734, London: Macmillan.
DELHEZ, R. & MITTEMEIJER, E. J. (1975). *J. Appl. Cryst.* **8**, 609–611.
GANGULEE, A. (1970). *J. Appl. Cryst.* **3**, 272–277.
KIDRON, A. & DE ANGELIS, R. J. (1971). *Acta Cryst.* A**27**, 596–599.
WARREN, B. E. (1969). *X-ray Diffraction*, pp. 264–275. Reading Mass.: Addison-Wesley.
WILSON, A. J. C. (1967). *Acta Cryst.* **23**, 888–898.
WILSON, A. J. C. (1968). *Acta Cryst.* A**24**, 478.
WILSON, A. J. C. (1969). *Acta Cryst.* A**25**, 584–585.
YOUNG, R. A., GERDES, R. J. & WILSON, A. J. C. (1966). *Acta Cryst.* **22**, 155–162.

A COMPARISON OF TWO COMPUTER METHODS FOR SEPARATION OF THE $\alpha_1\alpha_2$ DOUBLET

by

R. Delhez and E.J. Mittemeijer

Laboratory of Metallurgy, Delft University of Technology
Rotterdamseweg 137, Delft, The Netherlands

Transcription (abridged) of lecture given at the Tenth International Congress of Crystallography (Amsetrdam; 7 - 15 August 1975).
Abstract: Acta Cryst., A31, Part S3, S202 (1975).

1. Introduction

In line profile analysis it is often impossible to obtain the pure line profile - that is the line profile corrected for all the instrumental broadening - by any deconvolution procedure. In those cases separation of the $\alpha_1\alpha_2$-doublet of the characteristic Kα radiation used is still possible. The success of such a method is based upon the fact that an important part of the instrumental broadening arises from the presence of the α_2 component.

From Brill's work in 1928[1] up to now a number of methods for elimination of the α_2 component from the doublet have been proposed. Nowadays two methods have become common practice:

(i) The substitution correction. This elimination method is frequently referred to as the Rachinger correction, but the method is originated by DuMond & Kirkpatric in 1931[2,3].

(ii) The Fourier correction, which is developed by Gangulee in 1970[4].

Both methods have the following three basic assumptions [c.f. Fig. 3 in ref. 5]:

a. The α_1 and α_2 line profiles have the same shape.

b. The intensity ratio R $[= I_{\alpha_2}(\max)/I_{\alpha_1}(\max)]$ is known.

c. The doublet separation δ is known. The doublet separation is the distance between corresponding abscissa-values; an example is the distance between the maxima of the α_1 and α_2 line profiles.

From these assumptions it can be derived that the intensity of the α_1 line profile is given by the following summation:

$$I_{\alpha_1}(x) = \sum_{m=0}^{M} (-R)^m \, I_t(x-m\delta) \qquad (1)$$

At the right hand side of this equation only known quantities are present.

I.6

If $A(n)$ and $T(n)$ denote the Fourier coefficients of the α_1 and total line profile respectively, than $A(n)$ is given by the simple division:

$$A(n) = T(n)/P(n) \qquad (2)$$

where: $P(n) = 1 + R \exp\{-2\pi i n\delta/a\}$

("a" is the period over which the Fourier series have been evaluated). Eq. (1) is the basis for the substitution correction whereas eq. (2) is the basis for the Fourier correction, where the α_1 line profile follows after a synthesis with the calculated α_1 Fourier coefficients.

Both methods have been programmed for computer utilization. Here we would like to present a critical comparison on practical grounds of both methods.

2. Advantages of the Fourier correction mentioned in the literature

In the recent literature[4,6] the Fourier correction is preferred because of two advantages mentioned:

(i) The Fourier correction does not give oscillations at the high angle side in the calculated α_1 line profile, in contrast with the substitution correction. In the literature it is frequently said that these oscillations accompany the substitution correction (e.g. ref. 7).

(ii) The Fourier correction does not need an interpolation of data points in contrast with the substitution correction. It can be easily seen from eq. (1) that the substitution correction needs an interpolation of data points since the experimentally determined intensity values are in general not known at abscissa-values $x-m\delta$.

3. Discussion of the first advantage mentioned (abridged)

Three formulations for the doublet separation δ may be applied[8]

$$\delta_\lambda = 2\theta_2 - 2\theta_1 = 2 \arcsin (\sin\theta_1 + \Delta\lambda/2d) - 2\theta_1 \ , \qquad (3)$$

$$\delta_C = 2 \arcsin (\frac{\lambda_1}{\lambda_2} \sin\theta_1) - 2\theta_1 \ , \qquad (4)$$

$$\delta_B = 2 \tan\theta \ \Delta\lambda/\langle\lambda\rangle \ , \qquad (5)$$

where λ_1 en λ_2 follow from spectroscopic data for the peak values of the α_1 and α_2 wavelength distributions; $\Delta\lambda = \lambda_2 - \lambda_1$ and $\langle\lambda\rangle$ denotes the centroid wavelength.

The results with respect to the oscillations on the high angle side of the α_1 profile calculated with these formulations differ notably[8].

The Fourier correction and the substitution correction produce the same oscillations. Indeed one should not expect any difference in results between both methods since they are mathematically equivalent (proof in ref. 9). Apparently this was not realized by previous authors.

An angle dependent doublet separation in stead of a constant one diminishes the oscillations mentioned. Since line profile analysis is usually done on a sinθ scale it is efficient to use a doublet separation which is a constant on such a scale. δ_λ has this convenient property. δ_C, the close approximation of δ_λ, is of particular interest when it is impossible to determine the interplanar spacing d (which is necessary for δ_λ). Furthermore if an α_2-elimination is needed over a large range of θ-values including more than one line profile then δ_C serves as the basis for a computerized monochromator.

4. Discussion of the second advantage mentioned

According to previous authors [c.f. section 2] the Fourier correction does not need an interpolation of data points, in contrast with the substitution correction.

For the Fourier correction it is necessary to calculate the Fourier coefficients of the total line profile [c.f. eq. (2)]. This calculation can be done efficiently only if the data are equally spaced, because Fast Fourier Transform algorithms[10] are based on equally spaced data. Line profiles are usually measured with constant increments in 2θ. Nevertheless it is not recommended to perform the calculation of the Fourier coefficients on this 2θ scale, since it follows from the discussion on the formula for the doublet separation[8] that the angle dependent doublet separation δ_λ [eq. (3)] is preferable. Thus, if the Fourier correction is applied on the 2θ scale one has to calculate for every data point a set of α_1 Fourier coefficients, since every data point has its own doublet separation, which is needed for the calculation of $P(n)$. Therefore it is clear that the Fourier correction has to be applied on a scale where the doublet separation is a constant. From the formula for the doublet separation δ_λ [eq. (3)] it follows that this doublet separation is a constant on a $\sin\theta$ scale. Hence the 2θ scale has to be transformed into a $\sin\theta$ scale and accordingly the intensities measured have to be interpolated for the Fourier correction as well.

5. Conclusions

Summarizing:

(i) Both α_2 elimination methods produce the same oscillations at the high angle side of the α_1 line profile. These oscillations can be diminished if a properly calculated angle dependent doublet separation is used in stead of a constant one. We propose to apply δ_λ or δ_C [eqs. (3) and (4)].

(ii) In practice both α_2 elimination methods need an interpolation of data points.

Hence: The advantages mentioned in the literature for the Fourier correction do not hold.

Moreover we would like to go further and remark:

(i) The substitution correction can be applied on any scale such as a 2θ scale or a $\sin\theta$ scale.

(ii) The Fourier correction can only be applied on a $\sin\theta$ scale because only then the doublet separation is a constant.

(iii) The substitution correction is easier to handle: for application of the Fourier correction a computer is necessary whereas the substitution correction can be performed graphically.

(iiii) The computer time needed for the substitution correction is a factor of 5 less. This is true if Fast Fourier Transform algorithms are applied for the Fourier correction. Otherwise the computation time advantage for the substitution correction is even more distinct.

Hence: The substitution correction has to be preferred in practice.

1.6

References

1. Brill, R. (1928), Z. Kristallogr. 68, 394.
2. Rachinger, W.A. (1948). J.Sci.Instrum. 25, 254.
3. DuMond, J.W.M. and Kirkpatric, H.A. (1931). Phys.Rev. 37, 154.
4. Gangulee, A. (1970). J.Appl.Cryst. 3, 272.
5. Delhez, R. and Mittemeijer, E.J. (1977). Chemisch Weekblad Magazine, m103.
6. Kidron, A.and De Angelis, R.J. (1971). Acta Cryst. A27, 596.
7. Wagner, C.N.J.,in Cohen, J.B. and Hilliard, J.E. (Eds.), "Local atomic arrangements studied by X-ray diffraction", Vol. 36, (Gordon and Breach, New York, 1966), p. 234.
8. Delhez, R. and Mittemeijer, E.J. (1975). J.Appl.Cryst. 8, 609.
9. Delhez, R. and Mittemeijer, E.J. (1975). J.Appl.Cryst. 8, 612.
10. Brigham, E.O. (1974). The Fast Fourier Transform, pp. 91-109. Englewood Cliffs,New Jersey: Prentice Hall.

Reprinted from *J. of Appl. Crystallography*, Vol. 9, Part 3, June 1976

PRINTED IN DENMARK

SHORT COMMUNICATIONS

J. Appl. Cryst. (1976). **9**, 233

The elimination of an approximation in the Warren–Averbach analysis.

By R. Delhez and E. J. Mittemeijer, *Laboratory of Metallurgy, Delft University of Technology, Rotterdamseweg* 137, *Delft, The Netherlands*

(*Received* 17 *December* 1975; *accepted* 9 *February* 1976)

The Warren–Averbach analysis for the separation of particle size and strain involves a cosine and a logarithmic power series expansion. It is shown that the neglect of higher-order terms in the logarithmic series expansion introduces larger errors at small values of the strain than the cosine series while at larger values the dominance is less pronounced. Furthermore it is shown that the power series expansion for the logarithm is superfluous and as a result the Warren–Averbach analysis can be improved. In common practice the differences between the improved method and the original one can easily be 10% for particle-size Fourier coefficients and 30% for mean square strain values.

The separation of cold-work distortion and particle-size broadening in X-ray diffraction line profiles is usually obtained by applying the well known Warren–Averbach analysis (Warren, 1969). The method is based on a Fourier analysis of the pure line profile.

Each Fourier coefficient $A(n,l)$ – usually obtained after some deconvolution technique or α_2-elimination procedure – can be written as the product of a 'size' Fourier coefficient $A^S(n)$ and a 'distortion' Fourier coefficient $A^D(n,l)$ according to the convolution theorem. If the diffracting domains are thought to consist of columns of unit cells perpendicular to the diffracting planes, described as $(00l)$ planes, then

$$A^S(n)=N(n)/N_3 \tag{1}$$

$$A^D(n,l)=\langle\cos 2\pi lZ(n)\rangle \tag{2}$$

where $N(n)$ is the average number per column of pairs of unit cells a distance n cells apart, N_3 is the average domain size in unit cells perpendicular to $(00l)$ and $Z(n)$ is the difference between the displacements of two unit cells n cells apart. If $e(n)$ is defined by $e(n)=Z(n)/n$:

$$A(n,l)=N(n)/N_3\,.\,\langle\cos 2\pi lne(n)\rangle\,. \tag{3}$$

Since $A^D(n,l)$ is dependent on l and $A^S(n)$ is not, size and strain effects can be separated by taking the logarithm of (3):

$$\ln A(n,l)=\ln N(n)/N_3+\ln\langle\cos 2\pi lne(n)\rangle\,. \tag{4}$$

Two power series expansions are applied:

$$\begin{aligned}\langle\cos 2\pi lne(n)\rangle &= 1-\frac{\langle[2\pi lne(n)]^2\rangle}{2!}+R_4^{\cos}\\ &\simeq 1-2\pi^2l^2n^2\langle e^2(n)\rangle,\end{aligned} \tag{5}$$

$$\begin{aligned}\ln\,[1-2\pi^2l^2n^2\langle e^2(n)\rangle] &= -2\pi^2l^2n^2\langle e^2(n)\rangle+R_4^{\ln}\\ &\simeq -2\pi^2l^2n^2\langle e^2(n)\rangle\end{aligned} \tag{6}$$

where $R_4^{\cos}$ and $R_4^{\ln}$ are the remainders of the two series expansions. In practice terms in higher orders of l^2 are neglected. From (4), (5) and (6) it follows that

$$\ln A(n,l)\simeq\ln N(n)/N_3-2\pi^2l^2n^2\langle e^2(n)\rangle\,. \tag{7}$$

If at least two orders of a reflexion are available then values for $N(n)/N_3$ and $\langle e^2(n)\rangle$ can be obtained, numerically or graphically, from the slope and intercept of a plot of $\ln A(n,l)$ *versus* l^2.

Recently Mitra & Chaudhuri (1974) considered the errors originating from the series expansion for the cosine. They calculated the ratio of the third to the second term of this power series for some practical values of l, n and $e(n)$ (*cf.* their Table 1*). Here we will compare the errors arising from both series expansions.

It can be shown that (*cf.* Appendix 1):

$$|R_4^{\ln}|_{\min}=3|R_4^{\cos}|_{\max}\,. \tag{8}$$

Since the cosine is underestimated with $|R_4^{\cos}|$ and the logarithm is overestimated with $|R_4^{\ln}|$ it follows from (8) that the logarithmic series expansion introduces an error in the final result at least twice that of the cosine series expansion.

Let us also consider the ratio R of the relative errors caused by truncation of the series after the terms with l^2. Defining $q=2\pi^2l^2n^2\langle e^2(n)\rangle$, it follows from (5) and (6) with the additional assumption $e(n)=\sqrt{\langle e(n)^2\rangle}$ that:

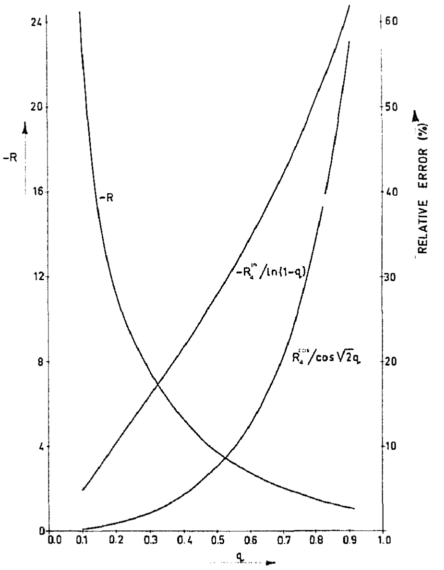

Fig. 1. The relative error in the series expansion for the cosine: $R_4^{\cos}/\sqrt{2q}$; the relative error in the series expansion for the logarithm: $R_4^{\ln}/\ln(1-q)$ and their ratio R as a function of $q=2\pi^2l^2n^2\langle e^2(n)\rangle$.

---

* This table contains two cases where the logarithmic series expansion is impossible, because of negative values of the argument.

$$R=\frac{R_4^{\ln}/\ln(1-q)}{R_4^{\cos}/\cos\sqrt{2q}}=\frac{[\ln(1-q)-(-q)]/\ln(1-q)}{[\cos\sqrt{2q}-(1-q)]/\cos\sqrt{2q}}. \qquad (9)$$

The relative errors in the cosine and logarithmic series expansions and their ratio R, as defined by (9), are plotted in Fig. 1. It is clear that at small values of q the neglect of higher-order terms in the logarithmic series is of much more importance than in the cosine series; at larger values of q, as are often observed in alloys and highly cold-worked metals, the difference becomes less pronounced.

In the literature the approximation for the logarithmic function is always encountered. The errors caused hereby are discussed above. However to our knowledge it has not been noticed that these errors can be reduced to nil because the series expansion for the logarithm can be simply avoided in the following way.

The direct substitution of the power series expansion for $\langle\cos 2\pi lne(n)\rangle$ according to (5) in (3) yields:

$$A(n,l)\simeq\frac{N(n)}{N_3}-\frac{N(n)}{N_3}2\pi^2l^2n^2\langle e^2(n)\rangle. \qquad (10)$$

Now the influences of size and strain are *not* separated as in (4). However if two orders of a reflexion are available the values of $N(n)/N_3$ and $\langle e^2(n)\rangle$ are readily obtained numerically, or graphically from a plot of $A(n,l)$ *versus* l^2.

Results of the usual Warren–Averbach method [equation (7)] were compared with the results based on (10) for experimental line profiles. For all n, values of $A^S(n)$ and values of $\langle e^2(n)\rangle$ obtained with (10) were smaller than the values deduced from (7), as is shown in Appendix 2. In a case where $\langle e^2(n)\rangle\simeq10^{-6}$ the differences between the values of $A^S(n)$ obtained from both methods were less than 2% for small values of n; for larger values of n differences of 10% and more were found. The differences in $\langle e^2(n)\rangle$ at small values of n were 15% and less; at larger values of n the differences increased: 30% and more.

In practice the second order of a reflexion is usually measured less accurately than the first order. Therefore spurious variations may be present on the Fourier coefficients of the second order. This will produce spurious ripples on the $A^S(n)$-curve. These ripples will be enhanced in the $A^S(n)$-curve obtained from (7) as compared to the $A^S(n)$-curve obtained from (10), as is shown in Appendix 2. Also $\langle e^2(n)\rangle$ obtained from (7) is more sensitive to spurious variations in the Fourier coefficients of the second order as compared to $\langle e^2(n)\rangle$ obtained from (10) (*cf.* Appendix 2).

A more refined multiple-order technique is possible by considering one more term in the series for $\langle\cos 2\pi lne(n)\rangle$. If terms in l^6 and higher orders are neglected, the Fourier coefficient of the total line profile can be expressed as:

$$A(n,l)\simeq C_1-C_2l^2+C_3l^4 \qquad (11)$$

where

$$C_1=N(n)/N_3$$
$$C_2=C_12\pi^2n^2\langle e^2(n)\rangle$$
$$C_3=C_12\pi^4n^4\langle e^4(n)\rangle/3.$$

In fact (11) is an improved formulation of the multiple-order technique proposed by Mitra & Chaudhuri (1974). As in (10), again the influences of size and strain are not separated, but the three coefficients C_1, C_2 and C_3 are readily obtained if three orders of a reflexion are available. After substitution of C_1 $[=N(n)/N_3]$ in C_2 and C_3 values for $\langle e^2(n)\rangle$ and $\langle e^4(n)\rangle$ are found.

Obviously the number of orders of a reflexion necessary for the evaluation of (10) and (11) can be reduced by one if $A^S(n)$ is approximated by $1-n/N_3$, as was done by Mitra & Misra (1967) who for the rest used the logarithmic series expansion.

We are indebted to Professor B. Okkerse and Dr F. W. Schapink for critically reading the manuscript.

Financial support of the Stichting voor Fundamenteel Onderzoek der Materie (F.O.M.) is gratefully acknowledged.

APPENDIX 1

Applying the formulation of Lagrange for the remainder (*e.g.* Jeffreys & Swirles, 1962) we arrive at the following expressions for $R_4^{\cos}$ and $R_4^{\ln}$:

$$R_4^{\cos}=\frac{l^4}{4!}\langle\varepsilon^4\cos\theta_1\varepsilon l\rangle\quad 0<\theta_1<1$$

$$R_4^{\ln}=-\frac{3l^4\langle\varepsilon^2\rangle^2}{4!}\,\frac{\langle\varepsilon^2\rangle\theta_2^4l^4/4+3\langle\varepsilon^2\rangle\theta_2^2l^2+1}{(1-\langle\varepsilon^2\rangle\theta_2^2l^2/2)^4}\quad 0<\theta_2<1$$

where

$$\varepsilon=2\pi ne(n).$$

A maximal estimate for the remainder $|R_4^{\cos}|$ is obtained if $\theta_1=1$ and a minimal estimate for $|R_4^{\ln}|$ follows if $\theta_2=0$. If $\langle\varepsilon^2\rangle^2$ may be approximated by $\langle\varepsilon^4\rangle$ equation (8) is obtained.

APPENDIX 2

Two orders of a reflexion are characterized by l_1 and l_2 $(l_2>l_1)$.

The suffices 7 and 10 are used to distinguish between results derived from (7) and (10) respectively.

For the usual Warren–Averbach method [equation (7)] it follows that

$$A^S(n)_7=\{A(n,l_1)\}^{l_2^2/(l_2^2-l_1^2)}.\{A(n,l_2)\}^{-l_1^2/(l_2^2-l_1^2)}$$
$$\langle e^2(n)\rangle_7=-1/2\pi^2n^2.\{\ln A(n,l_2)-\ln A(n,l_1)\}/(l_2^2-l_1^2)$$

and for the method based on (10):

$$A^S(n)_{10}=\{A(n,l_1)l_2^2-A(n,l_2)l_1^2\}/(l_2^2-l_1^2)$$
$$\langle e^2(n)\rangle_{10}=-1/2\pi^2n^2.\{A(n,l_2)-A(n,l_1)\}/\{A(n,l_1)l_2^2-A(n,l_2)l_1^2\}.$$

Since $l_2>l_1>0$ and since $A(n,l_1)/A(n,l_2)>1$ for $n\neq0$ if the line profiles contain both particle size and strain broadening, it follows that

$$A^S(n)_7/A^S(n)_{10}>1\quad\text{and}\quad\langle e^2(n)\rangle_7/\langle e^2(n)\rangle_{10}>1.$$

If it is assumed that the errors $\Delta A^S(n)$ and $\Delta\langle e^2(n)\rangle$ are determined entirely by the error in $A(n,l_2)$, it can be shown that

$$\Delta A^S(n)_7/\Delta A^S(n)_{10}>1\quad\text{and}\quad\Delta\langle e^2(n)\rangle_7/\Delta\langle e^2(n)\rangle_{10}>1.$$

Because $A(n,l_1)/A(n,l_2)$ usually increases with n the ratios mentioned increase with n.

References

Jeffreys, H. & Swirles, B. (1962). *Methods of Mathematical Physics*, p. 51. Cambridge Univ. Press.

Mitra, G. B. & Chaudhuri, A. K. (1974). *J. Appl. Cryst.* **7**, 350-355.

Mitra, G. B. & Misra, N. K. (1967). *Acta Cryst.* **22**, 454-456.

Warren, B. E. (1969). *X-ray Diffraction*, pp. 264-275. Reading, Mass.: Addison-Wesley.

I.8

Philosophical Magazine, 1977, Vol. 36, No. 5

CORRESPONDENCE

Correction for errors in microstrain values from X-ray diffraction line profiles

By Th. H. de Keijser and E. J. Mittemeijer
Laboratory of Metallurgy, Delft University of Technology, Rotterdamseweg 137, Delft, The Netherlands

[Received 9 May 1977]

Abstract

Before microstrain values are determined from broadened X-ray diffraction line profiles, one should correct for the broadening due to the experimental conditions. This broadening can be recorded from an ideally crystallized (standard) specimen. However, if one is obliged to use a standard specimen that diffracts in a 2θ-range different from that of the line profile to be investigated, errors in the mean-square-strain of the order of 50% may result. An easily applicable procedure is given to correct for such errors.

---

§ 1. Introduction

Microstrains contribute to the broadening of X-ray diffraction line profiles. Before microstrain values can be determined, the instrumental broadening—consisting of spectral broadening and broadening due to instrumental factors—should be eliminated from the experimental line profiles. This is usually done by the deconvolution method of Stokes (1948), for which knowledge of the instrumental profile is essential. At best, the 'instrumental' profile is recorded from a standard specimen of the same composition that is treated in the same way, as far as possible, as the specimen under investigation. Unfortunately, in many cases an 'instrumental' profile has to be taken from a standard specimen which is either different in composition or even made of a different material. A recent example can be found in the paper by O'Holleran, McKinstry and Stubican (1977) where microstrains were determined as a function of composition in the system Al_2O_3–Cr_2O_3 by applying pure Al_2O_3 as a standard specimen. Such a 'non-ideal' standard specimen has a lattice spacing different from that of the specimen under investigation and hence diffracts at a different 2θ-value. This leads to an improper elimination of the broadening due to the X-ray spectrum used. It is the purpose of this paper to show that large errors in the mean square strain values may result and also to propose an easily applicable procedure to correct for such errors.

§ 2. Correction for the difference in spectral broadening

Normally the characteristic K_α-doublet is used. In the case of a 'non-ideal' instrumental profile in a 2θ-range different from that of the line profile

I.8

to be investigated, corrections should be made for the incorrect doublet separation and for the incorrect width of each of the K_α components. The problem of the incorrect doublet separation can be solved by eliminating the α_2-component (e.g. Delhez and Mittemeijer 1975) from both the line profile under investigation and the non-ideal instrumental profile before a deconvolution procedure is applied. If these α_2-eliminations are omitted, considerable errors will arise ; these are not considered in this note.

The correction for the incorrect width of the remaining α_1-profile is performed in the following way. The spectral components of the exact and the measured (non-ideal) instrumental line profiles are denoted by g^s and $g_m{}^s$, respectively. The corresponding Fourier coefficients are $G^s(n)$ and $G_m{}^s(n)$, where n is the harmonic number. Applying the convolution theorem, the following relation between the exact Fourier coefficient $F(n)$ and the approximate one $F_m(n)$ of the pure line profile is obtained :

$$F_m(n)=\frac{G^s(n)}{G_m{}^s(n)}F(n), \tag{1}$$

where it is assumed that the difference in broadening owing to other instrumental conditions is negligible.

The x-axis is defined on a $\sin\theta$ scale and the centroids of the $g^s(x)$ and $g_m{}^s(x)$ profiles are identified with the origin of the x-axis. From the condition $\int g_m{}^s(x)\,dx=\int g^s(x)\,dx$ it follows that

$$g_m{}^s(x)=(1/r)g^s(x/r), \tag{2}$$

where $r=d/d_m$ and d and d_m are the lattice spacings of the ideal and non-ideal standard specimen, respectively. The relation between the corresponding Fourier coefficients is

$$G_m{}^s(n)=G^s(nr). \tag{3}$$

It is generally accepted that the wavelength distribution can be given by (e.g. Klug and Alexander 1974)

$$\{1+4(\lambda-\lambda_c)^2/w^2\}^{-1}, \tag{4}$$

where w is the width at half height and λ_c is the peak wavelength. Combination of (1), (3) and (4) results in

$$F_m(n)=\exp\left[-\frac{\pi nlw(1-r)}{\lambda_c}\right]F(n), \tag{5}$$

where l is the order of the reflection ; all (hkl) reflections can be considered as $(00l)$ ones (Warren 1969).

Following the Warren–Averbach analysis (Warren 1969) the Fourier coefficient $F(n)=A(n)+iB(n)$ of the pure line profile can be written as the product

$$F(n)=A^S(n)F^D(n,l), \tag{6}$$

where $A^S(n)$, the size Fourier coefficient, is real and independent of the order l of the reflection in contrast to the distortion Fourier coefficient $F^D(n,l)=A^D(n,l)+iB^D(n,l)$. The following expression is used for $\ln A^D(n,l)$:

$$\ln A^D(n,l)=-2\pi^2n^2l^2\langle e^2(n)\rangle \tag{7}$$

1.8

where $\langle e^2(n)\rangle$ is the mean-square-strain in the specimen under investigation. If two orders, l_1 and l_2, of a reflection are available $A^{\mathrm{S}}(n)$ and $\langle e^2(n)\rangle$ can be found separately from a plot of ln $A(n, l)$ versus l^2[†].

Defining $F_{\mathrm{m}}(n) = A_{\mathrm{m}}(n) + iB_{\mathrm{m}}(n)$ it follows from (5), (6) and (7) :

$$\ln A_{\mathrm{m}}(n, l) = -\pi nlw(1-r)/\lambda_c + \ln A^{\mathrm{S}}(n) - 2\pi^2 n^2 l^2 \langle e^2(n)\rangle. \tag{8}$$

From (8) it is clear that a plot of ln $A_{\mathrm{m}}(n, l)$ versus l^2 results in inaccurate values of $A^{\mathrm{S}}(n)$ and $\langle e^2(n)\rangle$ because of the spectral term $-\pi nlw(1-r)/\lambda_c$. The correction for the difference in spectral broadening is properly performed by plotting $\ln A_{\mathrm{m}}(n, l) + \pi nlw(1-r)/\lambda_c$ versus l^2. The correction can also be applied to the values of $A_{\mathrm{m}}{}^{\mathrm{S}}(n)$ and $\langle e^2(n)\rangle_{\mathrm{m}}$ that are obtained from the plot of ln $A_{\mathrm{m}}(n, l)$ versus l^2. Application of eqn. (8) gives[‡]

$$\langle e^2(n)\rangle_{\mathrm{m}} - \langle e^2(n)\rangle = \frac{w(1-r)}{2\pi n(l_1 + l_2)\lambda_c}. \tag{9}$$

The errors in mean-square-strain values caused by neglecting the above mentioned correction can be calculated from eqn. (9). As an example we refer to the previously mentioned paper by O'Holleran *et al.* (1977). By application of Al_2O_3 as a standard specimen, these authors found a maximum value of about 10^{-6} at room temperature for the mean-square-strain in the Al_2O_3–Cr_2O_3 system at 70 mol % Cr_2O_3. For this composition $r = d/d_{\mathrm{m}} \simeq 1{\cdot}03$. Using $w = 6 \times 10^{-4}$ Å (Compton and Allison 1935), $\lambda_c = 1{\cdot}54$ Å and $l_2 = 2l_1$ eqn. (9) gives[§]

$$\langle e^2(n)\rangle_{\mathrm{m}} - \langle e^2(n)\rangle = -0{\cdot}6 \times 10^{-6}/nl_1.$$

It should be noted that the Warren–Averbach analysis is accurate only for small values of nl.

Thus, it follows that for the mean-square-strain, relative errors up to 60% ($nl_1 = 1$) are possible irrespective of the error caused by an improper elimination of the doublet separation (important at the larger nl_1 values), which adds to the error calculated.

ACKNOWLEDGMENTS

We are indebted to Ir. R. Delhez for stimulating discussions and to Professor B. Okkerse and Dr. F. W. Schapink for critically reading the manuscript. Financial support of the Stichting voor Fundamenteel Onderzoek der Materie (F.O.M.) is gratefully acknowledged.

[†] Recently Delhez and Mittemeijer (1976) have shown that plotting $A(n, l)$ versus l^2 is more accurate. This difference in procedure does not affect the results presented here.

[‡] A similar expression can be obtained for the particle size Fourier coefficient. It is remarked that the mean particle size, which equals $\{-(dA(n)/dn)|_{n=0}\}^{-1}$, can be corrected directly by use of eqn. (5).

[§] The negative sign of the difference $\langle e^2\rangle_{\mathrm{m}} - \langle e^2\rangle$ implies that the maximum in the microstrain versus composition curve in fig. 1 of the paper by O'Holleran *et al.* (1977) is in fact higher and hence the error estimation above provides support for the conclusions of these authors.

1.8

References

Compton, A. H., and Allison, S. K., 1935, *X-rays in Theory and Experiment* (London : Macmillan), p. 734.

Delhez, R., and Mittemeijer, E. J., 1975, *J. appl. Crystallogr.*, **8**, 609 ; 1976, *Ibid.*, **9**, 233.

Klug, H. P., and Alexander, L. E., 1974, *X-ray Diffraction Procedures for Polycrystalline and Amorphous Materials*, 2nd edition (New York : John Wiley), p. 297.

O'Holleran, T. P., McKinstry, H. A., and Stubican, V. S., 1977, *Phil. Mag.*, **35**, 485.

Stokes, A. R., 1948, *Proc. phys. Soc.*, **61**, 382.

Warren, B. E., 1969, *X-ray Diffraction* (Reading, Massachusetts : Addison-Wesley), p. 264.

THE DETERMINATION OF SIZE AND STRAIN FROM THE ANALYSIS OF X-RAY DIFFRACTION LINE PROFILES USING A NON-IDEAL STANDARD SPECIMEN

by

Th.H. de Keijser and E.J. Mittemeijer

Laboratory of Metallurgy, Delft University of Technology
Rotterdamseweg 137, Delft, The Netherlands

1.9

Abstract

In practice a standard specimen used for the elimination of instrumental broadening, by deconvolution, is never ideal. The instrumental line profile always contains some additional broadening due to finite particle size and distortion present in the standard specimen. Further it is sometimes unavoidable to use a standard specimen of a material different from the material to be analyzed, leading to reflections at incorrect sinθ-values (different spectral broadening). Firstly the effect of these deficiencies on the Fourier coefficients of the pure line profile is analyzed. Secondly the consequences for size-strain analysis are considered.

A correction [eq. (3.4)] for the difference in spectral broadening between the exact and the approximate instrumental line profile is given. To avoid serious errors this correction should be performed before particle size and strain are determined according to the so-called Warren-Averbach analysis. Accurate relative determinations of size and strain are possible even in the case that the line profile under investigation and the line profile of the reference specimen are at different sinθ-values. It is suggested that standard specimens which cause noticeable structural broadening can be used profitably.

1. Introduction

The measured line profile h is the outcome of the folding of the structurally broadened profile f with the instrumental profile g. From the h and g profiles the pure profile f can be obtained by the deconvolution method of Stokes[1]. Because of unavoidable alignment errors[2] the instrumental profile has to be determined experimentally from a so-called standard specimen. With the origin for the g- and h-profiles chosen at the same value of $\sin\theta$ and F, G and H being the Fourier coefficients of the f-, g- and h-profiles respectively, it follows:

$$F(n) = \frac{A}{a}\frac{H(n)}{G(n)} = G(o)\,\frac{H(n)}{G(n)} \qquad (1.1)$$

where n is the harmonic number, A is the integrated intensity and a the period taken for g and h on a $\sin\theta$-scale. The Fourier coefficients F(n) are the basis for the size-strain analysis originally developed by Warren and Averbach[3,4].

Different sources of errors occuring in the Fourier coefficients have been considered in the literature. The errors caused by sampling and truncation of the profile have been treated by Brigham[5] and Young, Gerdes and Wilson[6], while the latter authors also calculated the errors in the Fourier coefficients caused by an inaccurate choice of background. Wilson[7,8,9] considered the influence of counting statistics.

So far little attention has been paid to the errors caused by an approximate instrumental line profile. In principle it is impossible to measure the exact g-profile. At best the "instrumental" profile is recorded from a standard specimen of the same composition that is treated in the same way, as far as possible, as the specimen used for the h-profile. In many cases an "instrumental" profile has to be taken from a standard specimen different in composition[10] or even made of an other material[11]. This leads to instrumental line profiles measured at incorrect θ-values. Furthermore some structural broadening may be present in the instrumental line profile[12].

A solution to the problem of the incorrect θ-value may be obtained by applying the profile fitting method[13]. In this method an instrumental line profile is approximated by a small number of Cauchy-functions. Several instrumental line profiles taken over a large range of θ-values are measured. The parameters for the Cauchy-functions are obtained by fitting. Normally an instrumental line profile is needed at an unmatched θ-value. The parameters necessary for the evaluation in terms of Cauchy-functions of that profile are obtained by interpolation. However, in case of size-strain analysis on the basis of the method developed by Warren and Averbach, which is adopted in our paper, the Fourier coefficients of the pure profile are required. Therefore a direct description in terms of Fourier coefficients is preferable. For the determination of Fourier coefficients of instrumental profiles at unmatched θ-values an analogous interpolation procedure can be followed as for the determination of the parameters of the Cauchy-functions.

Although the above mentioned interpolation procedures are possible methods for size-strain analysis, it should be recognized that these procedures are laborious and still don't give exact results. Moreover any change in the experimental conditions (e.g. slit width, X-ray spectrum[14], absorbtion in the specimen) obliges to measure again the instrumental profiles. This may be the reason that, to our knowledge, no Warren-Averbach analysis on the basis of the profile fitting method has been reported in the literature.

In this paper an alternative, analytical and quick method is proposed to correct for instrumental profiles measured at incorrect θ-values. The method is based on an analytical description of the Kα-doublet. An experimental justification for this description is given. Further the effect of the structural broadening present in the instrumental line profile is analyzed.

2. The effect of an approximate instrumental line profile on the Fourier coefficients of the pure profile

In the approximate instrumental line profile two types of deviations are distinguished:

(i) the physical profile f_o of the standard specimen is not a delta function, but it is (slightly) broadened by strain and finite particle size;

(ii) the instrumental profile g_m is measured at a position on the sinθ-scale different from that of the desired exact instrumental profile g.

In general the approximate instrumental profile is the convolution of f_o and g_m. The Fourier coefficients of the approximate instrumental profile are, according to eq. (1.1), equal to the product of the Fourier coefficients $G_m(n)$ of the function g_m and $F_o(n)$ of the function f_o; where $F_o(n)$ is normalized such that $F_o(o) = 1$.

Taking $G(o) = G_m(o) = 1$ and using eq. (1.1) it follows for the approximate Fourier coefficients of the pure profile which are obtained in practice

$$F_m(n) = \frac{G(n)}{G_m(n)} \frac{F(n)}{F_o(n)} \tag{2.1}$$

In order to find the relation between $F_m(n)$ and $F(n)$, $G(n)$ must be related to $G_m(n)$, which means that $G(n)$ must be known as a function of sinθ.

Recently we proposed the following model for the instrumental profile[15]. The instrumental line profile $g(x)$, with x defined on a sinθ-scale[16], is taken as the sum of the α_1 and α_2 components. The shape and position of the components is related to an instrumental profile $g_c(x)$ intermediate between that of the α_1 and α_2 components. $g_c(x)$ is considered as the convolution of the spectral profile $g_c^s(x)$ of the intermediate wavelength distribution and the profile $g_c^i(x)$ due to the broadening caused by the instrumental conditions. For $g_c^s(x)$ the generally accepted Cauchy wavelength distribution is adopted[2,17]. This leads to

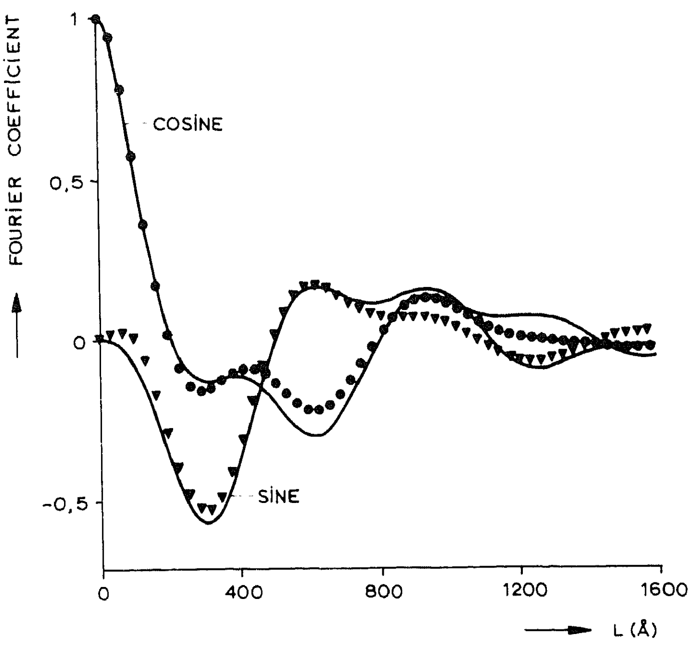

Fig. 1. Calculated and experimental Fourier coefficients as a function of the distance $L = n <\lambda_c>/2a$, *perpendicular to the reflecting planes, for the (444) reflection of silicon recorded with the CuKα doublet. Full lines: the cosine and sine coefficients calculated from eq. (2.2) with* $G_c^i(n) = 1$ *and* $\omega = 6.5 \times 10^{-4}$ Å^{17}.

The symbols ● and ▼ denote the cosine and sine coefficients respectively of the experimental profile. Divergence and receiving slits were 0.5° *and 0.05 mm respectively. Soller slits with* 4° *divergence were used. A standard silicon powder sample [Nat. Bur. of Standards SRM 640] was applied.*

$$G(n) = G_c^i(n) \frac{1}{1+R} [\exp - inR\alpha + R\exp in\alpha]\exp - \frac{\pi n w}{2da} \qquad (2.2)$$

where $G_c^i(n)$ is the Fourier coefficient of $g_c^i(x)$ normalized such that $G_c^i(o) = 1$; $\alpha = \pi\ (<\lambda_2> - <\lambda_1>)/d(1+R)a$ where $<\lambda_1>$ and $<\lambda_2>$ are the centroids of the α_1 and α_2 wavelength distributions respectively, d is the spacing of the reflecting planes and a is the period on a sinθ-scale used for the calculation of the Fourier coefficients; w is the width at half height of the intermediate wavelength distribution $g_c^s(\lambda)$. The centroid of $g_c^s(\lambda)$ is given by $<\lambda_c> = (<\lambda_1> + R<\lambda_2>)/(1+R)$.

In this paper the validity of eq. (2.2) is experimentally verified. It may be assumed that the instrumental broadening of a high angle reflection is entirely due to the X-ray spectrum used[13]. Then $g_c^i(x)$ is a delta-function and $G_c^i(n) = 1$ (the centroid of $g_c^i(x)$ chosen at $x = o$). From Fig. 1 it is concluded that eq. (2.2) gives a proper description of the spectral broadening, in particular for the smaller values of n, which are of interest in size-strain analysis.

$G_m(n)$ is obtained from eq. (2.2) replacing $G_c^i(n)$ by $G_{c,m}^i(n)$ and d by d_m, the spacing of the reflecting planes in the approximate standard specimen.

If d_m is chosen sufficiently close to d it can be shown[15] for the broadening due to the instrumental factors that for not too large n and not too small θ

$$\frac{G_c^i(n)}{G_{c,m}^i(n)} = 1 \qquad (2.3)$$

where the centroids of the g-profile and of the g_m-profile (which are at different sinθ values) are identified with the origin of the x-axis. With eqs. (2.1), (2.2) and (2.3) the Fourier coefficient F(n) of the pure line profile can be calculated.

In the following the consequences for size-strain analysis will be investigated.

3. The effect of an approximate instrumental line profile in size-strain analysis

Following the Warren-Averbach analysis[3,4] the normalized Fourier coefficients $F(n)/F(o)$ of a structurally broadened profile can be written as the product of a "size" Fourier coefficient $A^S(n)$ which is real and independent of the order l of the reflection and a "distortion" Fourier coefficient $F^D(n,l) = A^D(n,l) + i\ B^D(n,l)$.

It should be remarked that in the Warren-Averbach analysis the Fourier series evaluation of the pure (00l) line profile is performed over the range $l-\frac{1}{2}$ to $l+\frac{1}{2}$ of the variable $h_3 = 2a_3 \sin\theta/\langle\lambda_c\rangle$, where a_3 is the spacing of the (00l) planes[18]. In this paper the Fourier analysis is performed on a $\sin\theta$-scale over a range $a = \lambda/2a_3$.

The following expression was given for $A^D(n,l)$

$$\ln A^D(n,l) = -\ 2\pi^2 n^2 l^2 \langle e^2(n)\rangle \qquad (3.1)$$

where $\langle e^2(n)\rangle$ is the mean square strain in the specimen. If (at least) two orders of a reflection are available $A^S(n)$ and $\langle e^2(n)\rangle$ can be found separately from a plot of $\ln A(n,l)$ versus l^2. Recently Delhez and Mittemeijer[19] have shown that plotting $A(n,l)$ versus l^2 is more accurate. The relations between measured and true values for particle size and mean square strain and the conclusions presented in this paper are the same for both methods of separation.

By power series expansion the term in brackets of eq. (2.2) can be approximated:

$$[\exp - in R\alpha + R \exp in\alpha] \approx (1+R)\ [1 - n^2 R\alpha^2/2] \qquad (3.2)$$

Thus, within the approximation used, this factor is real.

Assuming the sine coefficients $B^D_o(n,l)$ of the standard specimen to be zero and using the relations $d = a_3/l$ and $2aa_3 = <\lambda_c>$ one obtains from eqs. (2.1), (2.2) and (2.3) with eq. (3.2)

$$A_m(n,l) = \frac{A^S(n)}{A^S_o(n)} \frac{A^D(n,l)}{A^D_o(n,l)} \exp - \frac{\pi n l w(1-r)}{<\lambda_c>} \frac{1-n^2l^2\beta}{1-n^2l^2r^2\beta} \qquad (3.3)$$

where $\beta = 2\pi^2(<\lambda_2> - <\lambda_1>)^2R/(1+R)^2<\lambda_c>^2$ and $r = d/d_m$. From eq. (3.3) it is clear that a plot of $\ln A_m(n,l)$ versus l^2 does not result in a determination of $A^S(n)/A^S_o(n)$ and $A^D(n,l)/A^D_o(n,l)$ separately, because of the factor $\exp - \frac{\pi n l w(1-r)}{<\lambda_c>}$. Since all quantities in the last two factors of eq. (3.3) are known a corrected Fourier coefficient can be defined

$$A^{corr}_m(n,l) = A_m(n,l) \quad \exp \frac{\pi n l w(1-r)}{<\lambda_c>} \frac{1-n^2l^2r^2\beta}{1-n^2l^2\beta} \qquad (3.4)$$

Using eq. (3.1), from eqs. (3.3) and (3.4) it is obtained

$$\ln A^{corr}_m(n,l) = \ln \frac{A^S(n)}{A^S_o(n)} - 2\pi^2n^2l^2 \; [<e^2(n)> - <e^2_o(n)>] \qquad (3.5)$$

where $<e^2_o(n)>$ is the mean square strain in the standard specimen. Following Delhez and Mittemeijer[19] the expression (3.5) should be replaced by

$$A^{corr}_m(n,l) = \frac{A^S(n)}{A^S_o(n)} - \frac{A^S(n)}{A^S_o(n)} \, 2\pi^2n^2l^2 \; [<e^2(n)> - <e^2_o(n)>] \qquad (3.6)$$

A plot of $\ln A^{corr}_m(n,l)$ versus l^2[eq. (3.5)] and a plot of $A^{corr}_m(n,l)$ versus l^2 [eq. (3.6)] both yield

$$A_m^S(n) = A^S(n)/A_o^S(n) \tag{3.7}$$ [20]

and $$\langle e_m^2(n)\rangle = \langle e^2(n)\rangle - \langle e_o^2(n)\rangle \tag{3.8}$$

The mean particle size and the particle size distribution may be obtained from eq. (3.7)[3]. N_3, the mean particle size expressed in units a_3, is obtained from $dA^S(n)/dn$ (for $n \to o$) $= -1/N_3$. Then the relation between the measured particle size $N_{3,m}$, the true particle size N_3 and the particle size $N_{3,0}$ of the standard specimen follows from (3.7)

$$(N_{3,m})^{-1} = (N_3)^{-1} - (N_{3,0})^{-1} \tag{3.9}$$

In an X-ray diffraction study of deformation in Ag-Si alloys by Zemitis, Kidron and Cohen[21] formulae related to eq. (3.8) and eq. (3.9) were used. These equations were applied for relative determinations. From the treatment given in this paper it may be concluded that accurate relative determinations using eqs. (3.8) and (3.9) are possible even in the case that the line profile under investigation and the line profile of the reference specimen are at different sinθ-values, provided the correction implied by eq. (3.4) has been performed. Furthermore from these relations the accuracy of size-strain analysis can be estimated.

If the corrections implied by eq. (3.4) and eqs. (3.8) and (3.9) are ignored errors in the values calculated for particle size and mean square strain will occur. Especially the accuracy of the mean square strain determined is heavily affected. A preliminary calculation already showed errors in the order of 50% to be possible[22]. In that calculation only the difference between the widths (w) of the spectral components of ideal and approximate instrumental profile were taken into account. In this paper also the influence of the difference in doublet separation between ideal and approximate instrumental profile and the influence of structural broadening by the standard specimen is considered. From the complete equations it follows that the error mentioned can be even larger.

From eq. (3.3) it follows

$$\left.\frac{dA_m(n,1)}{dn}\right|_{n\to 0} = -\frac{1}{N_{3,m}} - \frac{\pi l w(1-r)}{\langle\lambda_c\rangle} \qquad (3.10)$$

which means that $N_{3,m}$ can be determinated directly from the $A_m(n,1)$ values. Omittance of the spectral term in eq. (3.10) produces errors of a few percent in the value calculated for the particle size.

Finally, because determinations of particle size and strain can be performed independently of distortion [eq. (3.9)] and particle size [eq. (3.8)] in the standard specimen, it might be suggested that, for example with a view to extinction problems, for the determination of particle size a sligthly deformed standard specimen should be used and for the determination of distortion colloids as a standard specimen should be used.

Acknowledgements

We are grateful to Ir. R. Delhez for stimulating discussions and for supplying the Si (444) profile. Professor B. Okkerse and Dr. F.W. Schapink critically read the manuscript.

Financial support of the Stichting voor Fundamenteel Onderzoek der Materie (F.O.M.) is gratefully acknowledged.

I.9

References and footnotes

1. A.R. Stokes, Proc.Phys.Soc. London 61, 382 (1948).
2. H.P. Klug and L.E. Alexander, X-ray Diffraction Procedures (John Wiley and Sons, New York, 1974), pp 295 ff.
3. B.E. Warren and B.L. Averbach, J.Appl.Phys. 21, 595 (1950).
4. B.E. Warren and B.L. Averbach, J.Appl.Phys. 23, 497 (1952).
5. E.O. Brigham, The Fast Fourier Transform (Prentice Hall, Englewood Cliffs. New Yersey, 1974), pp. 91 ff.
6. R.A. Young, R.J. Gerdes and A.J.C. Wilson, Acta Cryst. 22, 15 (1966).
7. A.J.C. Wilson, Acta Cryst. 23, 888 (1967).
8. A.J.C. Wilson, Acta Cryst. A24, 478 (1968).
9. A.J.C. Wilson, Acta Cryst. A25, 584 (1969).
10. T.P. O'Holleran, H.A. McKinstry and V.S. Stubican, Phil.Mag. 35, 485 (1977).
11. N.C. Halder and E.E. Johnston, Z.Naturforsch. 30a, 825 (1975).
12. J.P. Urban, J.Appl.Cryst. 8, 459 (1975).
13. T.C. Huang and W. Parrish, Appl.Phys. Letters 27, 123 (1975).
14. Assuming that a high angle reflection of a standard specimen is broadened only by the X-ray spectrum used[13], a high angle reflection has to be measured again with change of X-ray spectrum.
15. R. Delhez, Th.H. de Keijser and E.J. Mittemeijer, J.Phys.E: Sci. Instrum, in the press.
16. R. Delhez and E.J. Mittemeijer, J.Appl.Cryst. 8, 609 (1975).
17. A.H. Compton and S.K. Allison, X-rays in Theory and Experiment (MacMillan, London, 1935).
18. All (hkl) reflections can be considered as (00l) ones: A.R. Stokes and A.J.C. Wilson, Proc. Cambridge Philos. Soc. 40, 147 (1944); B.E. Warren, Acta Cryst. 8, 483 (1955).
19. R. Delhez and E.J. Mittemeijer, J.Appl.Cryst. 9, 233 (1976).

20. For an ideal standard specimen $A_o^S(n) = 1$ [infinite particle size] for all n. In practice the standard specimen has a large, however finite, particle size $N_{3,0}$. Hence $A_o^S(n)$ tends to zero at large n. Combined with the effect of counting statistics this may be responsible [c.f. eq. (3.7)] for the large spurious ripples in the Fourier coefficients of a deconvoluted line profile at large n ($n > N_{3,0}$).
21. M.A. Zemitis, A. Kidron and J.B. Cohen, Scripta Met. 6, 875 (1972).
22. Th.H. de Keijser and E.J. Mittemeijer, Phil.Mag. 36, 1261 (1977).

II

Analysis of X-ray Diffraction Line Broadening of Specimens with Concentration Variations

The broadening of X-ray diffraction line profiles is analysed for three types of specimens containing concentration variations:

- powder samples where the concentration variation occurs within coherently diffracting crystallites or domains;
- powder blends where the concentration variations occur across the contact places of the particles (each particle consists of a number of crystallites or domains);
- monocrystals where the concentration variation extends over many coherently diffracting domains.

11.10

A note on the kinematical theory of x-ray diffraction from concentration profiles

E. J. Mittemeijer and R. Delhez

Laboratory of Metallurgy, Delft University of Technology, Rotterdamseweg 137 Delft, The Netherlands

(Received 14 November 1975)

A note is presented on the kinematical theory of x-ray diffraction from a diffusion zone in a monocrystalline system as given by Houska. Assuming a linear variation of spacing in a coherently diffracting domain it is possible to simplify the treatment of diffraction from a diffusion zone by definition of one factor which characterizes the shape of the intensity function. This treatment may have special importance for certain types of powder samples in which the same concentration profile is present in each particle.

PACS numbers: 61.10.D, 61.70.W

A theoretical treatment of diffraction from a diffusion zone in a monocrystalline system has been given by Houska.[1] He discusses the two cases of a very small domain and of a large domain and he considers the shape of the intensity function in each case. It will be shown here that the treatment of diffraction from a diffusion zone may be simplified defining a single factor which characterizes the shape of the intensity function for all cases including those of Houska. This may be useful for certain types of powder samples.

Applying the well-known Warren-Averbach theory[2] we arrive at the following Fourier series for the diffracted intensity of a coherently diffracting domain in which a lattice spacing variation due to a concentration profile is present:

$$P(h_3)=C\sum_{n=-(N_3-1)}^{N_3-1}F(n)\exp(2\pi inh_3),\qquad(1)$$

where

$$F(n)=\sum_{m_3=0}^{N_3-1-|n|}\exp[2\pi i(\Delta_{m_3+n}-\Delta_{m_3})l].\qquad(2)$$

Orthorhombic axis have been used, which transform reflections of (hkl) type into $(00l)$ type.[3] The reciprocal lattice vector is defined by $h_3\mathbf{b}_3$, where $|\mathbf{b}_3|=1/|\langle\mathbf{a}_3\rangle|$. The number of diffracting lattice planes is N_3. The displacement of the lattice plane m_3 from its reference position $m_3\langle\mathbf{a}_3\rangle$ is $\Delta_{m_3}\langle\mathbf{a}_3\rangle$. The quantity C is not of interest here. If it is assumed that the interplanar spacing increases linearly—with the fraction δ—from $\mathbf{a}_3$ up to $(N_3-2)\delta\mathbf{a}_3+\mathbf{a}_3$, we obtain after some calculations for the Fourier coefficient $F(n)$:

$$F(n)=\sin\pi\delta nl(N_3-|n|)/\sin\pi\delta nl.\qquad(3)$$

In this case "long-range" displacements exist, unlike in the case of Warren's strain broadening. Similar expressions for $F(n)$ have been obtained by Borie[4] and Houska.[1]

In practice the sine in the denominator of $F(n)$ may always be approximated by its argument. The replacement of the summation in Eq. (1) by an integration is justified in practice too. Hence it follows for the diffracted intensity $(N_3-1\approx N_3)$:

$$P(h_3)=C\int_{-N_3}^{N_3}\frac{\sin\pi\delta nl(N_3-|n|)}{\pi\delta nl}\exp(2\pi inh_3)\,dn.\qquad(4)$$

By definition of the factor $S=\delta lN_3^2$ and a replacement of variable n by $x=n/N_3$ Eq. (4) can be rewritten

$$P(h_3)=CN_3^2\int_{-1}^{1}\frac{\sin\pi Sx(1-|x|)}{\pi Sx}\exp[2\pi ix(N_3h_3)]\,dx.\qquad(5)$$

We now introduce the notion of comparable graphs for the shape of the intensity function of a particle with lattice spacing variations. As is well known, the intensity function of a particle without lattice spacing variation is given by $C\sin^2\pi N_3h_3/\sin^2\pi h_3$ having an absolute maximum proportional to N_3^2 and a width proportional to N_3^{-1}. Let us define a function which characterizes—independent of the total amount of diffracting material—the shape of the intensity function of a particle without lattice spacing variation. This can be realized by dividing the intensity values by CN_3^2 and multiplying the variable h_3 by N_3. In a similar way the intensity function of a particle with lattice spacing variations is normalized. We then obtain

$$P^n(h_3^n)=\int_{-1}^{1}\frac{\sin\pi Sx(1-|x|)}{\pi Sx}\exp(2\pi ixh_3^n)\,dx,\qquad(6)$$

where $P^n(h_3^n)=P(h_3)/CN_3^2$ with $h_3^n=h_3N_3$.

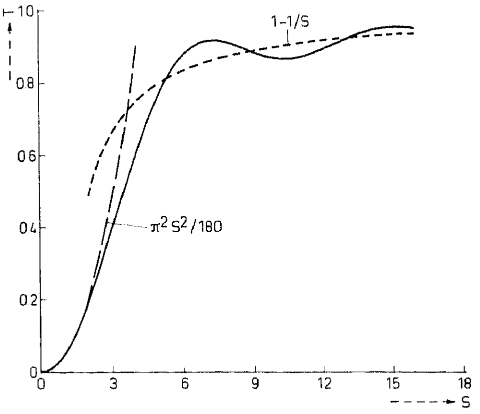

FIG. 1. The decrease in top intensity T versus the shape factor S.

Houska investigated the case of small domains, where particle size broadening dominates, and the case of large domains, where lattice spacing variation broadening dominates. However, the shape of the normalized diffraction profile is only adequately described by combination of δ, l and N_3 in the factor $S = \delta l N_3^2$, which characterizes the intensity function for all cases including those of Houska.

It is possible to give a simple description of the diffraction profile of a particle with lattice spacing variations. We define $T = 1 - P^n(h_3^n = lN_3)$, which represents the decrease in top intensity of the normalized intensity function. The relation $T = f(S)$ was computed and is shown in Fig. 1. From Fig. 1 it follows that for small values of S ($S < 1.5$) T is a parabolic function of S [a series expansion of Eq. (6) results in $T \approx \pi^2 S^2/180$]. Since T is small in this region of S, the shape of the profile is approximately the ideal one. For larger values of S ($2 < S < 4.5$) T varies linearly with S. In this region the subsidiary maxima rise at the cost of the originally absolute maximum at $h_3 = l$. We did not succeed in deriving a simple analytical expression for the approximate linear dependency of T as a function of S. In the last region ($S > 6$) T varies approximately inversely proportional to S [$T \approx 1 - 1/S$; see Eqs. (7)—(11)]. In this region the profile has approximately a rectangular shape [cf. Fig. 3(c) of Houska[1]].

Recently Wagendristel and Wolf[5] determined concentration profiles in CuNi-powder samples applying x-ray diffraction. Applying their technique it should be possible to examine powder samples where the same concentration profile is present in each coherently diffracting particle. Such powder samples may be obtained by the method of Kulifay,[6] also applied by Dessing[7] in preparing AuPt catalysts. The diffraction profiles of these powder samples may be described by the shape factor S as has been done in Fig. 1.

The authors are indebted to Professor H.J.A. Duparc, Professor B. Okkerse, and Dr. F.W. Schapink for helpful discussions on the manuscript. Financial support of the "Stichting voor Fundamenteel Onderzoek der Materie (F.O.M.)", is gratefully acknowledged.

Defining $\mathbf{a}_3$ and $\mathbf{a}_3^l$ as the two outermost interplanar spacings present, it follows for the difference $\Delta\mathbf{a} = \mathbf{a}_3^l - \mathbf{a}_3$ that

$$\Delta\mathbf{a} = (N_3 - 2)\delta\mathbf{a}_3 \approx N_3\delta\mathbf{a}_3. \quad (7)$$

The distance $|\Delta\mathbf{H}| = \Delta h_3 |\mathbf{b}_3|$ along the reciprocal lattice vector, where in the case of a (001)-reflection intensity can be found, conforms to

$$|\Delta\mathbf{H}| = \Delta h_3 |\mathbf{b}_3| = l(1/|\mathbf{a}_3| - 1/|\mathbf{a}_3^l|). \quad (8)$$

Using Eqs. (7) and (8) it is found for the shape factor $S = \delta l N_3^2$ that

$$S = \Delta h_3 N_3 |\mathbf{a}_3^l| / |\langle\mathbf{a}_3\rangle|. \quad (9)$$

Because the diffraction profile is of rectangular shape and the integrated intensity equals the constant CN_3, it follows for the top intensity of the normalized diffraction profile that

$$P^n(h_3^n = lN_3) = CN_3/\Delta h_3 C N_3^2 = 1/\Delta h_3 N_3. \quad (10)$$

Applying Eqs. (9) and (10) it is finally found that

$$T = 1 - P^n(h_3^n = lN_3) = 1 - |\mathbf{a}_3^l| / |\langle\mathbf{a}_3\rangle| S \approx 1 - 1/S. \quad (11)$$

---

[1] C.R. Houska, J. Appl. Phys. 41, 69 (1970).

[2] B.E. Warren, *X-Ray Diffraction* (Addison-Wesley, Reading, Mass., 1969), pp. 264ff.

[3] A.R. Stokes and A.J.C. Wilson, Proc. Cambridge Philos. Soc. 40, 197 (1944).

[4] B. Borie, Acta Crystallogr. 13, 452 (1960).

[5] A. Wagendristel and D. Wolf, Z. Metallkd. 65, 660 (1974).

[6] S.M. Kulifay, J. Am. Chem. Soc. 83, 4916 (1961).

[7] R.P. Dessing, thesis (University of Leiden, 1974) (unpublished).

CONCENTRATION VARIATIONS WITHIN SMALL CRYSTALLITES STUDIED BY X-RAY DIFFRACTION LINE PROFILE ANALYSIS

by

E.J. Mittemeijer and R. Delhez

Laboratory of Metallurgy, Delft University of Technology,
Rotterdamseweg 137, Delft, The Netherlands.

II.11

Abstract

An analysis is given of the X-ray diffraction line broadening caused by concentration variations occurring within coherently diffracting crystallites. The sine Fourier coefficients of the line profile are employed. The method is applied to sintered and unsintered AuPt alloy catalysts. In the interior of the crystallites of the sintered specimen the concentration maintained a constant value which very well agreed with the average composition. The surface region was enriched by gold, in agreement with experimental results from other methods and with theoretical predictions. Concentration variations in the unsintered specimen were much larger. The crystallites consisted of a platinum-rich nucleus surrounded by a gold-rich shell as may be expected from the preparation method (chemical reduction of platinum and gold ions in solution). In addition a method for correction of the "hook"-effect in line profile analysis is suggested.

1. Introduction

Concentration variations correspond to lattice parameter variations and - according to Bragg's law - may therefore be analyzed by X-ray diffraction. Such analyses were made for concentration variations occurring over distances many times larger than the dimensions of the coherently diffracting domains or crystallites [e.g. refs. 1 and 2]. To our knowledge until now no X-ray diffraction investigation of concentration variations occurring within the crystallites has been carried out.

It is well known that deviations from the average composition can occur in alloy catalysts. The concentration inhomogeneity is localized within the crystallites because significant variations of composition on a macroscale can usually be dismissed[3].

The purpose of this paper is to present a method for the analysis of X-ray diffraction line broadening caused by concentration variations within crystallites. The method will be applied to AuPt alloy catalysts.

2. Theory[4]

Particle size, cold work and concentration variations contribute to the X-ray diffraction line broadening. In this paper spacing changes due to concentration variations are considered only. The presence of strain from another origin is not considered, which is justified for alloy catalysts. Further the composition dependence of the structure factor is not taken into account. This is no serious limitation, since in many cases the structure factors are approximately equal and/or the concentration variation usually covers only a part of the possible composition range.

Recently the kinematical theory of X-ray diffraction from a crystallite with a linear concentration profile has been developed[5,6]. Non-linear concentration profiles will be dealt with below.

Applying the well-known Warren-Averbach theory[7] the following Fourier series is obtained[6] for the diffracted intensity of a binary A/B crystallite in which a lattice spacing variation due to a concentration profile is present:

$$P(h_3) = C \sum_{n=-(N_3-1)}^{N_3-1} F(n)\exp 2\pi i n h_3 \quad , \qquad (1)$$

where

$$F(n) = \sum_{m_3=0}^{N_3-1-|n|} \exp 2\pi i \; S_c(m_3,n) \qquad (2)$$

with

$$S_c(m_3,n) = \begin{cases} \Delta_{m_3+|n|}-\Delta_{m_3} & \text{for } n \geq 0 \\ \Delta_{m_3}-\Delta_{m_3+|n|} & \text{for } n \leq 0 \end{cases} \quad .$$

In the following only positive values of the harmonic number n will be considered. The quantity C comprises the usual angle dependent factors[7,8]. Orthorhombic axes have been used, which transform reflections of (hkl) type into (00l) type[9]. The reciprocal lattice vector is defined by $h_3 \; \underline{b}_B$ where $\underline{a}_B . \underline{b}_B = 1$ ($\underline{a}_A$ and $\underline{a}_B$ are the 00l spacings of the pure components A and B respectively). The number of diffracting lattice planes is N_3. The displacement of lattice plane m_3 from its reference position $m_3 \underline{a}_B$ is $\Delta_{m_3} \; \underline{a}_B$. In this case "long-range" displacements exist unlike in the case of Warren's strain broadening.

By denoting $c_{A,k}$ as the atomic fraction of component A in the k-th lattice plane and using Végard's law, which is valid for most binary systems[10], it follows

$$S_c(m_3,n) = \delta_a \sum_{k=m_3+1}^{m_3+n} c_{A,k} \quad , \qquad (3)$$

where $\delta_a = (|\underline{a}_A| - |\underline{a}_B|)/|\underline{a}_B|$.

The Fourier coefficient $F(n) = A(n) + iB(n)$ [eq. (2)] can be written as the product

$$F(n) = A^S(n)F^C(n,l) \quad , \tag{4}$$

where $A^S(n) = N_n/N_3$ (5)

and $F^C(n,l) = \langle \exp 2\pi i l\; S_c(m_3,n) \rangle$. (6)

$A^S(n)$, the "size" Fourier coefficient, is real and independent of the order l of the reflection in contrast to the "concentration" Fourier coefficient $F^C(n,l) = A^C(n,l) + iB^C(n,l)$. N_n denotes the number of pairs of lattice planes a distance n planes apart. The average in eq. (6) is the average over such pairs.

$F^C(n,l)$ is approximated for small values of n [c.f. eq. (3)] by

$$F^C(n,l) = 1 + 2\pi i l < S_c(m_3,n) > -2\pi^2 l^2 < S_c(m_3,n)^2 > \tag{7}$$

and thus $A(n,l) = A^S(n) - A^S(n)2\pi^2 l^2 < S_c(m_3,n)^2 >$ (8)

and $B(n,l) = A^S(n)2\pi l < S_c(m_3,n) >$ (9)

Eq. (9) makes evident that the presence of concentration variations within crystallites gives rise to non-zero sine Fourier coefficients indicating asymmetrical line broadening.

Obviously investigation of $\langle S_c(m_3,n) \rangle$ is more easily done than of $\langle S_c(m_3,n)^2 \rangle$. Therefore in the following it is attempted to obtain information on the concentration profile from the sine Fourier coefficients B(n,l) of the line profile.

Use of eq. (9) necessitates knowledge of the "particle size" Fourier coefficient $A^S(n)$: If two orders, l_1 and l_2, of a reflection are available values of $A^S(n)$ [and $\langle S_c(m_3,n)^2\rangle$] are obtained by plotting A(n,l) versus l^2[c.f. eq. (8) and see also ref. 11]. The particle size N_3 follows from $\{-(dA^S(n)/dn)|_{n\downarrow o}\}^{-1}$.

$\langle S_c(m_3,n)\rangle$ can be rewritten

$$\langle S_c(m_3,n)\rangle = \frac{1}{N_3-n}\sum_{m_3=o}^{N_3-1-n}(\Delta_{m_3+n}-\Delta_{m_3}) = \frac{1}{N_3-n}\sum_{m_3=o}^{n-1}(\Delta_{N_3-1-m_3}-\Delta_{m_3}) \; . \tag{10}$$

We shall restrict ourselves to symmetrical concentration profiles, which condition is usually met in practice. Then

$$\Delta_{N_3-1-m_3} = \delta_a N_3 \bar{c} - \Delta_{m_3-1} \tag{11}$$

where $\bar{c}$ is the known average composition of the crystallite. Substitution of eq. (11) into eq. (10) leads to

$$\langle S_c(m_3,n)\rangle = \frac{1}{N_3-n}\{n\,\delta_a N_3 \bar{c} - f(n)\} \tag{12}$$

where $$f(n) = \Delta_{n-1} + 2\sum_{k=o}^{n-2}\Delta_k \; . \tag{13}$$

Combination of eqs. (9) and (12) finally results in

$$f(n) = n\,\delta_a N_3 \bar{c} - \frac{B(n,l)}{A^S(n)}\,\frac{N_3-n}{2\pi l} \; . \tag{14}$$

All factors at the right hand side of eq. (14) are known. Hence f(n) can be calculated for successive values of n (n = 1,2...). Then, as follows from eq. (13), the Δ_n values (n = 0,1,2,....) can be calculated from the f(n) values applying the recursive equation

$$\Delta_n = f(n+1) - f(n) - \Delta_{n-1} \tag{15}$$

Because $\Delta_n = \delta_a \sum_{k=o}^{n} c_{A,k}$ [c.f. eq. (3)] also $\sum_{k=o}^{n} c_{A,k}$ can be calculated, implying the determination of the concentration profile. It should be noted that the above derivation only holds for not too large values of n [c.f. eq. (7) and section 4].

3. Experimental procedure

Supported AuPt catalysts were prepared by adding a solution of gold and platinum chlorides in aqua regia to a suspension of silica in a hydrazine solution at ± 80°C according to Kulifay[12,13]. The powders were sintered in a H_2 atmosphere during 15 h at 400°C.

The 200 en 400 CuKα line profiles were measured in steps of $1\text{-}3.10^{-2}$ °2θ applying the preset-time method with a Siemens ω-diffractometer equipped with a graphite monochromator. Background radiation was removed by linear interpolation. The α_2-component was eliminated according to Delhez and Mittemeijer[14]. The deconvolution method of Stokes[15] was applied using a Au standard powder sample. The difference in spectral broadening between the Au standard powder sample and the AuPt powder samples investigated was taken into account according to de Keijser and Mittemeijer[16]. The angle dependence of the Lorentz and polarization factors was corrected for corresponding to the rules set out in ref. 17.

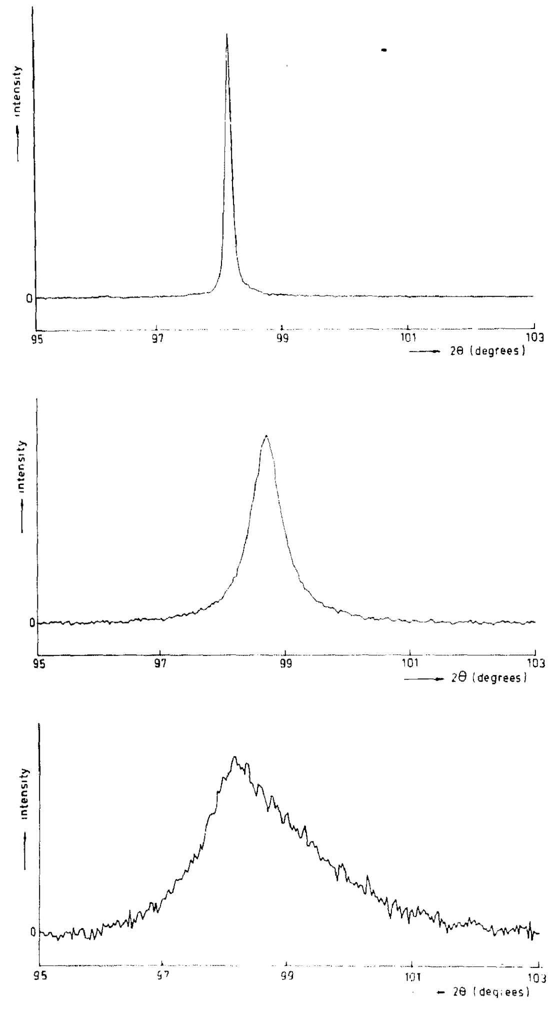

Fig. 1. 400 α_1-line profiles of the Au standard powder sample (a), the sintered AuPt [9 at% Pt] powder specimen (b) and the unsintered AuPt [14 at% Pt] powder specimen (c).

4. Results and discussion

The Figs. 1a, b and c show the 400 α_1-line profiles of the Au standard powder sample, a sintered AuPt catalyst (9 at% Pt) and an unsintered AuPt catalyst (14 at% Pt) respectively. It is seen that both AuPt specimens give rise to considerable line broadening. In the sintered specimen no large concentration variations within the crystallites are expected. The line profile should then be mainly symmetrically broadened due to small particle size, as is observed. The line profile of the unsintered specimen is substantially asymmetrically broadened which is indicative [c.f. eq. (9)] of considerable concentration variations.

On the basis of eq. (14) f(n) values can be calculated. It can be easily shown that theoretically $\{f(n)/n\}|_{n\downarrow o} = o$. From the example shown in Fig. 2 it follows that this is not observed in practice. This is attributed to the so-called "hook"-effect[8,18]. The first cosine Fourier coefficient A_o of the measured line profile, which is used for normalization of all Fourier coefficients F(n), is usually determined too small. This defect is often ascribed to a background level estimated too high owing to overlapping of long tails of neighbouring reflections. The usual method of correction for the "hook"-effect consists of extrapolating the straight portion of the cosine Fourier coefficient curve at small values of n to n = o[8]. This method is often invalidated because of the absence of such a straight portion.

If B'(n,l) and B(n,l) denote the sine Fourier coefficients obtained by normalization with the erronous A_o' and the correct A_o values respectively, it follows

$$B'(n,l) = \frac{A_o}{A_o'} B(n,l) \quad . \tag{16}$$

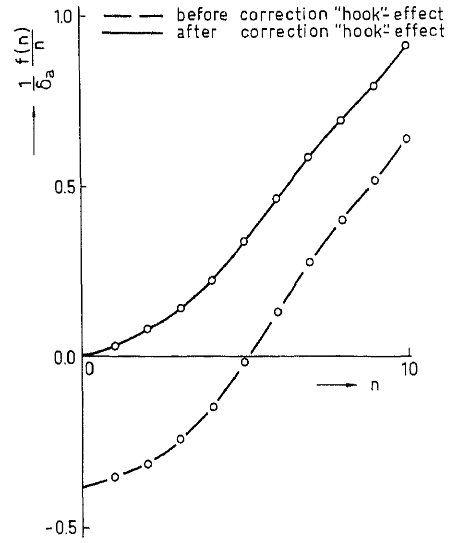

Fig. 2. *$\{f(n)/n\}/\delta_a$ versus n as obtained from the deconvoluted 200 line profile of the sintered AuPt specimen before (dashed curve) and after (bold curve) correction of the "hook"-effect [δ_a is a constant; c.f. eq. (3)].*

From eqs. (14) and (16) it is then obtained

$$\frac{f(n)}{n}\Big|_{n\downarrow o} = \delta_a N_3 \bar{c}\,(1 - \frac{A_o}{A'_o}). \tag{17}$$

Hence from the intercept of the ordinate the correct A_o value can be deduced. The f(n)/n values after the correction for the "hook"-effect are also shown in Fig. 2. It is suggested that the method based on eq. (17), which also holds if no concentration variations are present at all, may be a useful alternative for the usual correction for the "hook"-effect.

After carrying out the correction for the "hook"-effect according to eq. (17) the "integrated" concentration profile $|\underline{a}_3| \cdot \sum_{k=o}^{n} c_{Pt,k}$ was recursively calculated from the f(n)-values by applying eq. (15) [$\underline{a}_3$ is the fictituous unit cell parameter perpendicular to the reflecting planes: c.f. ref. 8]. The results for the sintered and unsintered specimens are shown in Figs. 3a and b. The concentration profiles calculated from the $|\underline{a}_3| \cdot \sum_{k=o}^{n} c_{Pt,k}$ data are shown in Figs. 4a and b.

For the calculation of the concentration profiles the 200 line profiles were employed instead of the 400 line profiles because of the higher counting accuracy attained. Using eq. (8), from both orders of the reflection the particle sizes were calculated to be 137 Å and 60 Å for the sintered and unsintered specimen respectively.

The results for the sintered specimen [Figs. 3a and 4a] show that in the interior of the crystallite the concentration maintains a constant value of 9 at% Pt, which agrees very well with the average composition. In the surface region enrichment by gold is observed. This is in agreement with Auger electron spectroscopical[19] and hydrogen adsorbtion[20] data. The enrichment of the surface region by the component with the lower heat of sublimation (i.e. gold) was also theoretically predicted[21,22].

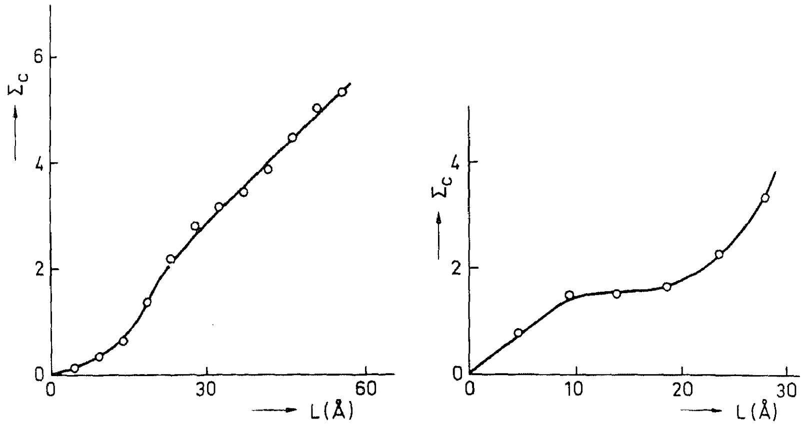

Fig. 3. The "integrated" concentration $\sum_c$ [= $|\underline{a}_3| \cdot \sum_{k=0}^{n} c_{Pt}$, *where* c_{Pt} *is the atomic fraction platinum and* $\underline{a}_3$ *is the fictituous unit cell parameter perpendicular to the reflecting planes*] *versus the distance L perpendicular to the reflecting planes for the sintered (a) and unsintered specimen (b).*

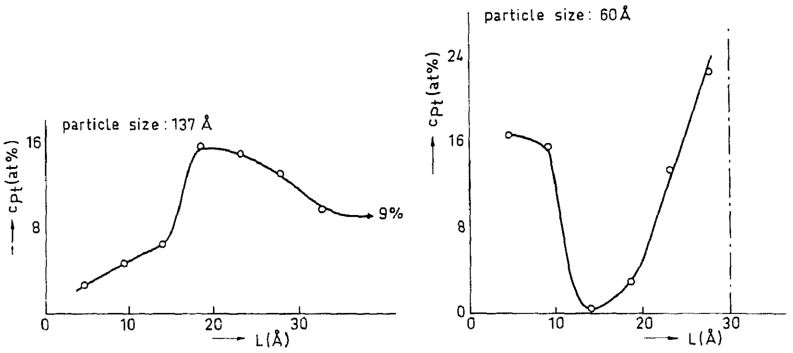

Fig. 4. The atomic fraction platinum c_{Pt} *versus the distance L perpendicular to the reflecting planes for the sintered (a) and unsintered specimen (b).*

The results for the unsintered specimen [Figs. 3b and 4b] show that the concentration variations are much larger than in the sintered specimen. For those concentration variations neither other experimental data nor theoretical predictions exist. Since the specimens are prepared by chemical reduction [c.f. section 3], it may be expected that the nucleus of the crystallite should be platinum-rich, surrounded by a gold-rich shell. This corresponds with the experimental observation. The platinum-enrichment of the surface, as compared to the average composition, is not understood at present. Although in our opinion this feature is no artifact of the measurements, it is noted that the X-ray data for the unsintered specimen were less accurate owing to a lower counting accuracy arising from the extremely broadened nature of the line profile [c.f. Fig. 1].

Finally it is remarked that for the specimens investigated the average concentration as determined from the concentration profile calculated equalled the value expected from specimen preparation.

Acknowledgements

The authors are very much indebted to Dr. Th.H. de Keijser and to Ir. P. Sonneveld of the Mathematics Department for supporting discussions. The stimulation by Dr. V. Ponec and Drs. F.J. Kuijers of the University of Leiden is gratefully recognized. Drs. F.J. Kuijers also prepared the AuPt alloy catalysts.

Professor B. Okkerse and Dr. F.W. Schapink critically read the manuscript.

Financial support of the Stichting voor Fundamenteel Onderzoek der Materie (FOM) is gratefully acknowledged.

II.11

References and footnotes

1. J.A. Carpenter, D.R. Tenney and C.R. Houska, J. Appl. Phys. 42, 4305 (1971).
2. R. Delhez, E.J. Mittemeijer and E.A. van den Bergen, J.Mat.Sci., in the press.
3. R.L. Moss, D. Pope and H.R. Gibbens, J. Catal. 46, 204 (1977).
4. by E.J. Mittemeijer.
5. C.R. Houska, J. Appl. Phys. 41, 69 (1970).
6. E.J. Mittemeijer and R. Delhez, J. Appl. Phys. 47, 1702 (1976).
7. B.E. Warren and B.L. Averbach, J. Appl. Phys. 21, 595 (1950).
8. B.E. Warren, X-ray Diffraction (Addison-Wesley, Reading, Mass., 1969), pp. 264 ff.
9. A.R. Stokes and A.J.C. Wilson, Proc. Cambridge Philos. Soc. 40, 197 (1944).
10. More complicated composition - lattice parameter dependencies can be dealt with analogously.
11. R. Delhez and E.J. Mittemeijer, J. Appl. Cryst. 9, 233 (1976).
12. S.M. Kulifay, J. Am. Chem. Soc. 83, 4916 (1961).
13. R.P. Dessing, thesis University of Leiden (1974).
14. R. Delhez and E.J. Mittemeijer, J. Appl. Cryst. 8, 609 (1975).
15. A.R. Stokes, Proc. Phys. Soc. 61, 382 (1948).
16. Th.H. de Keijser and E.J. Mittemeijer, Phil. Mag. 36, 1261 (1977).
17. R. Delhez, E.J. Mittemeijer, Th.H. de Keijser and H.C.F. Rozendaal, J. of Physics E 10, 784 (1977).
18. R.A. Young, R.J. Gerdes and A.J.C. Wilson, Acta Cryst. 22, 155 (1967).
19. F.J. Kuijers, personal communication (1977).
20. F.J. Kuijers, R.P. Dessing and W.M.H. Sachtler, J. Catal. 33, 316 (1974).
21. J.L. Meijering, Acta Met. 14, 251 (1966).
22. F.L. Williams and D. Nason, Surface Sci. 45, 377 (1974).

X-RAY DIFFRACTION LINE PROFILE ANALYSIS OF DIFFUSIONAL HOMOGENIZATION IN POWDER BLENDS

by

R. Delhez, E.J. Mittemeijer and E.A. van den Bergen

Laboratory of Metallurgy, Delft University of Technology,
Rotterdamseweg 137, Delft, The Netherlands.

Accepted for publication in Journal of Materials Science.

II.12

Abstract

A new nondestructive method - based on computer simulation of X-ray diffraction line profiles - is proposed to characterize homogenization in compacted binary powder blends. As a parameter to characterize the stage of homogenization the relative peak position is proposed. This parameter is easy to determine in practice: during homogenization the position of an X-ray diffraction maximum is traced. As compared to other methods the present one has the following advantages: (i) it is fast and simple and (ii) it allows a more severe test of the model of interdiffusion applied. Experiments were performed with compacted blends of copper and nickel powders at 800, 900 and 1000°C. At the start of homogenization diffusion was very fast. Experiments at lower temperatures revealed that this was due to surface diffusion at the contact places between the copper and nickel particles with an activation energy of about 12 kcal/mol. Because of the sensitivity of the relative peak position to the interdiffusion model adopted it was shown that the generally accepted concentric sphere model: nucleus of nickel and shell of copper, should be modified to include a prealloyed shell at the copper/nickel interface at $t = 0$. Then good correspondence between theory and experiment is obtained. Finally it was found that in the temperature range applied one diffusion mechanism is dominant with an activation energy of 32 kcal/mol, indicating grain boundary diffusion.

1. Introduction

The fabrication of alloys by diffusional homogenization of compacted powder blends is technologically important [1]. To control such processes characterization of the interdiffusion occurring in the powder blend is necessary.

X-ray diffraction line profile analysis appears to be a powerful quantitative nondestructive method to determine concentration profiles: A concentration profile corresponds to a lattice parameter profile and - according to Bragg's law - a spectrum of lattice parameters causes line broadening.

In recent years attention has been paid to the development of the theory of diffraction from concentration profiles in monocrystalline systems [2, 3]. For powder specimens a method for the interpretation of line broadening resulting from binary interdiffusion was proposed by Rudman [4]. This technique has been applied on interdiffused blends of copper and nickel powders [1, 5, 6]. From these studies it appeared that a concentric sphere gemometry may afford the best description of interdiffusion in compacts of blended metal powders: the minor component is represented by a spherical particle, the major component by a uniform shell around the sphere.

The purpose of this paper is to propose a new method to analyse interdiffusion in compacted powder blends. The method is based on computer simulations of the X-ray diffraction line profiles. A new parameter characterizing the stage of homogenization will be proposed: the relative peak position. The method has the following advantages:

(i) Simulations are simple and have to be done only once for a system;

(ii) The relative peak position is directly available from experiment and can be measured in a very short time. Thus diffusion processes may be followed in situ;

(iii) As compared to Rudman's "degree of interdiffusion" - which is obtained by an elaborate calculation - the relative peak position is more sensitive for the actual diffusion model.

Several results on the homogenization in blends of copper and nickel powders will be presented. Argument (iii) resulted in a modification of the usual concentric sphere model.

2. Experimental procedure

2.1. Sample preparation

Commercially available pure powders were used: Nickel (Koch-Light; 8500 W; $<\phi> \approx 14$ μm); Copper (Koch-Light; 8223 h; $<\phi> \approx 35$ μm). The powders were reduced in a 98% Ar/2% H_2 atmosphere at 350-400°C during 1 h. No measurable sintering occurred. Portions of the powders, all with 30 atomic percent Ni, were thoroughly mixed by tumbling together for about 12 h. The powder blends were cold pressed at $(8.28 \pm 0.02)10^8$ N/m^2. Discs were obtained with a diameter of about 13 mm and a thickness of about 2 mm.

The diffusion anneals were performed in a 98% Ar/2% H_2 atmosphere in a furnace controlled automatically to ± 2°C. The temperatures applied were 800, 900 and 1000°C. The annealing times were corrected for the time needed for the specimens to warm up [7]. After diffusion a surface layer (100-150 μm thick) was removed by grinding and mechanical polishing. The cold work thus induced was removed by an anneal at 500°C for 10 min. No interdiffusion occurred during this reheating.

2.2. Diffractometry

Line profiles were measured in steps of 0.01 °2θ applying the preset-time method with a Siemens ω-diffractometer, equipped with a graphite monochromator.

The 220 reflection was measured with CuKα radiation because (i) it is a good compromise between high intensity and angular (concentration) resolution and (ii) no overlap with neighbouring Kα and Kβ reflections occurs.

Angle position corrections due to specimen transparency, flat specimen, 3^o axial divergence (Soller slits were used) and specimen displacement were performed according to Wilson [8]. Background radiation was removed by linear interpolation. The α_2 component was eliminated according to Delhez and Mittemeijer [9]. The angle dependence of the Lorentz and polarization factors was corrected for according to the rules set out in [10]. The angle dependence of the structure factor F was taken into account as $F = x\ f_{Ni} + (1-x)\ f_{Cu}$, where x is the atomic fraction nickel. The angle dependencies of the atomic scattering factors f_{Ni} and f_{Cu} were obtained from [11].

3. Rudman's method

In this paper we intend to weigh the line profile simulation method (sections 5 and 6) against the Rudman method [4]. We also slightly modified the Rudman technique. Therefore it is appropriate to sketch briefly our version of the Rudman analysis.

If particle size and strain broadening are neglected and s is given by $2\ \sin\theta/\lambda [= 1/d(x)$, where $d(x)$ is the interplanar spacing], the volume fraction $p(x)\partial x$ of compositions between x and $x + \partial x$ follows from (c.f. [12])

$$p(x)\partial x = C_1 \frac{\frac{-\partial d(x)}{\partial x}\ v^2(x)}{d^2(x)}\ I(s)\partial x \qquad (3.1)$$

where C_1 is a constant (including the absorbtion factor which is approximately constant), $v(x)$ is the unit cell volume and $I(s)$ is the intensity corrected

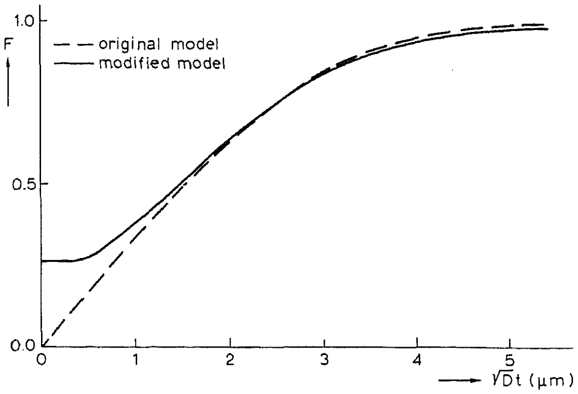

Fig. 1. The dependence of the degree of interdiffusion F on Dt, where D is the diffusion coefficient and t the annealing time, according to the original concentric sphere model and the modified one (c.f. section 6.2).

t(min)	T(°C)	F	D(cm²/s)
15	634	0.41	2.0×10^{-11}
15	664	0.46	2.6×10^{-11}
15	694	0.49	3.0×10^{-11}

Table 1.

Results of the experiments at relatively low temperatures. t = time of diffusion, T = annealing temperature, F = degree of interdiffusion and D = diffusion coefficient.

according to section 2.2. It should be pointed out that the previous investigators [1, 4 - 6] did not consider the concentration dependence of the unit cell volume. This implies that these authors did not correct for a 9% intensity lapse in the line profiles of their Cu/Ni powder specimens.

An effective penetration depth y(x) is defined

$$y(x) = \int_{o}^{x} p(x)\,\partial x \tag{3.2}$$

and then a plot of x versus y is analogous to normal concentration-penetration curves.

Rudman [4] proposed the degree of interdiffusion F as a parameter to characterize the stage of homogenization. F is defined by the ratio of the quantity of material which has crossed the Matano-interface after a given diffusion time to the quantity of material which will cross in infinite time:

$$F = \frac{\int_{x=o}^{x(y=y_M)} (y_M - y)\,dx + \int_{x(y=y_M)}^{x=1} (y - y_M)\,dx}{\bar{x}y_M + (1-y_M)(1-\bar{x})} = \frac{2\int_{x=o}^{x(y=y_M)} (y_M - y)\,dx}{2\bar{x}y_M} \tag{3.3}$$

where y_M represents the Matano-interface and $\bar{x}$ the average composition of the sample. For the concentric sphere model the ratio F is calculated analytically in the Appendix [let $\Delta_1 \to o$ and $\Delta_2 \to o$ in eq. (A-2)] in contrast with previous [5, 6] graphical integrations. The dependence of F on Dt, where D is the interdiffusion coefficient and t is the annealing time, is shown in Fig. 1. From the definition of F it is clear that this parameter is rather insensitive to considerable deviations from the concentric sphere model as will be illustrated in section 6.

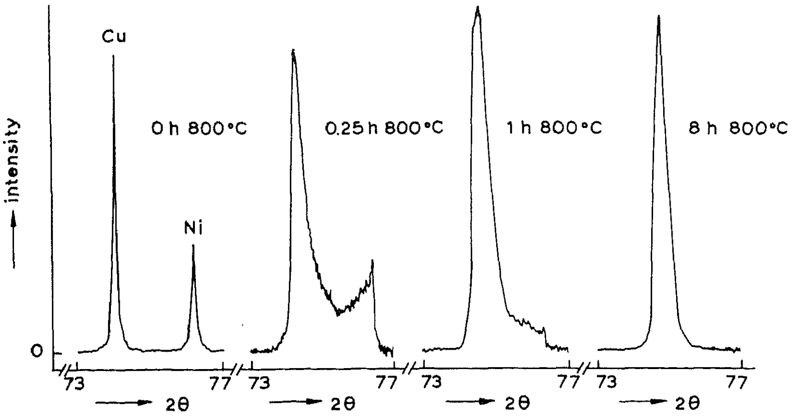

Fig. 2. 220 α_1 line profiles of an interdiffused Cu/Ni powder specimen for various annealing times at 800°C.

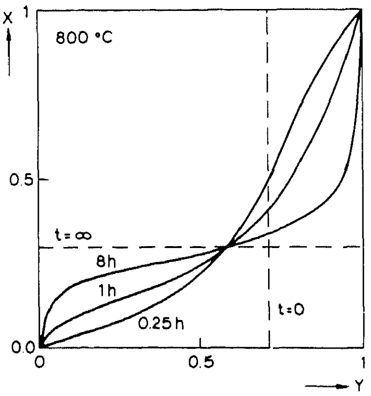

Fig. 3. Concentration-effective penetration curves as calculated according to the method outlined in section 3 from the line profiles of Fig. 2. x is the atomic fraction nickel and y is the effectice penetration distance (eq. 3.2).

4. Results with the Rudman method

Fig. 2 shows α_1-line profiles of a Cu/Ni powder specimen for various stages of interdiffusion. In Fig. 3 the corresponding concentration-effective penetration curves are given [eqs. (3.1) and (3.2)]*. The degree of interdiffusion F can be obtained by numerical integration of the concentration-effective penetration curves [eq. (3.3)]. The results are summarized in Fig. 4.

Adopting the concentric-sphere model a Dt value can be assigned to each experimental F value (Fig. 1). In Fig. 5 the Dt values obtained are plotted versus t. If the concentric sphere model is ideally suited to describe interdiffusion in these powder specimens, straight linesshould have been obtained, with slopes corresponding to the respective diffusion coefficients. Clearly this is not the case.

From Fig. 5 it is seen that at the start of homogenization diffusion is very fast. This effect was investigated by additional experiments at rather low temperatures, the results of which are gathered in table 1. Considering the insensitivity of F to changes in the model of diffusion (c.f. sections 3, 6.2) Dt values may be assigned to the F-values in the same way as before.

---

* The behaviour of these curves in the immediate neighbourhood of $y = o$ and $y = 1$ is not physically significant, because α_2-elimination [9] does not eliminate completely the broadening caused by the X-ray spectrum and the instrumental conditions. In principal deconvolution techniques [13] should give better results. However, in practive results obtained after deconvolution and after α_2-elimination show only small differences in the degree of interdiffusion [14].

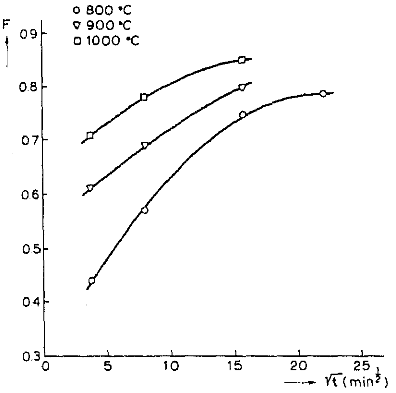

Fig. 4. The observed variation of the degree of interdiffusion F as a function of the annealing time t for Cu/Ni powder specimens interdiffused at 800, 900 and 1000°C.

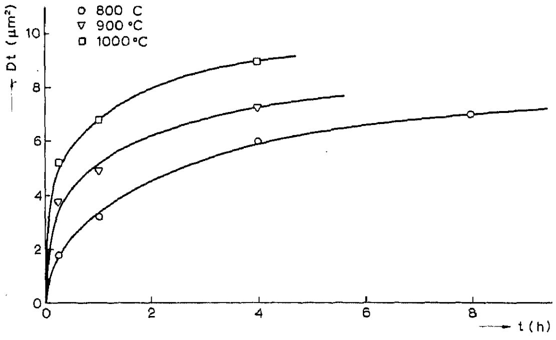

Fig. 5. Graphs of Dt versus t; Dt values are calculated according to the concentric sphere model from Fig. 1. Note that straight lines should have been obtained, with slopes corrsponding to the respective diffusion coefficients, if the concentric sphere model would hold.

Assuming an Arrhenius-type temperature dependence the activation energy of the fast diffusion process is estimated to be 12 kcal/mol. As compared with data on volume diffusion [15] this activation energy indicates surface diffusion [16]. At the contact places between the copper and nickel particles surface diffusion contributes significantly at the start of the homogenization at 800, 900 and 1000°C. The local character of this process is demonstrated by the α_1 line profile of the Cu/Ni powder specimen annealed at 634°C for 15 min. (Fig. 6). Apart from the nickel and copper peak two neighbouring maxima can be observed, which show that homogenization occurred locally not affecting the bulk of the copper and nickel particles.

From Fig. 5 it is seen that at large homogenization times the apparent diffusion coefficients become small. According to Heckel e.a. [1] this illustrates the effects of non-ideal mixing and non-uniform particle sizes. In section 7 an approach on the basis of an effective particle size will be presented to deal with this problem.

5. Line profile simulation method

Let us divide the radial concentration profile in the concentric sphere in segments (shells) corresponding to a constant change of concentration. Each segment k will diffract at a certain $s(= 2\sin\theta/\lambda)$-value, say s_k. We assume that all the segments give rise to a diffracted profile of the same shape. This implies that the structural broadening of a segment owing to its concentration variation is neglected as compared to the spectral and instrumental broadening. The intensity of the profile of segment k will be proportional to the amount of material of segment k. Then for the powder specimen the profile $i_k(s)$ of segment k can be written as

$$i_k(s) = C_2 \frac{1}{v^2_k} \frac{4}{3}\pi\{(R-r_{k-1})^3 - (R-r_k)^3\} f(s-s_k) \qquad (5.1)$$

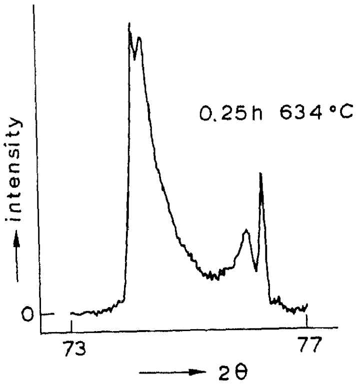

Fig. 6. 220 α_1 line profile taken from a Cu/Ni powder specimen annealed at 634^oC for 15 min.

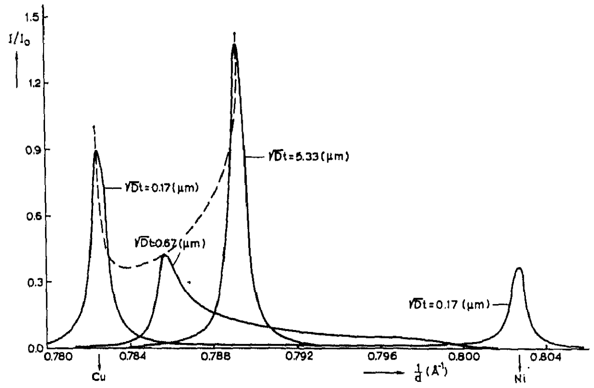

Fig. 7. Computer simulations of 220 α_1 line profiles of Cu/Ni powder specimens for various stages of interdiffusion according to the concentric sphere model. The behaviour of the copper-side peak maximum on annealing is indicated by the dashed curve.

where C_2 is a constant (including the absorbtion factor which is approximately constant), v_k is the average unit cell volume of segment k, R is the radius of the concentric sphere, the radii r_{k-1} and r_k enclose segment k in the sphere and f describes the shape of the diffracted profile such that f(o) = 1.

The total line profile of the powder specimen will be the sum of the profiles of all segments. Dividing the intensities by the peak intensity I_o of the major component before interdiffusion, the total line profile is given by

$$\frac{I(s)}{I_o} = \frac{v^2{}_B}{\{R^3-(R-r_B)^3\}} \sum_k \frac{1}{v^2{}_k} \{(R-r_{k-1})^3 - (R-r_k)^3\}.f(s-s_k) \qquad (5.2)$$

In order to obtain the shape function f the α_1 line profile of a standard nickel powder specimen was determined. The full width at half maximum was found to be 0.8 x 10^{-3} Å^{-1}. According to Edwards and Langford [17] the contribution of the spectral broadening to this width is (0.5 - 0.7) x 10^{-3} Å^{-1}. Hence the spectral broadening dominates over the broadening due to the instrumental conditions. It is generally accepted that the spectral α_1 component can be described by a Cauchy-function [18]. From the above we conclude that a reasonable approximation to the shape function is given by a Cauchy-function having a full width at half maximum of 0.8 x 10^{-3} Å^{-1}.

Results of simulations of the 220 line profile of an interdiffused Cu/Ni powder specimen on the basis of eq. (5.2) are shown in Fig. 7 for various stages of interdiffusion (the corresponding concentration profiles were calculated according to the concentric sphere model).

We propose to characterize homogenization by the relative peak position p_r defined as

$$p_r = (p-p_o)/(p_\infty-p_o) \qquad (5.3)$$

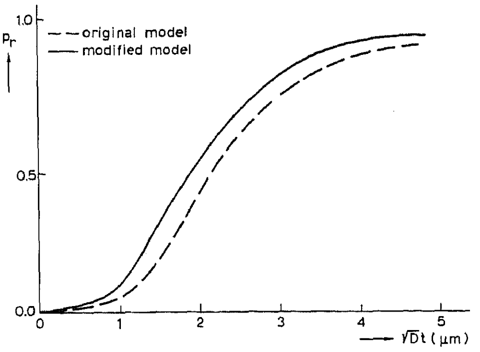

Fig. 8. The relative peak position p_r as a function of $\sqrt{Dt}$ according to the original concentric sphere model and the modified one (c.f. section 6.2).

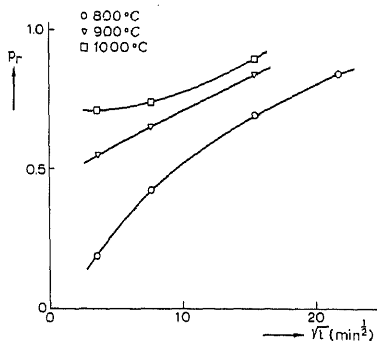

Fig. 9. The observed variation of the relative peak position p_r as a function of the annealing time t for Cu/Ni powder specimens interdiffused at 800, 900 and 1000°C.

where p is the actual peak position and p_0 and p_∞ correspond to the peak positions at the start and at the end of homogenization respectively. p_∞ can be calculated from the mean composition.

In our case (0.3 atomic fraction nickel) it is clear that the copper-side peak should be traced during interdiffusion: in Fig. 7 the behaviour of the copper-side peak maximum on annealing is also indicated (dashed curve).

On the basis of the line profile simulations according to the concentric sphere model the relative peak position is plotted as a function of Dt in Fig. 8. This plot plays the same role in our method as Fig. 1 in the Rudman method: once the value of p_r is established the value of Dt according to the concentric sphere model is obtained. It is clear that the relative peak position is much easier as well as much faster to determine than the degree of interdiffusion (c.f. section 3).

6. Results with the line profile simulation method

6.1. Comparison with the Rudman method

Experimentally determined values for the relative peak position are presented as a function of annealing time and temperature in Fig. 9. Using Fig. 8 a Dt value can be assigned to each p_r value according to the concentric sphere model, from which graphs of Dt versus t (as given in Fig. 5 for the Rudman method) can be constructed. Then the same conclusions as obtained before can be reached by similar reasoning.

Generally it can be said that the conclusions which are obtained by the Rudman method can also be provided by the line profile simulation method, which method is much simpler and faster to apply.

6.2. A modification to the concentric sphere model

Nothwithstanding the above, differences in results exist between the Rudman

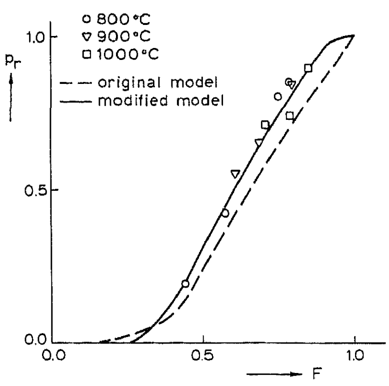

Fig. 10. The relative peak position p_r as a function of the degree of interdiffusion F for the original concentric sphere model (dashed curve) and the modified one (bold curve). The experimental points are also shown.

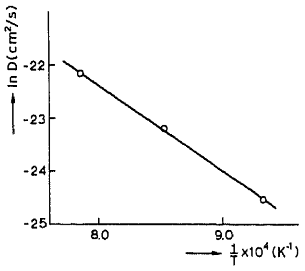

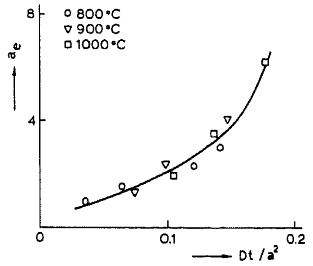

Fig. 11. Ln D versus 1/T. Only the ratios of the diffusion coefficients are physically significant. The given values of the diffusion coefficients result from the definition of $a_e = 1$ (c.f. Fig. 12). This does not affect the determination of the activation energy.

Fig. 12. The effective particle size a_e as a function of Dt/a^2, where a is the radius of the nucleus. The effective particle size was arbitrarely set equal to 1 for the experiment at 800^oC with 15 minutes annealing time.

method and the line profile simulation method: the dashed line in Fig. 10 represents the relation between the relative peak position p_r and the degree of interdiffusion F according to the concentric sphere model [$p_r \rightarrow Dt$ (Fig. 8); $Dt \rightarrow F$ (Fig. 1)]. The experimental points are also indicated. The correspondence between experiment and the concentric sphere model is not very satisfactory, because all experimental points lie above the dashed curve.

Now we recall the fast surface diffusion process which occurs at the start of the homogenization at 800, 900 and 1000°C, as is shown is section 4. The time required to establish local homogenization at the contact places between the copper and nickel particles by surface diffusion may be neglected with respect to the total annealing times at these temperatures. It was assumed that an initial concentration profile in the concentric sphere model with a prealloyed shell at the copper/nickel interface at t = o might give a better description of the homogenization behaviour observed at these temperatures. This model has been worked out in the Appendix. For the present case additional assumptions were made: (i) Homogenization in the prealloyed shell was considered as completed. (ii) The thickness $(\Delta_1 + \Delta_2)$ of the prealloyed shell was estimated from the low temperature experiments reported in section 4 by $(\Delta_1 + \Delta_2)^2 \simeq 2Dt \simeq 2\mu m$, where the radial dimensions Δ_1 and Δ_2 were taken equal. The dependence of F on Dt according to this modified concentric sphere model is also plotted in Fig. 1. It follows that in the range of F values which covers all experiments (0.45-0.90) the differences in Dt values between the original concentric sphere model and the modified one are negligible. This illustrates the insensitivity of the degree of interdiffusion to deviations from the concentric sphere model,as was mentioned in section 3. The relative peak position is much more sensitive to such deviations as follows from Fig. 8. In Fig. 10 the relation between p_r and F for the modified concentric sphere model is also given (bold line).

It can be seen that a good correspondence exists between the predictions of the modified concentric sphere model and the experiments.

7. Activation energy and diffusion mechanism

Without knowing the actual diffusion geometry in the powder specimens employed it is possible to determine the activation energy of the diffusion process. Assuming one diffusion mechanism to be dominant, it is recognized that equal values of the relative peak position at different temperatures imply identical stages of homogenization in the powder specimen. Hence the ratios of the diffusion coefficients at these temperatures are given by the ratios of the annealing times, which can be obtained by interpolation in Fig. 9. From an Arrhenius-plot the activation energy can be obtained (Fig. 11).

$$Q = 32 \text{ kcal/mol}$$

As compared with data on volume diffusion [15] this activation energy indicates grain boundary diffusion [16]. This agrees with previous results on polycrystalline Cu/Ni specimens [5, 19]. The result contradicts the statement of Heckel [1, 6] who claims volume diffusion to be dominant; however no activation energy was reported.

In section 4 the decrease in the apparent diffusion coefficients at large annealing times was noted (c.f. Fig. 5). This was attributed to deviations in the powder specimen from the diffusion geometry adopted: larger diffusion distances (e.g. contiguous nickel particles) become dominant at longer diffusion times causing a progressive decrease of the rate of homogenization. This problem can be dealt with as follows.

In the case of a concentration independent diffusion coefficient Fick's second law can be solved for concentric sphere geometries in terms of the dimensionless parameter Dt/a^2, where a is the radius of the nucleus (= nickel particle). Because at one annealing temperature the diffusion coefficient should be constant, the homogenization of non-ideally mixed powders with non-uniform particle sizes can be described by varying the radius a on annealing to accord with the (modified) concentric sphere model. We now introduce an effective particle size a_e, as suggested by Heckel [6]. After choosing a reference particle size a_r, it is possible for experiments with different annealing times at the same temperature to calculate the effective particle size $a_e = a/a_r$ in such a way that D remains constant. The results at different annealing temperatures can be related, because equal values of the relative peak position point to identical stages of homogenization. This implies that at the same values of the relative peak position one single effective particle size operates. In this way effective particle sizes at different temperatures can be brought into accordance, see Fig. 12. It is seen that all effective particle sizes observed lie approximately on a single curve. This illustrates that one single diffusion mechanism is dominant in the temperature range applied, as was assumed for the determination of the activation energy.

II.12

Appendix. The modified concentric sphere model

Metallographic evidence [5, 6] indicated that the geometry in binary powder specimens may be described by the concentric sphere geometry. A perfect distribution of the minor component A (in our case nickel) in the matrix of the major component B (in our case copper) is assumed. Then a concentric sphere with A and B constituting the sphere and the shell respectively may be a reasonable approximation of reality.

A general solution to Fick's second law with a concentration independent diffusion coefficient for diffusion in a sphere with impermeable surface was given by Crank (eq. 6.47 in [20]). In our case the concentration distribution $f(r)$ at $t = o$ is given by

$$o < r < a \quad f(r) = 1 \text{ and } a < r < b \quad f(r) = o \qquad \text{(case I)}$$

where a and b are the radii of the nucleus and the concentric sphere respectively.

In section 6.2 it is shown that a more realistic description of the homogenization behaviour is obtained if a prealloyed shell at the A/B interface is thought to be present at $t = o$. To a first approximation it is assumed that homogenization in the prealloyed shell leads to $c_L = 0.5$ (better approximations cause second order corrections). Then for the initial concentration distribution $f(r)$ it follows

$$o < r < a - \Delta_1 \quad f(r) = 1; \; a - \Delta_1 < r < a + \Delta_2 \quad f(r) = c_L$$

$$\text{and} \quad a + \Delta_2 < r < b \quad f(r) = o, \qquad \text{(case II)}$$

where $\Delta_1 + \Delta_2$ is the radial dimension of the prealloyed shell and

$$c_L = [a^3 - (a-\Delta_1)^3]/[(a+\Delta_2)^3 - (a-\Delta_1)^3].$$

Evaluation of the integrals in Crank's formula yields for case II

$$c(r) = \frac{a^3}{b^3} + \frac{2}{br}\sum_{n=1}^{\infty} \exp(-Dt\ \alpha_n^2)\ \frac{\sin \alpha_n r}{\sin^2\alpha_n b} \times$$

$$\times \frac{1}{2\alpha_n}\ \{(a-\Delta_1)\cos\ \alpha_n(a-\Delta_1) + (a+\Delta_2)\cos\ \alpha_n(a+\Delta_2) +$$

$$- \frac{\sin\ \alpha_n(a-\Delta_1)}{\alpha_n} - \frac{\sin\ \alpha_n(a+\Delta_2)}{\alpha_n}\} \qquad \text{(A-1)}$$

where $c(r)$ is the volume fraction of material A and α_n is the n-th positive root of the transcendental equation $b\alpha_n \cot b\alpha_n = 1$.

The quantity of material m_t which has crossed the interface after a given diffusion time t and the quantity of material m_∞ which will cross in infinite time follow from

$$m_t = 4\pi \int_0^{a/b} (1-c)\,(\tfrac{r}{b})^2\ d(\tfrac{r}{b}) + 4\pi \int_{a/b}^{1} c\,(\tfrac{r}{b})^2\ d(\tfrac{r}{b})$$

$$m_\infty = \frac{8\pi\ a^3}{3b^3}\ (1 - \frac{a^3}{b^3})$$

The degree of interdiffusion $F = m_t/m_\infty$ can be calculated from

$$F = 1 - \frac{16\pi}{b^4 m_\infty}\sum_{n=1}^{\infty} \exp(-Dt\ \alpha_n^2)\ \frac{1}{\sin^2\ \alpha_n b} \times$$

$$\times \frac{1}{2\alpha^2_n}\{(a-\Delta_1)\cos\ \alpha_n(a-\Delta_2)\cos\ \alpha_n(a+\Delta_2) +$$

$$- \frac{\sin\ \alpha_n(a-\Delta_1)}{\alpha_n} - \frac{\sin\ \alpha_n(a+\Delta_2)}{\alpha_n}\} \times \{a \cos\ \alpha_n a - \frac{\sin\ \alpha_n a}{\alpha_n}\} \qquad \text{(A-2)}$$

The formulae for the original concentric sphere model (case I) follow immediately from the formulae for the modified concentric sphere model (case II) if $\Delta_1 \to o$ and $\Delta_2 \to o$ in eqs. (A-1) and (A-2).

The dependence of F on Dt, as calculated from eq. (A-2), is plotted for both models in Fig. 1.

Acknowledgements

We are indebted to Professor B. Okkerse and Dr. F.W. Schapink for critically reading the manuscript.

Financial support of the Stichting voor Fundamenteel Onderzoek der Materie (F.O.M.) is gratefully acknowledged.

References

1. R.W. Heckel and M. Balasubramaniam, Met. Trans, 2 (1971) 379.
2. C.R. Houska, J. Appl. Phys. 41 (1970) 69.
3. E.J. Mittemeijer and R. Delhez, J. Appl. Phys. 47 (1976) 1702.
4. P.S. Rudman, Acta Cryst. 13 (1960) 905.
5. B. Fisher and P.S. Rudman, J. Appl. Phys. 32 (1961) 1604.
6. R.W. Heckel, Trans. ASM, 57 (1964) 443.
7. D.Y.F. Lai, "Diffusion in Body-Centered Cubic Metals". Proceedings International Conference of the American Society for Metals (Metals Park Ohio 1964) p. 269.
8. A.J.C. Wilson, "Elements of X-ray Crystallography" (Addison-Wesley, Reading Massachusetts, 1970) p. 34.
9. R. Delhez and E.J. Mittemeijer, J. Appl. Cryst. 8 (1975) 609.
10. R. Delhez, E.J. Mittemeijer, Th.H. de Keijser and H.C.F. Rozendaal, J. of Phys. E. 10 (1977) 784.
11. International Tables for X-ray Crystallography vols. III and IV, published for the International Union of Crystallography (The Kynoch Press, Birmingham 1962, 1974).
12. B.E. Warren, "X-ray Diffraction" (Addison-Wesley, Reading Massachusetts, 1969), section 4.3.
13. A.R. Stokes, Proc. Phys. Soc. 61 (1948) 382.
14. E.A. van den Bergen, R. Delhez and E.J. Mittemeijer, Phys.Stat.Sol. (a), in the press.
15. D.B. Butrymowicz, J.R. Manning and M.E. Read, J. Phys. Chem. Ref. Data 5 (1976) 103.
16. J. Askill, "Tracer Diffusion Data for Metals, Alloys and Simple Oxides" (Plenum Press, New York, 1970) p. 11.

17. H.J. Edwards and J.I. Langford, J. Appl. Cryst. 4 (1971) 43.

18. H.P. Klug and L.E. Alexander, "X-ray Diffraction Procedures for Polycrystalline and Amorphous Materials", 2nd edition (John Wiley, New York, 1974) p. 297.

19. G.O. Tronsdal and H. Sorum, Phys. Stat. Sol. 4 (1964) 493.

20. J. Crank, "The Mathematics of Diffusion" (Clarendon Press, Oxford, 1956) p. 92.

AN X-RAY DIFFRACTION STUDY OF DIFFUSIONAL HOMOGENIZATION IN RbCl/KCl POWDER BLENDS

by

E.A. van den Bergen, R. Delhez and E.J. Mittemeijer

Laboratory of Metallurgy, Delft University of Technology,
Rotterdamseweg 137, Delft, The Netherlands.

Accepted for publication in Physica Status Solidi (a).

II.13

Abstract

X-ray diffraction line profile analysis is used to study interdiffusion at 500, 575 and 650°C occurring in compacted RbCl/KCl powder blends. Two methods for the interpretation of the diffusion-induced line broadening are applied: the method of Rudman and a recently developed line profile simulation method. With respect to the determination of concentration profiles α_2-elimination and deconvolution of the X-ray line profiles are compared. The fast diffusion observed at the start of homogenization is ascribed to surface diffusion at the contact places between the RbCl and KCl particles with an activation energy of about 8 kcal/mol, whereas later on volume diffusion is shown to be dominant with an activation energy of 42 kcal/mol. Results of the line profile simulation method indicate that the concentric sphere model has a limited applicability to depict homogenization in powder blends of salts.

Durch Analyse der Röntgenbeugungsprofilen wird die Interdiffusion bei 500, 575 und 650°C in RbCl/KCl-Presslingen untersucht. Die Deutung der Konzentrationsverlauf-bedingten Linienverbreiterung erfolgt durch Anwendung der Rudman-Methode und einer kürzlich entwickelten Linienprofilsimulationsmethode. Entfaltung und α_2-Elimination der Röntgenbeugungsprofile werden bei der Bestimmung der Konzentrationsverteilung verglichen. Die Anfangsdiffusion ist schnell: Oberflächendiffusion mit einer Aktivierungsenergie von etwa 8 kcal/Mol; später herrscht Volumendiffusion mit einer Aktivierungsenergie von 42 kcal/Mol vor. Ergebnisse der Linienprofilsimulationsmethode zeigen, dass das konzentrische Kugelmodell nur beschränkt gültig ist zur Beschreibung der Diffusion in gepressten Mischpulversalzen.

1. Introduction

Lattice parameter variations broaden X-ray diffraction line profiles. Therefore line profile analysis appears to be a powerful nondestructive quantitative method to study concentration profiles. For monocrystalline specimens theory of diffraction from concentration profiles was developed in [1, 2]. For powder specimens the interpretation of the line broadening resulting from binary interdiffusion is possible according to the Rudman method [3] and a recently developed line profile simulation method [4]. Powder specimens are easier to prepare than single crystals and often have important technological implications [5, 6]. Considerable attention has been paid to homogenization im compacted metal powder blends [4, 5, 7-10]. From these studies it appeared that a concentric sphere model provides the best description of interdiffusion in mixed powders: one of the components is represented by a spherical particle, the other component by a uniform shell around this sphere.

It is the purpose of this paper to demonstrate that X-ray diffraction may be an important tool for studying diffusion in non-metal powder systems. In contrast with current methods in research on diffusion this technique is nondestructive and fast. The differences with previously investigated metal powder systems will be outlined.

2. Experimental procedure

2.1. Sample preparation

Commercially available pure powders were used: RbCl (Merck p.a.; $<\phi> \approx 35$ µm); KCL (Merck p.a.; $<\phi> \approx 35$ µm). Both powders were dried at 150^{o}C during 12 h. Equiatomic portions were thoroughly mixed by tumbling together for 12 h. In contrast with metal powder specimens a texture developed during compression: crystallites of KCl in a surface layer of the specimen showed a tendency to align their {100} planes parallel to the surface. Therefore this surface layer was removed after diffusion. In case the powder blend was cold pressed at $9.81\ 10^7$ N/m^2 the X-ray diffraction patterns revealed considerable homogenization. By milling a blend of Cu and Ni powders an analogous phenomenon was observed [11]. Because of this all powder blends were cold pressed at $2.45\ 10^7$ N/m^2 where no prealloying was observed. Discs were obtained with a diameter of about 13 mm and a thickness of about 2 mm.

The diffusion anneals were performed in a furnace controlled automatically to ± 5°C. The temperatures applied were 500, 575 and 650°C. The annealing times were corrected for the time needed for the specimens to warm up [12]. After diffusion a surface layer (170-200 μm) was removed by turning off cautiously. The cold work thus induced was eliminated by an anneal at 250°C for 30 min. No measurable interdiffusion occurred during this reheating.

2.2. Diffractometry

Line profiles were measured in steps of $0.01^{\circ}2\theta$ applying the preset-time method with a Siemens ω-diffractometer, equipped with a graphite monochromator.

The 220 reflection was measured with CuKα radiation because (i) it is a good compromise between high intensity and angular (concentration) resolution and (ii) no overlap with neighbouring Kα and Kβ reflection occurs.

Angle position corrections due to specimen transparency, flat specimen, 3° axial divergence (Soller slits were used) and specimen displacement were performed according to Wilson [13]. Background radiation was removed by linear interpolation. The α_2 component was eliminated according to Delhez and Mittemeijer [14]. The deconvolution method of Stokes [15] was applied using RbCl standard powder samples. The angle dependence of the Lorentz and polarization factors was corrected for according to the rules set out in [16].

The angle dependence of the structure factor S was taken into account as $S = xf_{KCl} + (1-x)f_{RbCl}$ where x is the molar fraction KCl. The angle dependencies of the atomic scattering factors f_{KCl} and f_{RbCl} were obtained from [17].

3. Methods of profile analysis

3.1. Rudman's method

A modified version of the original Rudman method [3] will be applied in this paper. The volume fraction $p(x)\partial x$ of compositions between x and $x + \partial x$ can be calculated from the line profile (c.f. [18]). In contrast with the previous investigators [3, 5, 7-10] the composition dependence of the unit cell volume is taken into account*). An effective penetration parameter y(x) is defined

$$y(x) = \int_0^x p(x)\,\partial x \tag{3.1}$$

and then a plot of x versus y is analogous to normal concentration-penetration curves.

Rudman [3] proposed the degree of interdiffusion F as a parameter to characterize the stage of homogenization. F is defined by the ratio of the quantity of material which has crossed the Matano interface after a given diffusion time to the quantity of material which will cross in infinite time

---

* The composition dependence of the unit cell volume causes a 15% intensity lapse in the line profiles of RbCl/KCl powder specimens. A corresponding 9% intensity lapse in the line profiles of Cu/Ni powder specimens was not corrected for in [3, 5, 7, 8].

$$F = \frac{\int_{x=o}^{x(y=y_M)} (y_M-y)\,dx + \int_{x(y=y_M)}^{x=1} (y-y_M)\,dx}{\bar{x}y_M + (1-y_M)(1-\bar{x})} = \frac{2\int_{x=o}^{x(y=y_M)} (y_M-y)\,dx}{2\bar{x}y_M} \qquad (3.2)$$

where y_M denotes the Matano-interface and $\bar{x}$ the average composition of the sample. Using the concentric sphere model the degree of interdiffusion can be calculated. From the definition of F it is clear that this parameter is insensitive to considerable deviations from the concentric sphere model, which may occur in practice.

3.2. Line profile simulation method

After division of the concentration profile into segments corresponding to a constant change in concentration, the total line profile is given by the sum of the profiles of all segments. The shape of each segment profile is described by a Cauchy function with a full width at half maximum of $1.2\ 10^{-3}\ \text{Å}^{-1}$ as followed from measurements of RbCl standard powder specimen. (A detailed description of the line profile simulation method is given in [4]).

The stage of homogenization can be characterized by the relative peak position p_r

$$p_r = (p-p_o)(p_\infty-p_o) \qquad (3.3)$$

where p is the actual peak position and p_o and p_∞ correspond to the peak positions at the start and at the end of homogenization respectively. p_∞ can be calculated from the mean composition. On annealing the position of an X-ray diffraction maximum is traced. The observed dependence of p_r on annealing time and temperature can be related to the calculated dependence obtained from line profile simulations. The relative peak position is much easier as well as much faster to determine than the degree of interdiffusion and is sensitive to deviations from the concentric sphere geometry which may occur in practice.

4. Results and discussion

From the line profiles (corrected according to section 2.2; an example is shown in Fig. 1) it immediately follows that RbCl is much faster contaminated by K^+ than KCl by Rb^+. This indicates a higher intrinsic diffusivity for K^+ compared to Rb^+ in agreement with [19].

4.1. Determination of concentration profiles and degrees of interdiffusion

Deconvolution potentially is the best method for purification of experimentally determined line profiles, but often only α_2 elimination is or can be employed. If considerable amounts of pure component material are still present after annealing, deconvolution is inappropriate because the Fourier series of the deconvoluted line profile diverges due to the presence

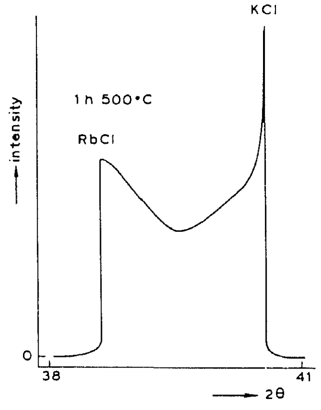

Fig. 1. Deconvoluted 220-line profile of a RbCl/KCl powder blend after a diffusion anneal of 1h at 500°C. The unfolded line profile was smoothed to remove spurious oscillations.

of δ-functions. The difference between concentration profiles obtained from line profiles purified either by deconvolution [15] or by α_2 elimination [14] is shown in Fig. 2. The α_2 elimination does not remove all instrumental and spectral broadening. Therefore the behaviour of the corresponding concentration profile in the neighbourhood of $y = o$ and $y = 1$ is not physically significant: the range of compositions seems to be wider than in reality.

For our experiments at 500, 575 and 650°C the concentration-effective penetration curves, as calculated according to section 3.1, were obtained from the deconvoluted line profiles, except for the experiment of 0.25 h at 500°C where the concentration profile was obtained from the α_2 eliminated line profile.

The degrees of interdiffusion F, obtained from the concentration-effective penetration curves according to eq. (3.2), are gathered in table 1. The incomplete removal of instrumental and spectral broadening by α_2 elimination leads to an apparently enhanced interdiffusion at the start of homogenization

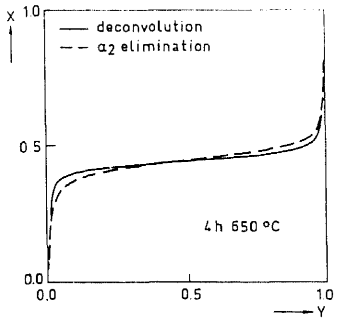

Fig. 2. Concentration-effective penetration curves calculated for the experiment at 650°C for 4h from the α_2-eliminated line profile (dashed curve) and the deconvoluted line profile (bold curve). x is the molar fraction KCl and y is the effective penetration distance.

and an apparently retarded interdiffusion near the end of homogenization. If F_{α_2} and F_d denote the degrees of interdiffusion obtained after α_2 elimination and after deconvolution respectively, we expect $F_{\alpha_2} > F_d$ for small F and $F_{\alpha_2} < F_d$ for large F. This corresponds with the experimental finding (table 1). Up to now this behaviour has neither been recognized nor observed in the literature where the results of α_2 elimination and deconvolution were compared [3, 8]. Furthermore it can be concluded that for about 50/50 blends deconvolution should be preferred over α_2 elimination if it is expected that F > 0.4. Hence some results obtained in [8, 9] may be inaccurate.

T	500°C			575°C			650°C		
t(h)	F_{α_2}	F_d	p_r	F_{α_2}	F_d	p_r	F_{α_2}	F_d	p_r
0.25	0.32	0.29*	0.03	0.55	0.54	0.75	0.78	0.79	0.93
1.0	0.45	0.44	0.19	0.71	0.72	0.91	0.86	0.88	0.96
2.0	0.53	0.52	0.40	0.78	0.79	0.93	0.89	0.91	0.97
4.0	0.60	0.60	0.78	0.83	0.84	0.94	0.89	0.92	0.97

* unreliable value (see text)

Table 1.

Degrees of interdiffusion as calculated from α_2-eliminated line profiles (F_{α_2}) and deconvoluted line profiles (F_d) and the relative peak position p_r. T is the annealing temperature and t is the annealing time.

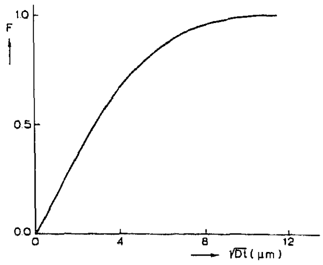

Fig. 3. The dependence of the degree of interdiffusion F on Dt, where D is the diffusion coefficient and t is the annealing time, according to the concentric sphere model for the RbCl/KCl powder specimens: the spherical KCl nucleus with $\langle\phi\rangle = 35$ *μm, is surrounded by a uniform RbCl shell of 5.1 μm thickness from the equi-atomic proportion RbCl/KCl.*

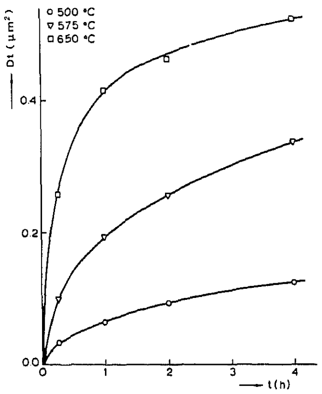

Fig. 4. Graphs of Dt versus t. De Dt values are calculated according to the concentric sphere model from Fig. 3. Note that straight lines should have been obtained, with slopes corresponding to the respective diffusion coefficients, if the concentric sphere model would hold.

t(min)	T(^{o}C)	F	D(cm^2/s)
15	373	0.20	1.7×10^{-11}
15	400	0.23	2.1×10^{-11}
15	442	0.25	2.5×10^{-11}

Table 2.

Results of the experiments at lower temperatures. T is the annealing temperature, t is the annealing time, F is the degree of interdiffusion and D is the diffusion coefficient.

4.2. Influence of surface diffusion

For the concentric sphere model* the F versus Dt curve, with D is the diffusion coefficient and t is the annealing time, can be calculated and it is shown in Fig. 3. Using this figure a Dt value can be assigned to each experimental F value. In Fig. 4 the Dt values obtained are plotted versus t. If the concentric sphere model is ideally suited to describe interdiffusion in these powder specimens, straight lines should have been obtained, with slopes corresponding to the respective diffusion coefficients. This is not the case.

From Fig. 4 follows that diffusion is very fast at the start of homogenization. This effect was investigated by additional experiments at lower temperatures, the results of which are gathered in table 2. Owing to the insensitivity of

---

* In case there are equal portions of both components it is generally assumed [7, 8, 9] that the material with the lower melting point (i.e. RbCl) envelopes the particles of the material with the higher melting point (i.e. KCl) at the start of homogenization.

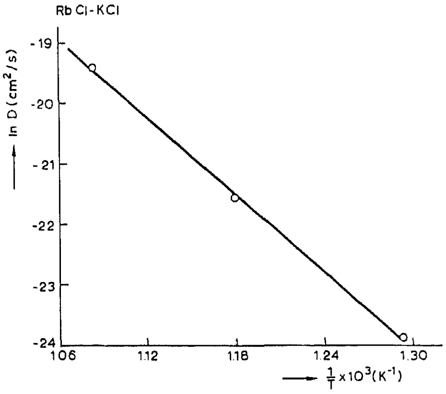

Fig. 5. Ln D versus 1/T. Only the ratios of the diffusion coefficients are physically significant. The absolute values of the diffusion coefficients result from the definition of $a_e = 1$ *(c.f. Fig. 6). This does not affect the determination of the activation energy.*

F to changes in the model of diffusion [4] Dt values may be assigned to the F values in the same way as before. Assuming an Arrhenius type temperature dependence the activation energy of the fast diffusion process is estimated to be 8 kcal/mol. Compared with data on volume diffusion [19] this activation energy indicates surface diffusion [20]. At the contact places between the RbCl and KCl particles surface diffusion contributes significantly at the start of homogenization of 500, 575 and 650^{o}C.

4.3. Activation energy and diffusion mechanism

If one diffusion mechanism is dominant, equal values of the degree of interdiffusion at different temperatures imply identical stages of homogenization in the powder specimen. Hence the ratios of the diffusion coefficients at these temperatures are given by the ratios of the annealing times, which can be obtained by interpolation from table 1. From an Arrhenius plot the activation energy can be obtained (Fig. 5)

$$Q = 42 \text{ kcal/mol}.$$

This value agrees with other data for volume diffusion in the RbCl/KCl system [19]. In view of results obtained on interdiffusion in Cu/Ni powder specimens at comparable annealing temperatures, where a dominant grain boundary diffusion was found [4, 7], this seems surprising. However it was experimentally shown [6] that grain boundaries do not enhance the cation diffusivities of these salts.

From Fig. 4 follows that at large annealing times the apparent diffusion coefficients become small. This may be attributed to deviations in the powder specimen from the diffusion geometry adopted: larger diffusion distances (e.g. contiguous KCl particles) become dominant at longer diffusion times causing a

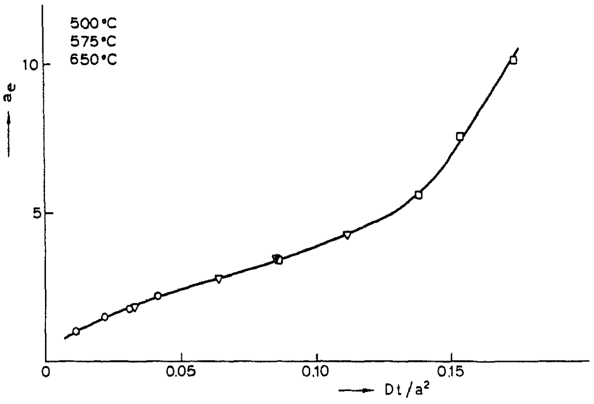

Fig. 6. The effective particle size a_e as a function of Dt/a^2, where a is the radius of the KCl nucleus. The effective particle size was arbitrarily set equal to 1 for the experiment at 500°C with 15 min. annealing time.

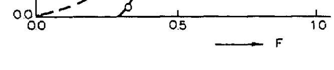

Fig. 7. The relative peak position p_r as a function of the degree of interdiffusion F for the original concentric sphere model (dashed curve) and the modified one (bold curve). For the latter the thickness of the prealloyed shell was estimated from the experiments at lower temperatures by $\sqrt{2Dt}$ at about 4·µm. The experimental data are plotted too.

progressive decrease of the rate of homogenization. The actual diffusion geometry can be described by means of an effective particle size [8]. For experiments with different annealing times at the same temperature the diffusion coefficient should be constant. This is accomplished by varying the effective particle size $a_e = a/a_r$, where a_r is an arbitrarily chosen reference particle size and a is the radius of the KCl nucleus*. The results at different annealing temperatures can be related, because equal values of the degree of interdiffusion point to identical stages of homogenization. This implies that at the same values of F one single effective particle size operates. In this way effective particle sizes at different temperatures can be brought into accordance, see Fig. 6. It is seen that all effective particle sizes observed lie on a single curve. This illustrates that one single diffusion mechanism is dominant in the temperature range applied, as was assumed for the determination of the activation energy.

4.4. Deficiencies of the concentric sphere model

To investigate the validity of the concentric sphere model results obtained from the relative peak position and the degree of interdiffusion will be interrelated. The relation between p_r and F calculated for the concentric sphere model is plotted in Fig. 7 (dashed curve) together with the experimental data: theory does not agree satisfactorily with experiment. Recalling the fast surface diffusion process at the start of homogenization (c.f. section 4.2) a better description of the diffusion behaviour may be obtained if a prealloyed layer at the interface of both components is assumed to be present at $t = o$. Such a modification to the concentric sphere model hardly effects

---

* This is justified by the fact, that Fick's second law with a concentration independent diffusion coefficient can be solved for concentric sphere geometries in terms of the dimensionless parameter Dt/a^2

the dependence of F on Dt in the range of F values of interest, but it does change the dependence of p_r on Dt (see section 3). For the RbCl/KCL powder blends investigated the relation between p_r and F according to this modified concentric sphere model is also plotted in Fig. 7 (bold curve). Although the presence of a prealloyed shell is an improvement for the first stages of homogenization, no improvement is observed for the later stages. Two other models have been proposed in the literature: an alternate layering of sheets of the two components [21] and an alternate packing of cubes [22], where the laminar thickness and the cube edge are adjustable parameters [7]. Only the latter model(restricted to equi-atomic powder blends)seems to be of interest for these salts, because RbCl and KCl cleave along the {001} faces. Then a {100} texture should have been present, but this was not observed with our specimens (see section 2.1).

For an overall description of homogenization the concentric sphere geometry remains attractive because it is applicable to powder blends of any average composition and the experimentally determinable particle size of one of the components enters into the equations.

Acknowledgements

The authors are grateful to Professor W.G. Burgers for his guidance in selecting the RbCl/KCl system. Professor B. Okkerse and Dr. F.W. Schapink critically read the manuscript.

Financial support of the Stichting voor Fundamenteel Onderzoek der Materie (F.O.M.) is gratefully acknowledged.

References

1. C.R. Houska, J. Appl. Phys. 41, 69 (1970).
2. E.J. Mittemeijer and R. Delhez, J. Appl. Phys. 47, 1702 (1976).
3. P.S. Rudman, Acta Cryst. 13, 905 (1960).
4. R. Delhez, E.J. Mittemeijer and E.A. van den Bergen, J.Mat.Sci., in the press.
5. R.W. Heckel and M. Balasubramaniam, Met. Trans. 2, 379 (1971)
5. J. Benard and J. Cabane, in: Sintering and Related Phenomena, Eds. G.C. Kuczynski, N.A. Hooton and C.F. Gibbon, Proceedings International Conference, 1965, Gordon and Breach, Science Publishers, New York 1967 (p. 1).
7. B. Fisher and P.S. Rudman, J. Appl. Phys. 32, 1604 (1961).
8. R.W. Heckel, Trans. ASM. 57,443 (1964).
9. P.H. Holloway and G.O. Mohanty, J. Phys. Chem. Solids 32, 2656 (1973).
10. S. Leber and R.F. Hehemann, Trans. AIME 230, 100 (1964).
11. A. Wagendristel, K. Persy and E. Tschegg, Planseeberichte für Pulvermetallurgie 21, 241 (1973).
12. D.Y.F. Lai, in: Diffusion in Body-Centered Cubic Metals, Proceedings International Conference of the American Society for Metals, Metals Park (O.) 1964 (p. 269).
13. A.J.C. Wilson, Elements of X-ray Crystallography, Addison-Wesley, Reading Massachusetts 1970, p. 34.
14. R. Delhez and E.J. Mittemeijer, J. Appl. Cryst. 8,609 (1975).
15. A.R. Stokes, Proc. Phys. Soc. 61, 382 (1948).
16. R. Delhez, E.J. Mittemeijer, Th.H. de Keijser and H.C.F. Rozendaal, J. of Phys. E 10, (1977) 784.
17. International Tables for X-ray Crystallography vols. III and IV, published for the International Union of Crystallography, The Kynoch Press, Birmingham 1962, 1974.

18. B.E. Warren, X-ray Diffraction, Addison-Wesley, Reading Massachusetts 1969, section 4.3.

19. M. Kantola and R. Lindström, Ann. Acad. Sci. Fenn. A VI 222, 3 (1967).

20. J. Askill, Tracer Diffusion Data for Metals, Alloys and Simple Oxides, Plenum Press, New York 1970, p. 11.

21. P. Duwez and C.B. Jordan, Trans. ASM 41, 194 (1949).

22. S. Weinbaum, J. Appl. Phys. 19, 897 (1948).

ON THE ANALYSIS OF X-RAY DIFFRACTION LINE PROFILES FROM SMALL EPITAXIAL BINARY DIFFUSION COUPLES: DETERMINATION OF CONCENTRATION PROFILE AND INFLUENCE OF TDS

by

R. Delhez and E.J. Mittemeijer

Laboratory of Metallurgy, Delft University of Technology,
Rotterdamseweg 137, Delft, The Netherlands.

II.14

Abstract

The *in situ* nondestructive determination of the concentration profile in a small epitaxial binary diffusion couple by X-ray diffraction line profile analysis is considered. On the basis of the work by Houska and collaborators a direct method is presented for the determination of the concentration profile from an X-ray intensity band. The method has the advantages that only a single order of the reflection is required and that neither iterative nor trial and error calculations are necessary as compared to previous methods. It is further shown that linear interpolation between both extremeties of the intensity band is a poor approximation to the actual background profile. The background mainly consists of Thermal Diffuse Scattering (TDS) which peaks at the Bragg positions and may contribute significantly to the integrated intensities measured. An iterative method is proposed to calculate the TDS background. Both the direct method for determining the concentration profile and the calculation and subsequent elimination of the TDS background are applied to experiments with Cu/Ni bicrystals where the copper is either electrocrystallized or deposited from the vapour phase onto the 111 nickel substrate.

1. Introduction

Concentration variations correspond to lattice parameter variations and - according to Bragg's law - may therefore be analyzed by application of diffraction methods. These are highly attractive, because in situ nondestructive investigations are possible. Small diffusion zones are accessible, which is of great technological importance in view of the many applications of microelectronic devices.

X-ray diffraction methods have been applied to powder specimens for concentration variations occurring over distances many times the size of the coherently diffracting domains or crystallites[1-4] as well as for concentration variations occurring within the coherently diffracting crystallites[5].

Solid state interdiffusion is commonly studied using specimens with a plane geometry (c.f. Fig. 1). The power of X-ray diffraction for studying interdiffusion in epitaxial bimetallic diffusion couples was demonstrated by Houska and collaborators[6-10]. Two different procedures were employed for the determination of concentration profiles from X-ray diffraction line profiles: (i) An iterative method using two or more orders of a reflection and (ii) a computer simulation method where the line profile is calculated from an assumed concentration profile, which is modified until satisfactory agreement exists between simulation and experiment (this method is also applied in refs. 11 and 12). The need for at least two orders of a reflection and the iterative nature of the procedure in the first method and the trial and error adaptation of the concentration profile assumed in the second method may be considered as disadvantages of the methods mentioned.

The purpose of this paper is to extend the work by Houska and co-workers by proposing a direct method for the determination of the concentration profile from a single order of a reflection. Moreover it will be shown that the concentration profile calculated may be strongly influenced by the mode of background

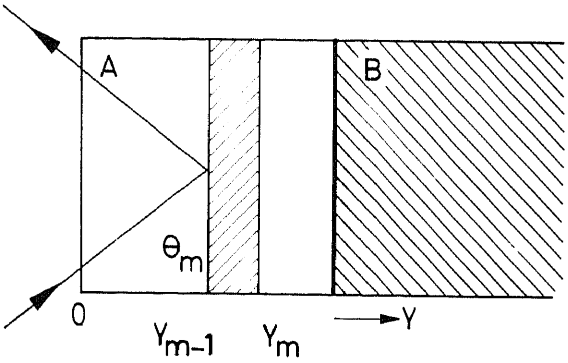

Fig. 1. *Schematic representation of specimen and diffraction geometry.*

elimination. When the background is mainly determined by Thermal Diffuse Scattering (TDS), the background profile should be calculated instead of eliminated by some interpolation procedure between the arbitrarily chosen extremeties of the line profile.

2. Theoretical considerations

2.1. Determination of the concentration profile

Consider the geometry of Fig. 1: the specimen may be thought to consist of a series of segments parallel to the free surface by adopting some fixed change in concentration; the composition of each segment may be considered constant. In this way the gradual change in composition is approximated by a series of steps as is commonly done.

Applying the kinematical diffraction theory[13] the following expression is obtained for the integrated intensity P_m of segment m extending from the penetration distance y_{m-1} to y_m:

$$P_m = P_o.C.LP_m.F_m^2 \cdot \frac{1}{v_m^2}.A_m.V_m \qquad (1)$$

where P_o is the power in the primary beam; $C = r_e^2.\lambda^3$, with r_e and λ being the classical radius of the electron and the X-ray wavelength respectively; LP_m comprises the Lorentz and polarization factors; F_m^2 is the squared modulus of the structure factor (including the Debije-Waller factor) and v_m is the unit cell volume. The absorbtion by the segments 1 to m-1 is described by

$$A_m = \exp. \frac{-2}{\sin \theta_m} \sum_{i=1}^{m-1} \mu_i \, \Delta y_i \qquad (2)$$

and the absorbtion in segment m is included in

$$V_m = g_m(1 - \exp. \frac{-2}{\sin \theta_m} \mu_m \Delta y_m)/2\mu_m \tag{3}$$

where θ_m is the angle of incidence, μ_m is the linear absorbtion coefficient and $\Delta y_m = y_m - y_{m-1}$. The orientation factor g_m $(0 \leq g_m \leq 1)$ is introduced, since in the specimens employed in practice often only a fraction of the material is in epitaxial position[6,11,12].

Houska and collaborators[6-10] approximated the product $A_m V_m$ with

$$A_m V_m \simeq \frac{g_m \Delta y_m}{\sin \theta_m} \exp. \frac{-2}{\sin \theta_m} \int_0^{y'_m} \mu(y)\,dy \tag{4}$$

where $y'_m = (y_{m-1} + y_m)/2$ [14]. It should be noted that the approximation (4) is only valid for small values of the thickness Δy_m of the segment. In case the segments extend over several microns, as can be the case for the end regions of the concentration profile, the procedures based on eq. (4) cannot be used.

In this paper a direct method will be applied for the determination of the concentration profile:

$$y_i = y_{i-1} + \Delta y_i \qquad (i = 1, 2, \ldots\ldots) \tag{5a}$$

where according to eqs. (1-3)

$$\Delta y_i = \frac{-\sin \theta_i}{2\mu_i} \ln\{1 - \frac{P_i . v_i^2 . 2\mu_i}{P_o . C . LP_i . F_i^2 . A_i . g_i}\} \tag{5b}$$

In this way the concentration profile can be recursively calculated, starting from the free surface (y = 0), when the power P_o in the primary beam is known. P_o can be obtained either by direct measurement[15,16] or by indirect calculation[17]. The direct method has the advantages that neither iterative nor trial and error procedures are required and that only a single order of a reflection is required. The latter aspect may be of great practical importance; since the penetration depth depends on the Bragg angle, the reflection to be measured can be chosen in relation to the plating thickness applied to provide optimal information (thin plating: low order, thick plating: high order), as will be illustrated in section 4.

2.2. Elimination of the background

Commonly the intensities measured are corrected for background radiation by applying a linear interpolation between both extremeties of the intensity bands[6]. The background regions of a Cu/Ni bicrystal before diffusion-annealing are shown in Fig. 2. Note that the signs of the slopes of the background profile at both sides of each Bragg reflection are opposite, and that no constant background level is reached. Therefore a linear background is a poor approximation to the actual background profile. The type of background observed (Fig. 2) is characteristic for Thermal Diffuse Scattering (TDS).

TDS contributes significantly to the integrated intensities measured, as is illustrated by the following calculations of the ratio α (= integrated TDS intensity/integrated kinematical intensity) for copper and nickel in the 222 up to 555 MoKα line profiles at room temperature (Cu/Ni bicrystals and MoKα radiation were employed in this investigation as well as previous studies[6-8,10]). The results are gathered in table 1. These calculations are based on the approximate, analytical expression for first order TDS (higher order TDS can be neglected) derived by Nilsson for cubic single crystals[18]. The usefulness of the Nilsson approach was demonstrated by numerical calculations[19,20] and by experimental evidence[21].

In the following calculation of the background of an intensity band from a diffusion zone it is assumed that the background consists dominantly of TDS. Since the TDS-profile from each segment extends over the whole 2θ-range investigated, overlap should be taken into account. The background for segment i is determined by the total TDS contribution from all M segments, so we have

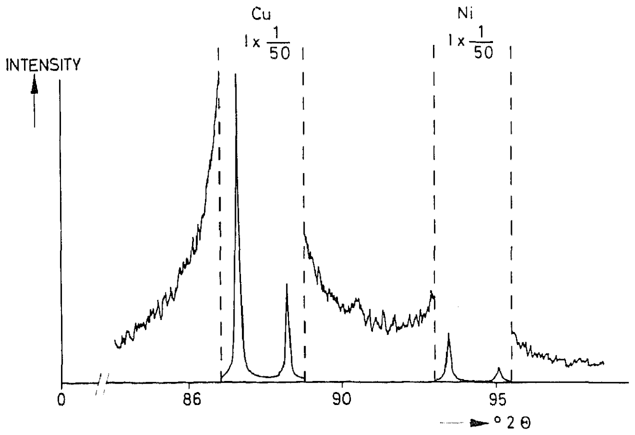

Fig. 2. The 444 MoKα intensity band recorded from a Cu/Ni bicrystal before diffusion-annealing. The intensity scale for the background regions is 50x larger than for the Bragg reflections. The TDS character of the background is less pronounced for Ni, since the integrated kinematical Bragg intensity and α are smaller (c.f. Table 1).

	integration range 2θ	α_{Cu} *in %*	α_{Ni} *in %*	*integration range 2θ*	α_{Cu} *in %*	α_{Ni} *in %*
222	1.08°	9.4	5.9	.54°	5.6	3.5
333	1.77°	21.0	13.1	.885°	12.6	7.8
444	2.79°	37.6	23.2	1.395°	22.5	13.9
555	4.97°	59.5	35.4	2.485°	35.6	21.1

Table 1.

The ratio α (= integrated TDS intensity/integrated kinematical intensity) for Cu and Ni at room temperature in the 222, 333, 444 and 555 MoKα line profiles according to Nilsson's formula[18]*. The elastic constants needed are taken from ref. 22. The 2θ integration ranges given are 1/2 and 1/4 respectively of the separation of the Cu and Ni Bragg positions. The ω integration range is 10°.*

$$b_i = \sum_{j=1}^{M} \alpha_{ij} P_j, \qquad (6)$$

where α_{ij} denotes the ratio of the integrated TDS intensity of segment j at the 2θ range of segment i to the integrated intensity P_j (without background b_j) of segment j. The α_{ij} values can be calculated from the Nilsson formula[18]. Because the P_j values are unknown, the b_i values cannot be determined directly. By assuming that the main contribution to TDS in segment j originates from segment j a first estimate of the background is obtained from

$$b_i^1 = \sum_{j=1}^{M} \frac{\alpha_{ij}}{1 + \alpha_{jj}} P_j^t, \qquad (7)$$

where P_j^t is the observed intensity (including background b_j) of segment j. Since the TDS profiles of the different segments overlap, b_i^1 is an overestimate. Then the following iterative method can be applied to determine the integrated intensities:

$$P_i^k = P_i^t - b_i^k \qquad (8a)$$

$$b_i^{k+1} = \sum_{j=1}^{M} \alpha_{ij} P_j^k \qquad (8b)$$

The correct values of b_i and P_i are approached alternatingly by under- and overestimates (k = 1, 2, ...). Calculations should be continued until all segments give rise to P_i or b_i values which differ less than an arbitrarily fixed fraction from the previous set obtained in the iterative procedure. It was found that normally 3-10 iterations (depending on the reflection considered) suffice if for any segment a 5% difference between the last two iterations is allowed.

In our opinion the calculation of the background in the manner proposed above gives a physically more sound base for the calculation of concentration profiles from X-ray diffraction line profiles than a linear interpolation procedure. This will be illustrated in section 4.

3. Experimental procedure

3.1. Sample preparation

Mechanically polished nickel monocrystals with a 111 surface were electropolished until they were microscopically flat and no deformation was detectable with optical and scanning electron microscopy and X-ray diffraction. Two types of specimens will be considered:

(i) Thick specimens (about 14 μm copper) were prepared by electrocrystallization of copper from a plating bath prepared and purified according to Schultze[23]. All electroplating was done under a plastic hood to prevent dust contamination. The current density applied was 0.5 mA/cm^2 (= about 100 Å/min). The thickness of the deposited layer was determined by an X-ray fluorescence technique[24].

(ii) Thin specimens (about 2 μm copper) were prepared by vapour deposition of copper in a bell jar in a vacuum of about 10^{-5} Torr. The thickness of the deposited film was measured with a Deposition Control Master Omni II (Sloan). The temperature of the nickel substrate was 250°C; the deposition rate was 100 Å/min.

The specimens were diffusion-annealed in a N_2 filled fused quartz capsule at temperatures in the range 550-925°C.

3.2. Diffractometry

Before and after interdiffusion occurred the intensity bands were stepscanned, applying MoKα radiation, with a Siemens ω-diffractometer equipped with a quartz crystal monochromator. Because of the mosaic structure of the sample, at each value of the angle 2θ, intensity measurements should be performed over a range of angles ω and χ, the ω axis being perpendicular to the diffractometer plane and the χ axis being in the plane of diffraction perpendicular to the ω axis. Integration over χ is established by removing the Soller slits thus allowing for $\pm 4^{o}$ axial divergence. Integration over ω is performed by rocking the crystal. The integrated intensity at each 2θ position was taken as the integrated intensity of the rocking curve. The rocking curves were measured in the following way: the angular velocity of the ω scan was automatically changed from 0.5 ^{o}/s to a lower velocity (usually 0.02 ^{o}/s) when the counting rate exceeded a predefined level, since the error due to counting statistics is lowered when counting time increases with counting rate[25].

Angle position correctionsdue to specimen displacement were performed according to Wilson[26]. The α_2 component was eliminated according to Delhez and Mittemeijer[27] and the ratio $R[= I_{\alpha_2}(\max)/I_{\alpha_1}(\max)]$ was determined for each intensity band[28]. The angle dependence of the Lorentz and polarization factors was corrected for[29]. The angle dependence of the structure factor was taken into account as $F = x F_{Ni} + (1-x)F_{Cu}$ where x is the atomic fraction nickel; the angle dependence of the structure factors F_{Ni} and F_{Cu} (and also the data for the corresponding Debije-Waller factors) were obtained from ref. 30.

4. Results and Discussion

In Fig. 3a the 555 $MoK\alpha_1$ intensity band of a specimen with a thick Cu layer (c.f. section 3.1) is shown after a diffusion anneal of 1 h at 925^{o}C. From the integrated intensities measured before interdiffusion it was found that for this specimen the orientation factor g = 1, indicating perfect epitaxy.

To calculate the concentration profile according to the direct method outlined in section 2.1 the intensity band was divided into 20 segments over the 2θ range between the pure copper and pure nickel positions, denoted by $2\theta_{Cu}$ and $2\theta_{Ni}$ respectively. The integrated intensity of each segment was determined. In accordance with the experience of Houska and co-workers[7] we found that

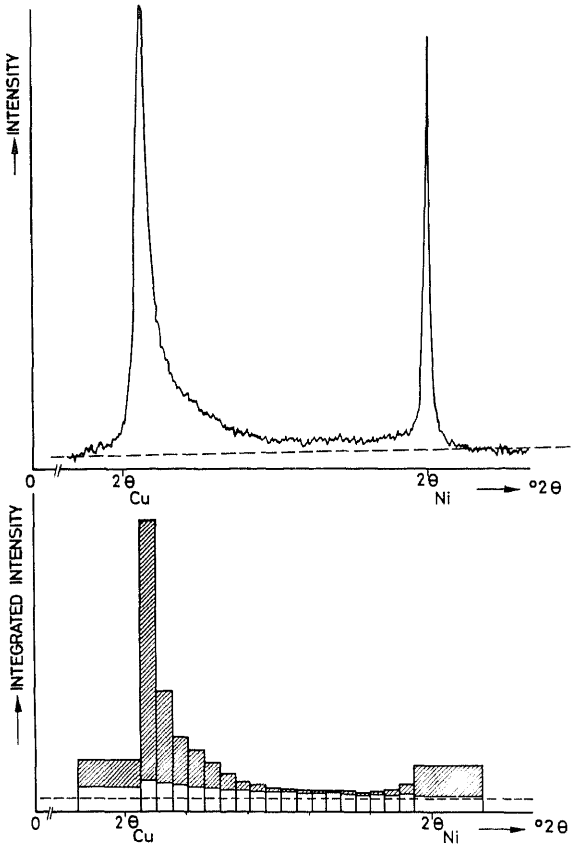

Fig. 3. (a): The 555 MoKα_1 intensity band recorded from a thick Cu/Ni bicrystal diffusion-annealed for 1 h at $925^{\circ}C$; a linear background is indicated; (b): the corresponding histogram of integrated intensities of the segments into which the intensity band is divided; the not hatched area represents the TDS background calculated; the background level as obtained from linear interpolation is also indicated; (c): the concentration profiles as calculated for the background corrections according to the TDS calculation (○) and the linear interpolation (△) respectively.

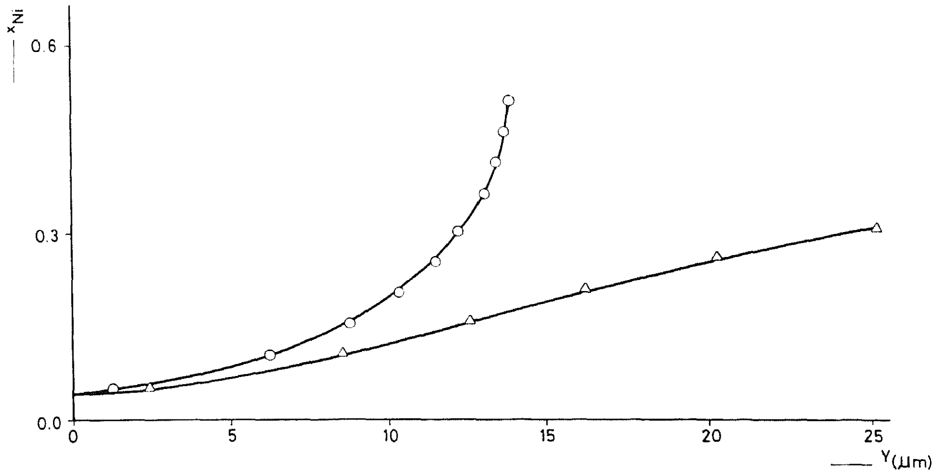

Fig. 3c. See opposite page for figure caption.

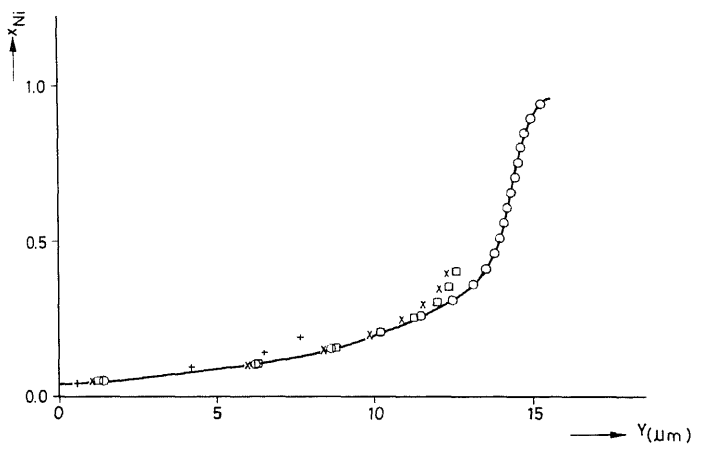

Fig. 4. The concentration profiles as calculated from the 222 (+), 333 (×), 444 (□) and 555 (○) MoKα_1 intensity bands for the Cu/Ni bicrystal diffusion-annealed for 1 h at 925°C. It should be noted, that the lower the order of the reflection the smaller part of the concentration profile which can be obtained reliably, owing to decreasing peneration depths of the X-rays.

purification of the measured profiles by deconvolution appeared unsuccessful. Therefore only α_2 elimination was employed which implies that some instrumental broadening remains in the profile and consequently intensity diffracted by material in the diffusion zone may be found outside the $2\theta_{Cu}$-$2\theta_{Ni}$ range. Since this will affect in particular the integrated intensities of the first and of the last segment[6], the integrated intensities of these two segments were obtained by integrations starting at $2\theta_{Cu}-\Delta 2\theta'$ and finishing at $2\theta_{Ni} + \Delta 2\theta'$ respectively where $\Delta 2\theta'$ was chosen as $0.15 \times (2\theta_{Ni}-2\theta_{Cu})$. The choice of $\Delta 2\theta'$ is arbitrary, provided that all the intensity diffracted by the material in the diffusion zone outside the $2\theta_{Cu}$-$2\theta_{Ni}$ range is included (see also below).

Next the integrated TDS background intensities were calculated according to the method proposed in section 2.2[31]. The results are presented in the form of a histogram in Fig. 3b. In this figure also the background level is indicated as obtained from a linear interpolation between the $(2\theta_{Cu}-\Delta 2\theta')$ and $(2\theta_{Ni}+\Delta 2\theta')$ positions.

The concentration profiles calculated from the integrated intensities corrected for the TDS background as well as corrected for the linear background are shown in Fig. 3c. A large discrepancy is observed. The results obtained by the linear background are inconsistent with the values of the diffusion coefficient[32] and the annealing time. Any linear background is arbitrary and lacks a physical basis (c.f. discussion of Fig. 2 in section 2.2).

Further evidence in favour of the TDS background correction can be obtained from Fig. 4 where the concentration profiles are plotted as calculated from the 222, 333, 444 en 555 intensity bands after elimination of the respective TDS background profiles. For this thick specimen it should be noted that the lower the order of the reflection the smaller the part of the concentration profile which can be obtained reliably, owing to decreasing penetration depths of the X-rays (This stresses the need for a method where the concentration profile is obtained from a single order of the reflection). It is seen from Fig. 4 that the results of the intensity bands coincide very well as far as penetration depths of the X-rays allow comparison.

It was found that large changes in $\Delta 2\theta'$ (100% or more) do not affect the concentration profiles calculated, indicating also that the method of the TDS background calculation is sound.

Fig. 5a shows the 222 $MoK\alpha_1$ intensity band of a specimen with a thin Cu layer (c.f. section 3.1) after a diffusion anneal of 16 h at 550°C. From the integrated intensities measured before interdiffusion it was found that the orientation factor $g = 0.70$ for the vapour deposited copper layer. For the calculation of the concentration profile it was assumed that g_m in eq. (5.6) was constant (0.70) for the segments in the region originally occupied by the pure copper layer (In the nickel region $g = 1$), because previous experiments did not show a concentration dependence of g[33]. The TDS background calculated is shown in Fig. 5b. Finally the concentration profile calculated is plotted in Fig. 5c together with the concentration profile calculated from the 333 intensity band. The results for both orders coincide satisfactorily especially in the surface region; at relatively large penetration depths some disagreement is observed. The result from the 222 intensity band, however, is considered to be the most reliable, since the TDS calculations revealed that in the 2θ region corresponding to the larger penetration depths about 60% of the diffracted intensity in the 333 intensity band is TDS, whereas this percentage is 25 for the 222 intensity band. With respect to the TDS background the 111 intensity band would be even more useful but the effects of instrumental broadening are too large. The 222 intensity band is the best compromise.

The fact that the vapour deposited layer is not as perfectly epitaxial as the electrocrystallized one[34] may have affected the shape of the concentration profile determined, especially at this relatively low annealing temperature (see also refs. 11 and 12). However a discussion on the diffusion process taking place is beyong the scope of the present paper[35].

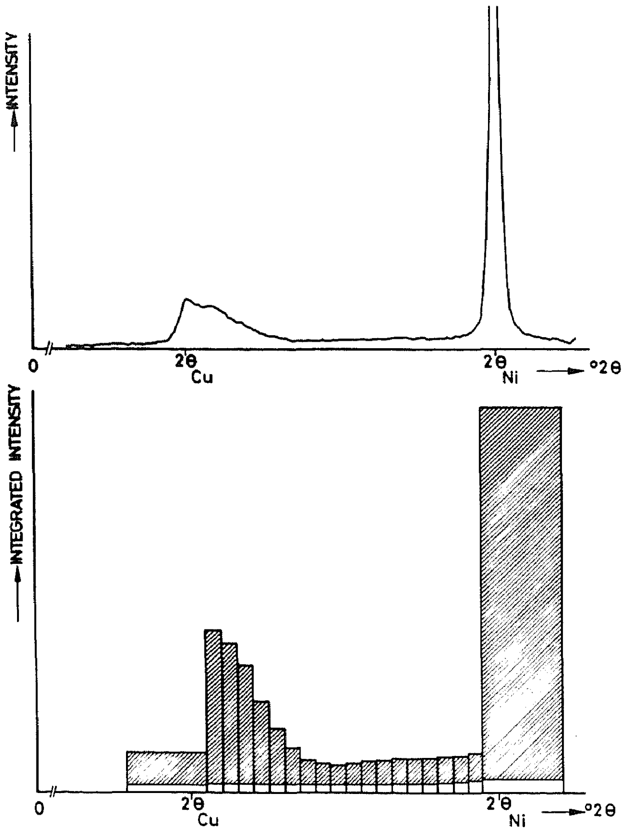

Fig. 5. (a): The 222 MoKα_1 intensity band recorded from a thin Cu/Ni bicrystal diffusion-annealed for 16 h at $550^{o}C$; (b): the corresponding histogram of integrated intensities of the segments into which the intensity band is divided; the not hatched area represents the TDS background calculated; (c): the concentration profiles as calculated from the 222 (+) and 333 (×) MoKα intensity bands.

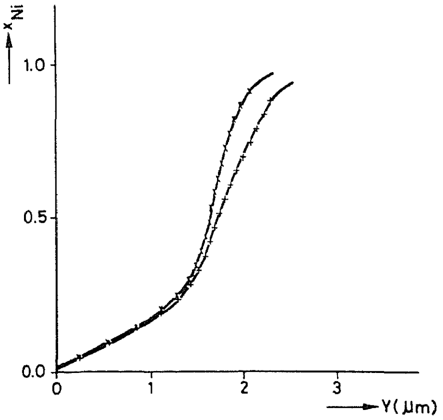

Fig. 5c. See opposite page for figure caption.

Concluding: (i) In practice a single order of the reflection may be selected which can be used most profitably for the calculation of the concentration profile. Hence a method which needs only one order of the reflection should be favoured. The direct method proposed in this paper avoids the trial and error calculations employed in the computer simulation method. (ii) The background mainly consists of TDS which can be eliminated according to section 2.2.

Acknowledgements

We are very much indebted to Professor C.R. Houska for a written discussion. Professor B. Okkerse and Dr. F.W. Schapink critically read the manuscript. Financial support of the Stichting voor Fundamenteel Onderzoek der Materie (F.O.M.) is gratefully acknowledged.

II.14

References and footnotes

1. B. Fisher and P.S. Rudman, J. Appl. Phys. 32 1604, (1961).
2. R.W. Heckel, Trans. ASM 57, 443 (1964).
3. R. Delhez, E.J. Mittemeijer and E.A. van den Bergen, J. Mat. Sci., in the press.
4. E.A. van den Bergen, R. Delhez and E.J. Mittemeijer, Phys. Stat. Sol. (a), in the press.
5. E.J. Mittemeijer and R. Delhez, to be published.
6. D.R. Tenney, J.A. Carpenter and C.R. Houska, J. Appl. Phys. 41, 4485 (1970).
7. J.A. Carpenter, D.R. Tenney and C.R. Houska, J. Appl. Phys. 42, 4305 (1971).
8. J. Unnam, J.A. Carpenter and C.R. Houska, J. Appl. Phys. 44, 1957 (1973).
9. J. Unnam and C.R. Houska, J. Appl. Phys. 47, 4336 (1976).
10. C.R. Houska, F. Dietrich and G. Subbaraman, Thin Solid Films 44, 217 (1977).
11. M. Murakami, D. de Fontaine and J. Fodor, J. Appl. Phys. 47, 2850 (1976).
12. M. Murakami and D. de Fontaine, J. Appl. Phys. 47, 2857 (1976).
13. B.E. Warren, X-ray Diffraction (Addison-Wesley, Reading, Mass., 1969).
14. Then for each segment m $\int_0^{y_m} \mu(y)dy$ can be determined from measurements of P_m from at least two orders of a reflection. Subsequently an iterative procedure can be employed to determine the concentration profile from the $\int_0^{y_m} \mu(y)dy$ data. This approximate expression for A_mV_m is also used in the computer simulation method.
15. D.R. Chipman, Acta Cryst. A25, 209 (1969).
16. O. Inkinen, Acta Cryst. A25, 214 (1969).
17. e.g. P_o (as well as the plating thickness) may be obtained from integrated intensity measurements before interdiffusion.
18. N. Nilsson, Arkiv för Fysik 12, 247 (1957).
19. M.J. Cooper and K.D. Rouse, Acta Cryst. A24, 405 (1968).
20. B.T.M. Willis, Acta Cryst. A25, 277 (1969).

21. M. Renninger in: J.B. Newkirk and G.R. Mallet (eds.), Adv. in X-ray analysis vol. 10, (Plenum Press, New York, 1967), p. 42.

22. K.H. Hellwege (Ed.) "Landolt-Börnstein Numerical Data and functional Relationships in Science and Technology", New Series, Group III, vols. 1 and 2 (Springer Verlag, Berlin, 1966, 1969).

23. W.A. Schultze, Thesis, Delft University of Technology (1970).

24. H.A. Liebhafsky and P.D. Zemany, Anal. Chem. 28, 455 (1956).

25. L.V. Azaroff, R. Kaplow, N. Kato, R.J. Weiss, A.J.C. Wilson and R.A. Young, X-ray Diffraction (Mc.Graw Hill, New York, 1974), p. 495.

26. A.J.C. Wilson, Elements of X-ray Diffraction (Addison-Wesley, Reading, Mass. 1970) p. 34.

27. R. Delhez and E.J. Mittemeijer, J. Appl. Cryst. 8, 609 (1975).

28. R. Delhez, Th.H. de Keijser and E.J. Mittemeijer, J. Phys. E, in the press.

29. R. Delhez, E.J. Mittemeijer, Th.H. de Keijser and H.C.F. Rozendaal, J. Phys. E 10, 784 (1977).

30. International Tables for X-ray Crystallography vols. III and IV, published for the International Union of Crystallography (The Kynoch Press, Birmingham, 1962, 1974).

31. The α-values for copper and nickel were calculated from Nilsson's formula[18] using the appropriate elastic constants[22]. For the alloys a linear interpolation between the copper and nickel α-values was used.

32. D.B. Butrymowicz, J.R. Manning and M.E. Read, J. Phys. Chem. Ref. Data 5, 103 (1976).

33. C.R. Houska, personal communication, 1977.

34. E.J. Mittemeijer, R. Delhez, R. van Rooijen and V. Hoyer, J. Cryst. Growth 36, 249, (1976).

35. R. Delhez and E.J. Mittemeijer, to be published.

III

Electron Diffraction Investigations of Diffusion-annealed Specimens

Transmission electron microscopical investigations of small diffusion zones yield information

- on the diffusion process from the change of the moiré spacing;
- on the microstructure of the diffusion zone.

Thin Solid Films, *41* (1977) 173–178

THE EFFECT OF INTERDIFFUSION ON MOIRÉ PATTERNS OF THIN BIMETALLIC FILMS

T. VAN DIJK* AND E. J. MITTEMEIJER
Laboratory of Metallurgy, Delft University of Technology, Rotterdamseweg, 137 Delft (The Netherlands)
(Received June 17, 1976; accepted August 24, 1976)

Observations are described of a diffusion-induced change in the spacing of moiré fringes from thin bimetallic films at low temperatures where the diffusion coefficients are small ($<10^{-15}$ cm^2 s^{-1}). Experiments were carried out with specimens consisting of a layer of approximately 400 Å Cu vapour deposited onto an electropolished Ni substrate approximately 1000 Å thick. After annealing in the electron microscope at different temperatures an increase in the average spacing M of the moiré fringes was observed. It was found that $1-M_0/M$ varies linearly with $t^{1/2}$, where M_0 is the original moiré spacing and t is the annealing time at a given temperature. According to a highly simplified model of electron diffraction the diffusion coefficient can be obtained from the slope of the $1-M_0/M$ *versus* $t^{1/2}$ plot. From experiments at 450 °C, 500 °C and 550 °C the frequency factor D_0 and the activation energy Q for diffusion were established: $D_0 = 0.2$ cm^2 s^{-1}, $Q = 54.6$ kcal mol^{-1}. These values are in good agreement with published data for volume diffusion in the Cu–Ni system at higher temperatures.

1. INTRODUCTION

The many applications of thin metal films in modern electronic devices enhance the interest in diffusion measurements at low temperatures where the diffusion coefficient is small ($<10^{-15}$ cm^2 s^{-1}). Recently Gupta[1] discussed critically various methods of determining such small diffusion coefficients, *e.g.* electrochemical serial sectioning, radioactivity monitoring on the front or back surface of the specimens and a microsectioning technique by Ar ion backsputtering; Gupta considers the last method to be the most versatile. All of these methods are destructive and/or require rather complicated techniques.

This paper reports an investigation of the relation between the diffusion process and the change in the moiré patterns of thin bicrystals observed in the electron microscope operating under standard conditions. In principle this technique is non-destructive.

Consider a thin film of metal A which is deposited epitaxially onto a substrate of metal B. It is well known[2,3] that in the case of parallel moiré patterns the spacing M_0 of the moiré fringes is given by

---

* Present address: Twente University of Technology, Enschede, The Netherlands.

$$M_0 = \frac{d_A d_B}{d_A - d_B} \tag{1}$$

where d_A and d_B are the spacings corresponding to the chosen reflections of crystals A and B.

This paper deals with variations in M_0 observed as a result of diffusion in bicrystals of Cu/Ni.

2. EXPERIMENTAL PROCEDURE

Nickel (99.999%; Johnson, Matthey and Co., Ltd.) was electropolished in a Tenupol (Struers) at −70 °C with a current density of 15 mA mm^{-2} in a solution of 6% perchloric acid in methanol. Most crystallites in the nickel foils were oriented with the (100) plane parallel to the surface.

Copper (99.999%; Johnson, Matthey and Co., Ltd.) was vapour deposited onto the electropolished nickel specimen in an ordinary bell-jar in a vacuum of about 10^{-5} Torr. The thickness of the deposited film was measured by a Deposition Control Master Omni II (Sloan). The temperature of the substrate during deposition was 250 °C; the deposition rate was 40 Å min^{-1}. Under these conditions perfectly epitaxial films were obtained. Usually approximately 400 Å of copper was deposited.

The moiré fringes were studied in a Philips EM300 electron microscope fitted with a heating stage and operating at 100 kV. The diffusion anneals were performed *in situ* in a vacuum of about 10^{-5} Torr with the electron beam turned off. The diffusion temperatures applied were 450 °C, 500 °C and 550 °C. Moiré fringes in bright field and in dark field were recorded for several areas of the specimen using a calibrated instrumental magnification of 126 000 ×.

3. RESULTS AND DISCUSSION

During annealing, the moiré patterns changed as a result of diffusion in the bicrystal. Ultimately the fringes disappeared. For example, fringe patterns were observed for up to 16 h at 500 °C.

The most striking feature of the moiré patterns was the increase in the average moiré spacing. In the following we shall treat only this aspect.

3.1. *Reproducibility of the measurements*

The moiré spacing was measured in several different areas before and after each diffusion anneal. Assuming that the moiré spacing after diffusion is constant, there are several experimental reasons for expecting some variation in the moiré spacing: (a) errors in the measurements on the photograph; (b) variations in the magnification factor of the microscope; (c) imperfections in the specimen which disturb the moiré pattern; (d) local thickness changes. Because of this, we found it necessary to determine the mean moiré spacing. Therefore for each diffusion experiment the results obtained for several areas, each consisting of 5–10 fringes, were averaged.

Several identical experiments were done to investigate the reproducibility. The mean (220) moiré spacings, together with the standard deviation and the number of areas for which the moiré spacing was measured, are given in Table I for three specimens subjected to an annealing treatment at 550 °C for 1 h in the microscope. Similarly the results for two specimens after an anneal for 2 h at 500 °C are shown in Table II. It can be concluded that the reproducibility of the mean moiré spacing is very satisfactory.

TABLE I

REPRODUCIBILITY OF THE MEAN (220) MOIRÉ SPACING *M*

Specimen	*M* (Å)	*s* (Å)	*n*
750409	60.00	2.01	9
750424	60.78	0.88	9
750612	60.69	0.64	6

Three experiments of 1 h at 550 °C (*s* is the standard deviation; *n* is the number of areas where the moiré spacing was measured).

TABLE II

REPRODUCIBILITY OF THE MEAN (200) MOIRÉ SPACING *M*

Specimen	*M* (Å)	*s* (Å)	*n*
750604	77.52	1.32	16
750626	77.78	2.70	6

Two experiments of 2 h at 500 °C (*s* is the standard deviation; *n* is the number of areas where the moiré spacing was measured).

3.2. *The moiré spacing as a function of the time of diffusion*

The results of all of our measurements at 500 °C are shown in Fig. 1 where $1 - M_0/M$ is plotted against $t^{1/2}$ (M is the mean moiré spacing after a time t of diffusion). From this figure a linear relationship between $1 - M_0/M$ and $t^{1/2}$ is observed, in agreement with the model to be presented in Section 4.

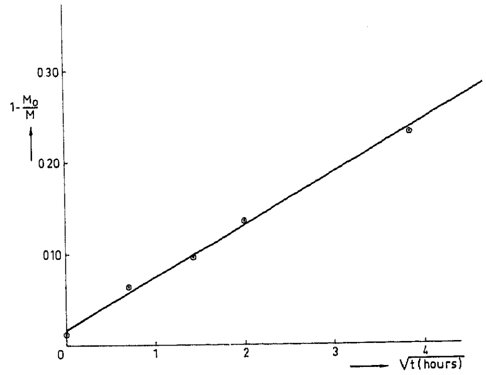

Fig. 1. $1 - M_0/M$ as a function of $t^{1/2}$ at 500 °C.

The line should pass through the origin ($M = M_0$ if $t = 0$), but this is not observed. This may be due to an error in the magnification factor of the microscope, which in this case may be too small. However, there could be another explanation. In calculating the moiré spacing M_0 before diffusion it was assumed that both lattices were not strained to reduce the misfit between them. Matthews[4] has already noted that all observed moiré spacings are too large compared with calculated values, thus indicating the presence of strain in the lattices to reduce misfit. If we interpret the difference between the observed and calculated moiré spacings as being caused by misfit relaxation, it follows from our measurements that the lattice parameter of each crystal is changed by 0.02 %, giving rise to a reduction of misfit of 1.5 %. The remaining 98.5 % is accommodated by misfit dislocations.

4. A MODEL

On annealing the bicrystal AB a diffusion zone will be created.

It is well known that networks of misfit dislocations are present in the interface of epitaxial bicrystals[4, 5]. After diffusion the misfit dislocations become distributed in the alloyed volume[6]. In the model of Vermaak and van der Merwe[7, 8] the misfit dislocations are distributed over subinterfaces in subzones after diffusion. However, this model does not allow us to calculate the displacement vector[9] after diffusion because it is not only a function of distance x along the operating reciprocal lattice vector but also of depth z in the diffusion zone.

We therefore propose the following simple model to describe the effect of interdiffusion on the moiré patterns. Before diffusion the specimen consists of a layer of thickness z_A of crystal A and a layer of thickness z_B of crystal B. After a certain time of diffusion there will be a concentration profile in the specimen. We assume that the diffusion coefficient is constant and hence the quantity of material that has crossed the interface is the same for both directions. To obtain an expression for the moiré spacing M after diffusion, we calculate the average spacings $\bar{d}_A$ and $\bar{d}_B$ in crystals A and B respectively. If Vegard's law holds,

$$\bar{d}_A = (1 - x_{B,A})d_A + x_{B,A}d_B \tag{2}$$

$$\bar{d}_B = (1 - x_{A,B})d_B + x_{A,B}d_A \tag{3}$$

where $x_{B,A}$ is the fraction of material B present in crystal A after a certain time of diffusion and $x_{A,B}$ is defined analogously. If the quantity m of material that has crossed the interface is expressed in distance units along the z axis, it follows that

$$x_{B,A} = m/z_A \qquad x_{A,B} = m/z_B \tag{4}$$

where in terms of the diffusion coefficient D and the time t of diffusion[10]

$$m = (Dt/\pi)^{1/2} \tag{5}$$

Since $\bar{d}_A\bar{d}_B \approx d_A d_B$ it follows that for the ratio M_0/M according to eqn. (1)

$$\frac{M_0}{M} = \frac{\bar{d}_A - \bar{d}_B}{d_A - d_B} \tag{6}$$

Finally, the combination of eqns. (2), (3), (4), (5) and (6) leads to

$$1-\frac{M_0}{M}=\left(\frac{1}{z_A}+\frac{1}{z_B}\right)\left(\frac{Dt}{\pi}\right)^{1/2} \tag{7}$$

From eqn. (7) it is concluded that a plot of $1-M_0/M$ *versus* $t^{1/2}$ should be a straight line. This corresponds very well with the experimental results (Section 3.2, Fig. 1). It also follows from eqn. (7) that the diffusion coefficient can be calculated from the slope of that straight line, provided that z_A and z_B are known.

5. CALCULATION OF THE DIFFUSION COEFFICIENTS

As remarked in Section 4, the diffusion coefficients can be calculated from eqn. (7) if the thicknesses z_A and z_B are known. The thickness of the copper layer is known from experiment. The thickness of the nickel layer is estimated at 1000 Å. This estimation is sufficiently accurate because the diffusion coefficient does not depend strongly on the value for the thickness of the nickel layer since this value is much larger than that of the copper layer. Furthermore, variations in the thickness of the layer are smoothed by the averaging procedure described before.

TABLE III

DIFFUSION COEFFICIENTS FROM EXPERIMENTS AT THREE DIFFERENT TEMPERATURES

T (°C)	D (cm^2 s^{-1})
450	2.33×10^{-18}
500	2.42×10^{-17}
550	2.23×10^{-16}

The diffusion coefficients calculated from our experiments at 450 °C, 500 °C and 550 °C are shown in Table III. It should be noted that results were available for only one time of diffusion at 450 °C and at 550 °C.

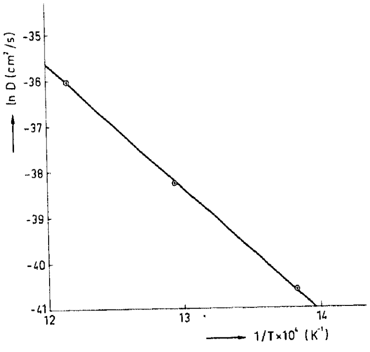

Fig. 2. Ln D as a function of $1/T$.

The temperature dependence of the diffusion coefficient is given by $D = D_0 \exp(-Q/RT)$, where D_0, Q, R and T are, respectively, the frequency factor, the activation energy, the gas constant and the absolute temperature. D_0 and Q can be obtained from a plot of ln D *versus* $1/T$. This is done for our experiments in Fig. 2. From the intercept and slope of the straight line we find

$$D_0 = 0.2\,\mathrm{cm^2\,s^{-1}} \qquad Q = 54.6\,\mathrm{kcal\,mol^{-1}}$$

It should be noted that the value for the slope of the straight line in Fig. 2, and hence the value of Q, is independent of the values used for z_A and z_B. The values obtained for D_0 and Q indicate that volume diffusion occurred and in fact are in agreement with the values for D_0 and Q found for volume diffusion at much higher temperatures[11].

Further work is in progress in order to investigate more details of this experiment.

ACKNOWLEDGMENTS

We are greatly indebted to Dr. R. Delhez and Dr. F. W. Schapink for stimulating discussions and to Professor B. Okkerse and Mr. A. M. Beers for reading the manuscript critically. We also thank Mr. H. Weerheijm for assistance with the vapour deposition experiments.

Financial support from the Stichting voor Fundamenteel Onderzoek der Materie (F.O.M.) is gratefully acknowledged.

REFERENCES

1 D. Gupta, *Thin Solid Films, 25* (1975) 231.
2 G. A. Bassett, J. W. Menter and D. W. Pashley, *Proc. R. Soc. London, Ser. A, 246* (1958) 345.
3 J. R. White, *J. Appl. Phys., 45* (1974) 588.
4 J. W. Matthews, *Philos. Mag., 6* (1961) 1347.
5 J. H. van der Merwe, in H. Herman (ed.), *Treatise on Materials Science and Technology*, Academic Press, New York, 1973, p. 1.
6 J. W. Matthews, *Thin Solid Films, 25* (1975) 199.
7 J. S. Vermaak and J. H. van der Merwe, *Philos. Mag., 10* (1964) 785.
8 J. S. Vermaak and J. H. van der Merwe, *Philos. Mag., 12* (1965) 453.
9 P. B. Hirsch, A. Howie, R. B. Nicholson, D. W. Pashley and M. J. Whelan, *Electron Microscopy of Thin Crystals*, Butterworths, London, 1971.
10 Y. Adda and J. Philibert, *La Diffusion dans les Solides*, Presses Universitaires de France, Paris, 1966, p. 136.
11 See, for example, the compilations of data in *Diffusion Data, 2* (1968) 271; *4* (1970) 440.

DISLOCATION WALL FORMATION DURING INTERDIFFUSION IN THIN BIMETALLIC FILMS

by

A.M. Beers and E.J. Mittemeijer

Laboratory of Metallurgy, Delft University of Technology
Rotterdamseweg 137, Delft, The Netherlands

Accepted for publication in Thin Solid Films.

III.16

Summary

TEM observations are described of the diffusion-induced behaviour of misfit dislocations originally present in the interface of thin bimetallic films. Experiments were carried out with specimens consisting of a layer of approximately 500 Å Cu vapour deposited onto an electropolished Ni substrate approximately 1000 Å thick. Diffusion anneals were performed *in situ* in the electron microscope at annealing temperatures in the range 450-600°C. The dislocation behaviour in Cu/Ni bicristals with originally a (100) interface was photographed and video-recorded. A cross-grid of misfit dislocations parallel to <110> directions was present in the original interface. The Burgers vectors were of type $\frac{1}{2}\underline{a}$ <110> lying in the interface. During diffusion the misfit dislocations became distributed in the diffusion zone. When $\sqrt{2Dt}$ (where D is the diffusion coefficient and t is the annealing time at a given temperature) exceeded a value of 40-50 Å, the dislocations started to align vertically forming dislocation walls along <110> directions parallel to the original interface. This resulted in a dislocation cell structure. Lengthwise the dislocation walls grew with shocks. The elastic strain energy of a finite edge dislocation array was estimated. Using this result an energy criterion for the formation of dislocation walls was derived. From this criterion it followed that dislocation wall formation may start to occur when $\sqrt{2Dt} \approx 45$ Å, in good correspondence with the experimental finding. Some additional observations of recrystallization phenomena during interdiffusion are reported.

1. Introduction

It is well known that networks of misfit dislocations can be found in the interface of epitaxial bicrystals[1,2]. On annealing the bicrystal a diffusion zone will be created. Matthews[3-5] concluded that the interfacial dislocations become distributed in the alloyed volume. From a theoretical point of view Vermaak and van der Merwe[6,7] suggested that the misfit dislocations in the diffusion zone may rearrange themselves into vertical alignment, thus forming dislocation walls. In interdiffused thin bicrystals fragments of dislocation walls have been observed only locally[8,9]. This paper deals with *in situ* observations of the diffusion-induced behaviour of the misfit dislocations in (100) Cu/Ni bicrystals, resulting in the formation of dislocation walls.

In general research on diffusion in thin metal films is of technological importance. In particular the study of the structure of the diffusion zone may eventually contribute to a better model to describe the broadening of the moiré spacings observed on annealing from which van Dijk and Mittemeijer[10] recently deduced diffusion coefficients.

2. Experimental procedure

In a vacuum of (1-2) 10^{-5} Torr copper (99.999%; Johnson, Matthey and Co., Ltd) was vapour deposited onto an electropolished[10] nickel (99.999%; Johnson, Matthey and Co., Ltd) specimen approximately 1000 Å thick. The temperature of the substrate during deposition was 250°C; the deposition rate was 60-100 Å/min. Under these conditions continuous, perfectly epitaxial copper films were obtained. The mean thickness of the deposited film was 485 ± 10 Å as measured with a quartz crystal oscillator (Deposition

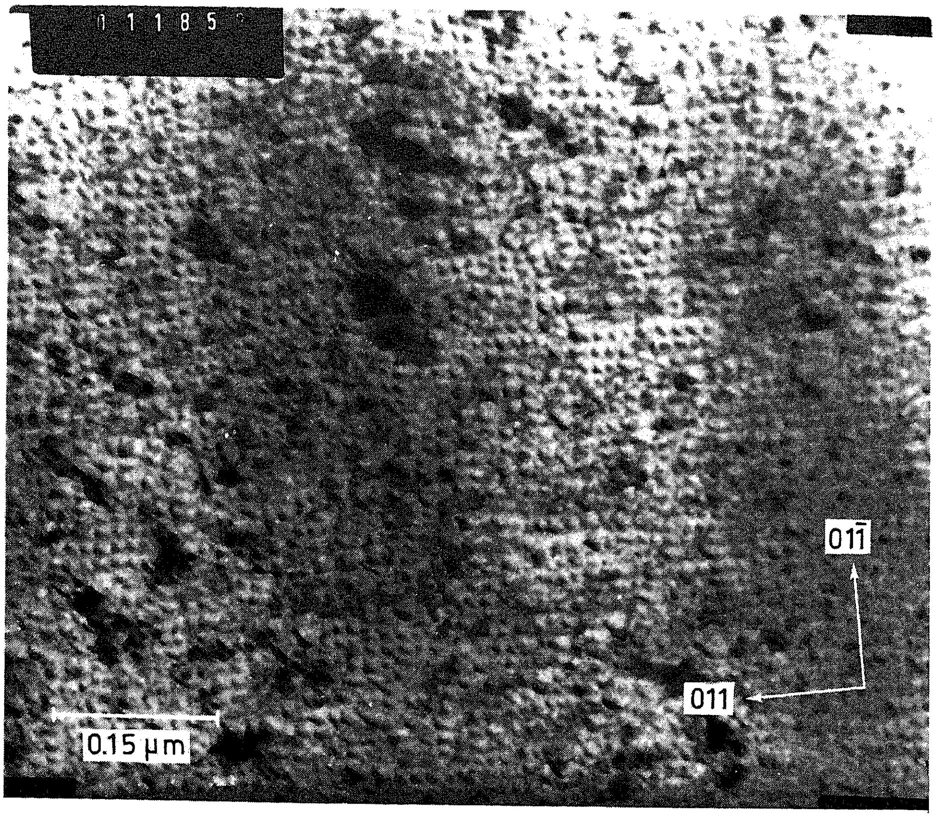

Fig. 1. Bright field image of (100) Cu/Ni bicrystal before interdiffusion. A practically square network of misfit dislocations along the <110> directions in the interface can be observed.

Control Master Omni II; Sloan) which was calibrated by quantitative neutron activation analysis of copper.

Diffusion anneals were performed *in situ* in the electron microscope (Philips EM 300 operating at 100 kV) by means of a calibrated heating stage in a vacuum of about 10^{-5} Torr. The annealing temperatures applied were in the range 450-600°C. The misfit dislocation configurations were recorded on photographic plates. Using a TV camera (Philips PW 6326) mounted in the microscope the dislocation behaviour could also be reproduced on a TV monitor and video-recorded (IVC 711).

3. Results and discussion

Using specimens with (100), (110), (211) and (310) interfaces, experiments were performed at different annealing temperatures with varying annealing times. In this section results concerning specimens with a (100) interface will be reported. Observations on specimens with the other interfaces have not been satisfactorily interpreted yet.

3.1. Misfit dislocations before interdiffusion

As can be seen from Fig. 1 misfit dislocations in the interface constitute a cross-grid with lines parallel to <110> directions. In an analogous way as performed by Matthews[5,11] the Burgers vectors were determined to be of type $\frac{1}{2}\,\underline{a}$ <110> lying in the interface. Thus these misfit dislocations are edge dislocations with Burgers vectors in the film plane (in this way the misfit is accommodated most efficiently).

In the literature on (100) Cu/Ni bicrystals there is disagreement concerning the Burgers vectors of the misfit dislocations: Burgers vectors

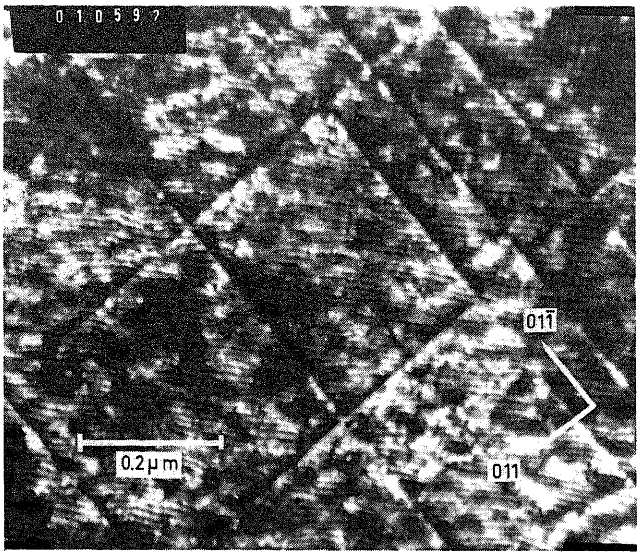

Fig. 2a. $00\bar{2}$ Dark field image of an interdiffused (100) Cu/Ni bicrystal (2h at 500°C). The bold lines along the <110> directions correspond to dislocation walls. The fringes parallel to a <100> direction constitute a (200) moiré pattern.

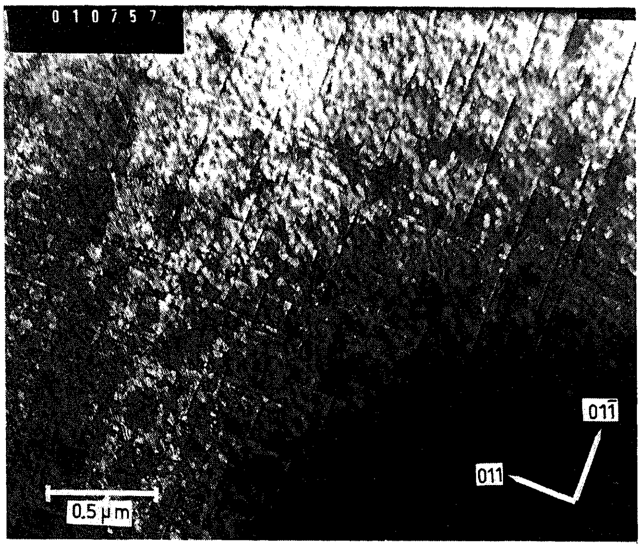

Fig. 2b. Bright field image of the same specimen as in Fig. 2a. In order to show that dislocation wall formation occurred over large areas a smaller magnification was applied.

lying in the interface have been found[11,12], as is the case with our specimens, as well as Burgers vectors inclined at 45° to the film plane[12]. For copper vapour deposited onto a nickel substrate recent experimental[12] and theoretical[13] results indicate the Stranski-Krastenov growth mode, a mechanism involving three-dimensional islands. Then, as suggested earlier by Shinohara and Hirth[14], the island dimension normal to the interface may be decisive for the dislocation structure obtained. If this normal dimension is large, before coalescence dislocations will glide into the interface in the interface plane, resulting in Burgers vectors lying in the interface; if the normal dimension is small, after coalescence dislocations will glide in from the free surface leading to the 45° dislocation structure.

Apart from the misfit dislocations, strain in the lattices may contribute to the accommodation of the misfit. In that case moiré spacings and misfit dislocation spacings larger than the "theoretical" ones are observed. In our Cu/Ni specimens it was found that about 11% of the misfit was accommodated by lattice strain, corresponding to an average misfit dislocation spacing of about 110 Å (instead of 99 Å "theoretical").

3.2. Dislocation wall formation during interdiffusion

From the theoretical work of Vermaak and van der Merwe[6,7] it is conceivable that a climb force exists promoting distribution of the dislocations in the diffusion zone. Vermaak and van der Merwe suggested that the misfit dislocations may rearrange themselves into vertical alignment, thus forming dislocation walls (c.f. Fig. 3a). This should lead to dislocation cells. In interdiffused thin Pd/Au[8] and Ag/Cu[9] couples fragments of dislocation walls have been observed only locally. To our knowledge no diffusion-induced dislocation cell formation in thin metal films has

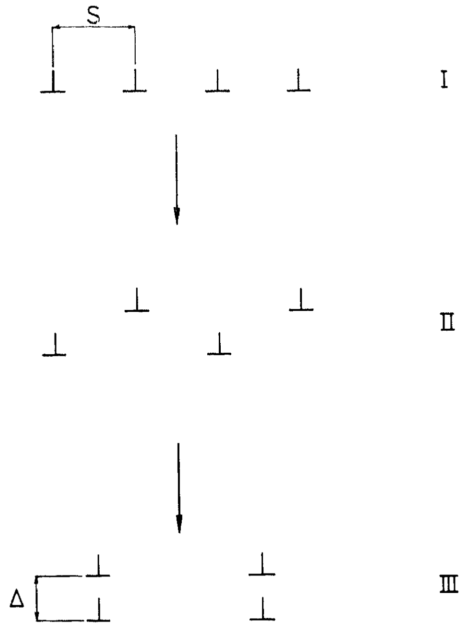

Fig. 3a.
This diagram schematically displays subsequent misfit dislocation configurations: before diffusion a cross-grid of misfit dislocations is present in the original interface (stage I); on annealing the misfit dislocations are distributed in the diffusion zone (stage II); a rearrangement into vertical alignment results in the formation of dislocation walls (stage III).

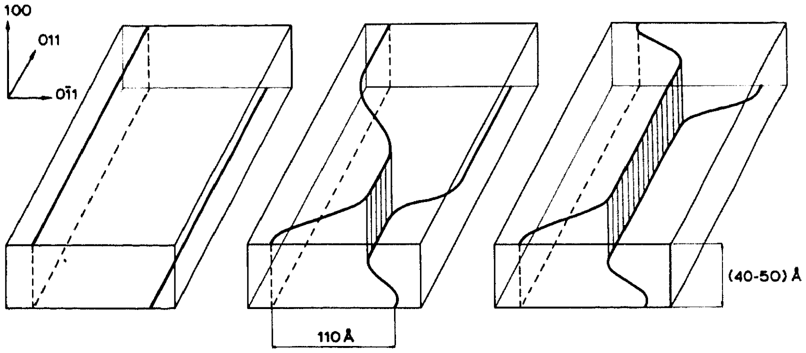

Fig. 3b.
Two dislocations lying along a <110> direction parallel to the original interface but at different depths in the diffusion zone align vertically part by part.

been reported yet. In our (100) Cu/Ni bicrystals we believe to have observed dislocation wall formation over the entire area investigated. In Figs. 2a and b the bold lines along the <110> directions parallel to the original interface correspond to the dislocation walls; the fringes parallel to a <100> direction form a (200) moiré pattern*. Using the diffusion coefficient D as calculated from the broadening of the average moiré-spacing[10,15] it was found that dislocation wall formation started when $\sqrt{2Dt}$ = (40-50)Å independent of temperature (t = annealing time). From this and from energy considerations to be presented in section 4 we believe the dislocation walls to be made up of two dislocations at this stage of interdiffusion. Unfortunately the dislocations in the wall could not be resolved separately because of the ferromagnetism of the electropolished nickel substrate and the small separation of the dislocations. However, the $\underline{g}.\underline{b} = 0$ criterion was successfully applied to confirm that the Burgers vectors of the dislocations in the wall were of type $\frac{1}{2}\,\underline{a}$ <110> and parallel to the original interface.

Video-recordings made during interdiffusion revealed that lengthwise growth of the dislocation walls occurred with shocks. A "zip"-wise growth mode is suggested where the two separate dislocations lying parallel but at different depths in the diffusion zone align vertically part by part (Fig. 3b).

3.3. Recrystallization during interdiffusion

As diffusion proceeded the growth of new grains was sometimes observed (Fig. 4). Most often these grains nucleated at the edge of the hole in the

---

* As compared to the dislocation walls, the misfit dislocations which are not arranged in walls, are difficult to observe (c.f. Figs. 1 and 2). It has been observed earlier that often the individual misfit dislocations give only small image contrast (c.f. Fig. 1 and Fig. 1 in ref. 1).

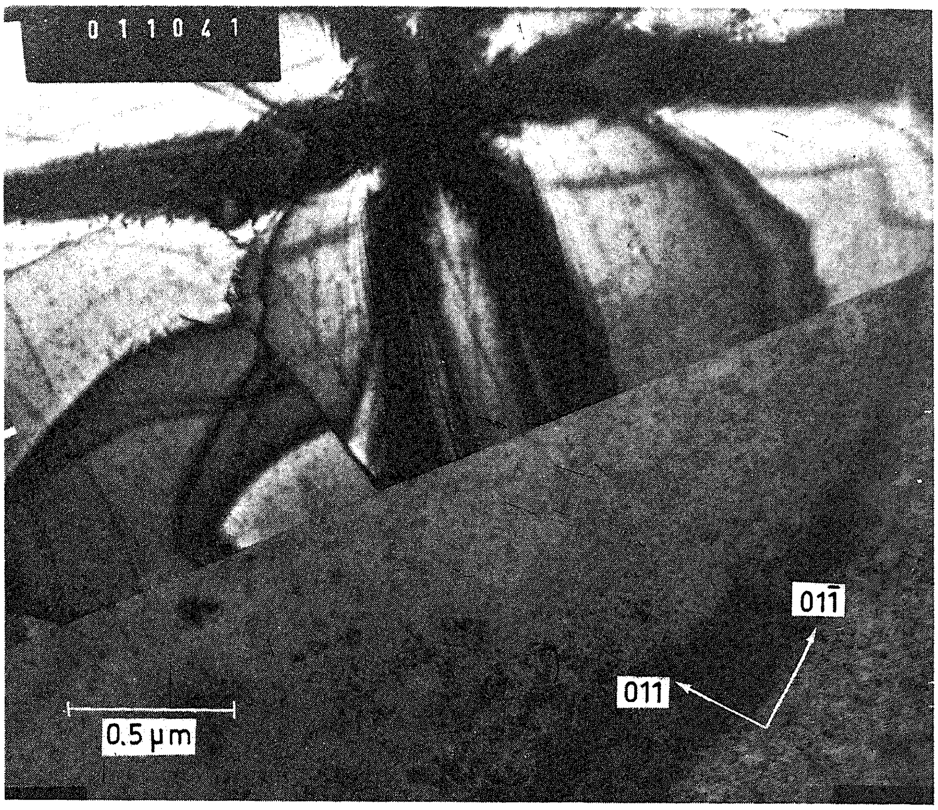

Fig. 4. Recrystallization. The upper side of this electron micrograph shows a new-formed grain after a diffusion anneal of 8h at 450°C (note the bend extinction contours indicating lattice curvature) while at the lower side the matrix can be observed. The orientation relationship between matrix and new grain is (100)//(110). In contrast with the matrix neither misfit dislocations nor moiré fringes can be observed in the new grain.

jet-electropolished specimen; a few times new grains developed at grain boundaries. The observation of new-formed grains at these places indicates that recrystallization in these specimens may occur at later stages of homogenization. The boundaries of these new grains advanced by leaps and bounds during grain growth. The bend extinction contours (c.f. Fig. 4) indicate lattice curvature of the new grain. This may be attributed to the misfit which still has to be accommodated for between upper and lower surfaces of the incompletely homogenized specimen[8]. This type of curved grains was also observed in Pd/Au[8] and Ni/Pd[5] thin bicrystals. It has been suggested[8] that the boundaries of the new grains are made up of the original misfit dislocations. Such dislocation walls, however, should be distinguished from the ones formed in the matrix as reported in section 3.2.

4. An energy criterion for dislocation wall formation during interdiffusion

It is assumed that on annealing all misfit dislocations become distributed by climb in a diffusion zone of magnitude $\sqrt{2Dt}$[16]. This is schematically represented in Fig. 3a. By estimating and comparing the energies of the dislocation configurations of stages II and III in this diagram the value of $\sqrt{2Dt}$ at which dislocation wall formation may start will be predicted.

Analogous to Vermaak and van der Merwe[6] the elastic strain energy* E_d per unit length of a single edge dislocation in an intermediate stage (II) may be approximated by the well-known expression[17]

$$E_d = \frac{\mu b^2}{4\pi(1-\nu)} \ln \frac{R_d}{r_o} \qquad (1)$$

---

* In comparing energies of different dislocation configurations the dislocation core energy does not play a role and is therefore omitted from the present discussion.

where μ and ν, the shear modulus and the Poisson ratio respectively, are considered to be constant; b is the magnitude of the Burgers vector; r_o is the radius of the core and R_d is the radius of the stress field which is taken as half the average dislocation spacing.

An expression for the elastic strain energy e_w per unit surface of a finite dislocation wall consisting of k edge dislocations with a spacing Δ has been derived in the Appendix [eq. (A-4)]. Then the elastic strain energy E_w per unit length of a single dislocation in stage III may be given by

$$E_w = \Delta . e_w = \frac{\mu b^2}{4\pi(1-\nu)} \{\frac{\Delta}{2} A(k,\Delta,R_w) + \ln \frac{e\Delta}{2\pi r_o}\} \qquad (2)$$

with $$A = \frac{1}{\Delta^2} (2L \ln \frac{R_w^2/4L^2+1}{1/k^2+1} + \frac{R_w^2}{2L} \ln \frac{R_w^2+4L^2}{R_w^2}) - \frac{1}{k\Delta} \ln(1+k^2)$$

where $2L(= k\Delta)$ is the height of the wall and R_w is the radius of the stress field of the wall.

The energy difference $\Delta E \equiv E_w - E_d$ equals zero when

$$\frac{\Delta}{2} A(k,\Delta,R_w) + \ln \frac{e\Delta}{2\pi} = \ln R_d \qquad (3)$$

In calculating the root Δ_c of this transcendental equation only estimations for the values of R_d and R_w have to be made. From the definition of ΔE and eq. (3) it follows that $\Delta E \leq 0$ when $\Delta \geq \Delta_c$. Hence, when $\sqrt{2Dt} \geq \Delta_c$ dislocation walls may be formed because they are energetically more favourable than a distribution of the dislocations throughout the alloyed volume. The existence of a minimal $\sqrt{2Dt}$ value for the start of wall formation is in agreement with experiment (c.f. section 3.2).

It should be recognized that in case e_w is approximated by using the expression for the infinite edge dislocation wall [eq. (A-3)] no such critical value Δ_c is found: the walls would always be more favourable energetically. This contradicts with expectation as well aswith our observations. Therefore reasonable results are only expected from eq. (3) where the expression for the finite edge dislocation wall is used.

Finally a numerical value for Δ_c will be presented. It is generally accepted[17] that energy calculations of dislocation configurations are inaccurate, because the radius of the stress field (i.e. in our case R_d,R_w) cannot be known exactly. However, because of the logaritmic dependence the energies are not very sensitive to changes in R. Usually approximations are made on the basis of the average spacing. For the formation of a dislocation wall from two original misfit dislocations (k = 2) it appears reasonable to estimate R_d by S/2 (S is the average misfit dislocation spacing before interdiffusion) and accordingly R_w by S. For our (100) Cu/Ni bicrystals with S = 110 Å one obtains Δ_c = 46 Å. Hence when $\sqrt{2Dt}$ exceeds this value dislocation wall formation may start. In view of the assumptions made the calculated value of $\sqrt{2Dt}$ is in surprisingly good correspondence with the experimental results (40-50 Å; section 3.2): only a rough estimation of this value is expected from the model used.

From the above it may also be understood why Shinohara and Hirth[14] did not observe dislocation wall formation in their interdiffused (100) Ni/Cu bicrystals: since the nickel layer thickness of their specimens was in range (15-70)Å the size of the diffusion zone may have been too small as compared to Δ_c. Also the presence of dislocation walls in interdiffused Pd/Au[8] and Ag/Cu[9] specimens can be understood because the respective diffusion zones were large enough as compared to Δ_c.

III.16

Acknowledgements

We are indebted to Ir. M. de Bruin of the Interuniversity Reactor Institute, Delft, for performing neutron activation analyses and to Mr. H. Weerheym for assistance with the vapour deposition experiments. Professor B. Okkerse, Dr. F.W. Schapink and Ir. R. Delhez critically read the manuscript.

Financial support of the Stichting voor Fundamenteel Onderzoek der Materie is gratefully acknowledged.

Appendix

The elastic strain energy of a finite edge dislocation array.

Consider a dislocation wall consisting of k evenly spaced edge dislocations (with spacing Δ) all of the same Burgers vector. The wall is perpendicular to the slip plane of each dislocation. A cartesian coordinate system (xyz) is chosen. The dislocations lie in the y-z plane parallel to the z-axis. The origin is chosen at the middle of the array.

For an infinite edge dislocation array (symmetrical tilt boundary) the stresses and the energy were calculated by Read and Shockley[18]. A finite edge dislocation array, however, has long range stresses which make the strain energy calculation somewhat complicated.

Li[19,20] demonstrated that when $x > \Delta$ the shear stress σ_{xy} can be approximated by

$$\sigma_{xy} = \frac{\mu b}{2\pi(1-\nu)} \frac{x}{\Delta} \left\{ \frac{y+L}{x^2+(y+L)^2} - \frac{y-L}{x^2+(y-L)^2} \right\} \qquad \text{(A-1)}$$

where μ is the shear modulus, b is the magnitude of the Burgers vector, ν is the Poisson constant and $L = k\Delta/2$. When $x < \Delta$ the shear stress resembles that of the infinite edge dislocation array.

According to a well-known procedure[17] the strain energy per unit surface of the wall follows from

$$e_w = \frac{b}{2} \frac{1}{2L} \int_{r_o}^{R_w} \sum_{n=1}^{k} \sigma_{xy_n} \, dx \qquad \text{(A-2)}$$

where r_o is the radius of the core and R_w is the radius of the stress field of the wall. Li calculated the strain energy of a finite edge dislocation wall by substituting σ_{xy} according to eq. (A-1) into eq. (A-2) for the whole range $r_o < x < R_w$. However, as eq. (A-1) is valid only when $x > \Delta$, we believe that a better approximation of the elastic strain energy of the wall is obtained by calculating the energy contributions e_1 and e_2, for the ranges $r_o < x < \Delta$ and $\Delta < x < R_w$ respectively, in the following way:

When $x < \Delta$ the shear stress can be approximated by that of the infinite edge dislocation array[20]. It can be easily shown that energy contributions of this shear stress are negligible when $x > \Delta$. Hence e_1 equals the expression of the strain energy of an infinite edge dislocation array[17]

$$e_1 = \frac{\mu b^2}{4\pi(1-\nu)} \frac{1}{\Delta} \ln \frac{e\Delta}{2\pi r_o} \qquad \text{(A-3)}$$

where e is the Naperian base.

After substituting eq. (A-1) into eq. (A-2) for the range $\Delta < x < R_w$, replacing the summation by an integration and adding the resulting e_2 to e_1, we eventually obtain for the total elastic strain energy of a finite edge dislocation array

$$e_w = \frac{\mu b^2}{4\pi(1-\nu)} [\tfrac{1}{2}\{\frac{1}{\Delta^2} (2L \ln \frac{R_w^2+4L}{\Delta^2+4L^2} + \frac{R_w^2}{2L} \ln \frac{R_w^2+4L^2}{R_w^2}) +$$

$$- \frac{1}{2L} \ln \frac{\Delta^2+4L^2}{\Delta^2} \} + \frac{1}{\Delta} \ln \frac{e\Delta}{2\pi r_o}] \qquad \text{(A-4)}$$

A consequence of the above mentioned procedure of Li[19] is that in his formulation with increasing Δ the strain energy of the finite edge dislocation array can become smaller than the strain energy of the infinite one*. This unrealistic behaviour of e_w does not occur applying our expression (eq. A-4), since e_2 approaches zero for increasing Δ as can be seen from Fig. A-1.

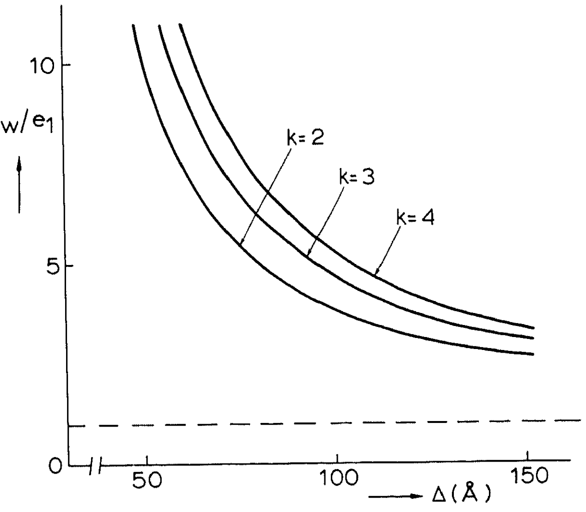

Fig. A-1. The ratio of the elastic strain energy of the finite edge dislocation wall to the one of the infinite edge dislocation wall (e_w/e_1) versus the dislocation spacing Δ for 2,3 and 4 dislocations in the finite dislocation wall. Calculations were performed with R_w = 1000 Å and r_o = 12.5 Å (≈ 5b for Cu/Ni specimens). The horizontal asymptote e_w/e_1 = 1 has been indicated (dashed line).

---

[*] It should be pointed out here that, as compared to our formulation, a further difference in the result of Li occurs because his formula accounts for the extra stresses which "eliminate the normal stresses in the cores of the dislocations and at the external surface". This does not alter however the objection mentioned above.

III.16

References

1. J.W. Matthews, Philos. Mag., 6(1961)1347.
2. J.H. van der Merwe, in H. Herman (ed.), Treatise on Materials Science and Technology, vol. 2, Academic Press, New York, 1973, p. 1.
3. J.W. Matthews, Philos. Mag., 8(1963)711.
4. J.W. Matthews, in M.H. Francombe and H. Sato (eds.), Single Crystal Films, Pergamon Press, New York, 1964, p. 165.
5. J.W. Matthews, Thin Solid Films, 25(1975)199.
6. J.S. Vermaak and J.H. van der Merwe, Philos. Mag. 10(1964)785.
7. J.S. Vermaak and J.H. van der Merwe, Philos. Mag. 12(1965)453.
8. J.W. Matthews and J.L. Crawford, Philos. Mag., 11(1965)977.
9. Y.G. Nakagawa and J.G. Greenfield, Acta Met., 21(1973)335.
10. T. van Dijk and E.J. Mittemeijer, Thin Solid Films, 41(1977)173.
11. J.W. Matthews, Surface Sci., 31(1972)241.
12. A. Chambers and D.C. Jackson, Philos. Mag., 31(1975)1357.
13. J.W. Matthews, D.C. Jackson and A. Chambers, Thin Solid Films, 26 (1975)129.
14. K. Shinohara and J.P. Hirth, Thin Solid Films, 16(1973)345.
15. A.M. Beers, E.J. Mittemeijer and R. Delhez, Proceedings of the International Conference on the Occasion of 50th Anniversary of the Discovery of Electron Diffraction, London, 19-21 September 1977, in the press.
16. W. Seith, Diffusion in Metallen, Springer Verlag, Berlin, 1955, p. 9.
17. J.P. Hirth and J. Lothe, Theory of Dislocations, Mc Graw-Hill Book Company, New York, 1968.
18. W.T. Read and W. Shockley, Phys.Rev., 78(1950)275.
19. J.C.M. Li, Acta Met., 8(1960)563.
20. J.C.M. Li, in G. Thomas and J. Washburn (eds.), Electron Microscopy and Strength of Crystals, Interscience Publishers, New York, 1963, p. 713.

EFFECTS OF INTERDIFFUSION ON THE MISFIT DISLOCATION CONFIGURATION AND THE MOIRÉ PATTERNS OF THIN BIMETALLIC FILMS

by

A.M. Beers, E.J. Mittemeijer and R. Delhez

Laboratory of Metallurgy, Delft University of Technology
Rotterdamseweg 137, Delft, The Netherlands

Accepted for publication in Proceedings of the International Conference on the Occasion of 50th Anniversary of the Discovery of Electron Diffraction, London, 19-21 September 1977.

III.17

Abstract

Effects of interdiffusion on the moiré patterns and misfit dislocation configurations as observed by TEM in thin bimetallic films are reported. With specimens consisting of a Cu layer vapour deposited onto an electropolished Ni substrate *in situ* diffusion experiments were carried out at 450 - 600 °C. On annealing (i) the average moiré spacing increased - from which diffusion coefficients were deduced - and (ii) the misfit dislocations, originally present as a square cross-grid in the (100) Cu/Ni interface, became distributed in the alloyed part of the bicrystal and formed dislocation walls, a process which eventually resulted in a three-dimensional dislocation cell structure. Comparing the elastic strain energies of a quasi-continuous distribution of the misfit dislocations in the diffusion zone and an arrangement in walls, an energy criterion for dislocation wall formation was formulated. It followed that wall formation may start when $\sqrt{2Dt} \simeq 45$ Å (where D is the diffusion coefficient and t is the annealing time), in good correspondence with the experimental finding at different temperatures.

1. Introduction

Reviewing special aspects of diffusion in thin films Balluffi and Blakely concluded, that "there is an urgent need for high resolution experiments which will yield detailed information regarding the fine structure and composition of the diffusion zone"[1]. In this context the development of methods for non-destructive *in situ* determination of diffusion coefficients at low temperatures is desired. The purpose of this contribution is (i) to relate the diffusion-induced change in the average moiré spacing to the interdiffusion process (section 3) and (ii) to study the behaviour of the misfit dislocations upon annealing (section 4).

2. Experimental

Thin epitaxial Cu/Ni bicrystals were prepared by vapour deposition of a continuous copper layer (usually about 485 Å thick) onto an electropolished[2] nickel substrate (approximately 1000 Å thick) as described elsewhere[3].

Diffusion anneals at 450, 475, 500, 550 and 600 °C were performed in the electron microscope (Philips EM 300). The microscope image was either photographed or video-recorded.

On each micrograph moiré fringes were measured at 5 or more sites where the fringe pattern was reasonably perfect over at least about 500 Å. The average moiré spacing M_t for each diffusion anneal was taken as the arithmetic mean of the average moiré spacing of N electron micrographs. Assuming that these N averages are distributed normally (standard deviation s), the standard deviation σ in M_t was determined: $\sigma = s/\sqrt{N}$. Experimental values of M_t, σ and N are shown in Table 1.

$T(^{\circ}C)$	450		475	500			550					600	
$\sqrt{t}(s^{\frac{1}{2}})$	120.0*	207.8*	134.2*	0	84.9	120.0	0	30.0*	54.8	73.5	84.9	0	60.0
N	8	8	8	15	10	6	7	6	7	10	7	23	2
M_t (Å)	162.5	166.1	163.7	158.7	164.4	169.2	162.0	163.4	182.6	186.3	191.0	157.9	246.7
σ (Å)	4.1	1.4	1.2	1.1	0.9	1.6	3.4	1.8	2.4	2.1	6.2	0.7	6.4
$D(cm^2/s)$	$2.45\ 10^{-18}$		$3.12\ 10^{-18}$	$7.15\ 10^{-18}$			$1.06\ 10^{-16}$					$1.26\ 10^{-15}$	

Table 1.

*Summary of experimental results: N is the number of micrographs; M_t is the average moiré spacing, converted into an imaginary (100) moiré spacing, after annealing time t; σ is the standard deviation in M_t; T is the temperature and D is the diffusion coefficient (c.f. section 2). * denotes, that in calculating D M_o = 157.2 Å (σ = 0.4 Å; N = 49) which is the average over all specimens.*

3. Determination of the diffusion coefficient from the increase of the average moiré spacing

During annealing the moiré patterns changed as a result of diffusion in the bicrystal. The most striking feature was the distinct increase in the average moiré spacing (up to 56% for 1h at 600 °C; c.f. Table 1).

Using a simple model[2] to interpret the increase in the average moiré spacing it followed that

$$1 - \frac{M_o}{M_t} = \left(\frac{1}{z_A} + \frac{1}{z_B}\right) \left(\frac{Dt}{\pi}\right)^{\frac{1}{2}} \qquad (1)$$

where z_A and z_B are the layer thicknesses before interdiffusion, D is the diffusion coefficient, t is the annealing time and M_o is M_t at $t = 0$. According to eq. (1) a plot of $1-M_o/M_t$ versus $\sqrt{t}$ should be a straight line passing through the origin*. This agrees with experimental finding as shown for 550 °C in Fig. 1.

After insertion of the appropriate values of z_{Cu} and z_{Ni} in eq. (1) the diffusion coefficients were calculated (see Table 1). The dependence of ln D on the reciprocal of the absolute temperature T is shown in Fig. 2. From this Arrhenius plot it is found that frequency factor $D_o = 180$ cm^2/s and activation energy $Q = 68.7$ kcal/mole for the straight line passing through the points for 500, 550 and 600 °C (correlation coefficient[4] 0.99995).

---

* In the calculation of $1-M_o/M_t$ previously[2] M_o was taken as the "*theoretical*" moiré spacing (139.7 Å) before interdiffusion.

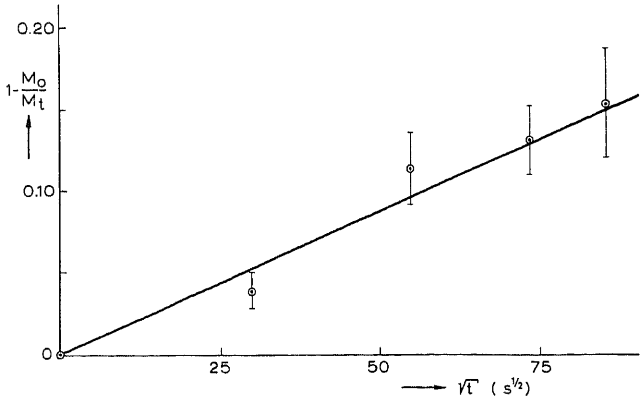

Fig. 1. $1-M_0/M_t$ versus $\sqrt{t}$ at 550^{0}C.

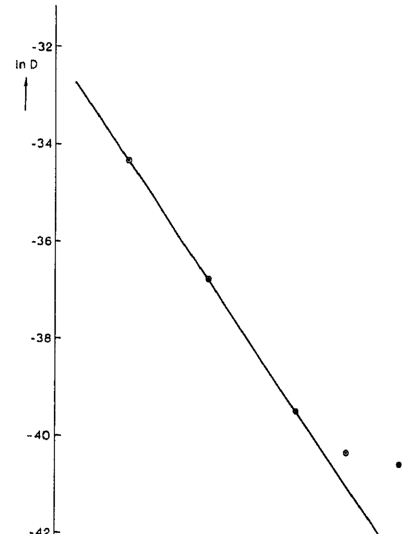

Fig. 2. ln D versus 1/T (D in cm^2/s).

For the data presented in Fig. 2 the average moiré spacings M_o and M_t were usually (Table 1) determined from the *same* specimen in order to prevent difficulties inherent in the use of different specimens (e.g. layer thickness differences; c.f. section 4). However, if these differences are considered negligibly small, a better estimate of M_o is obtained by averaging over all specimens. Then, in the same way as above, it is found that D_o = 39 cm^2/s and Q = 65.8 kcal/mole (correlation coefficient 0.99986).

It should be noted that according to the model used the slope of the straight line and hence the value of Q is independent of the values of z_A and z_B. The value obtained for Q indicates volume diffusion[5]. As can be seen from Fig. 2 the experimental results at 450 and 475 °C do not fall on the straight line observed for 500, 550 and 600 °C. It is proposed here that non-equilibrium vacancy concentrations and/or the presence of voids[6] in the vapour deposited layer contribute to this deviation: at lower annealing temperatures the influence of such defects will become increasingly important. A recent study[7] on diffusion in thin films indicates "time dependence" of diffusion coefficients, which was attributed to diffusion generated structure changes. Indeed, in terms of eq. (1), a "time dependent" diffusion coefficient (not included in Table 1) was found with one specimen diffusion annealed at 450 °C.

4. Formation of dislocation walls

Before interdiffusion the misfit dislocations in the (100) interface of the Cu/Ni bicrystals constituted a square cross-grid with lines parallel to <110> directions (Fig. 3a). The misfit dislocations were of edge character with Burgers vectors of type ½ a<110> lying in the interface. The average misfit dislocation spacing was found to be about 110 Å (c.f. 99 Å for unstrained lattices) indicating[8] that coherency strain in the

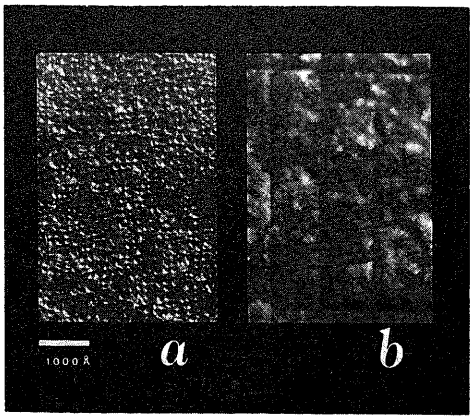

Fig. 3. $00\bar{2}$ Dark field image (a) of (100) Cu/Ni bicrystal before interdiffusion. The misfit dislocations form a practically square network. $00\bar{2}$ Dark field image (b) after a diffusion anneal of 2h at 500°C. The bold lines correspond to the dislocation walls. Also a (200) moiré fringe pattern can be observed clearly. The sides of both micrographs are along the <110> directions parallel to the original interface.

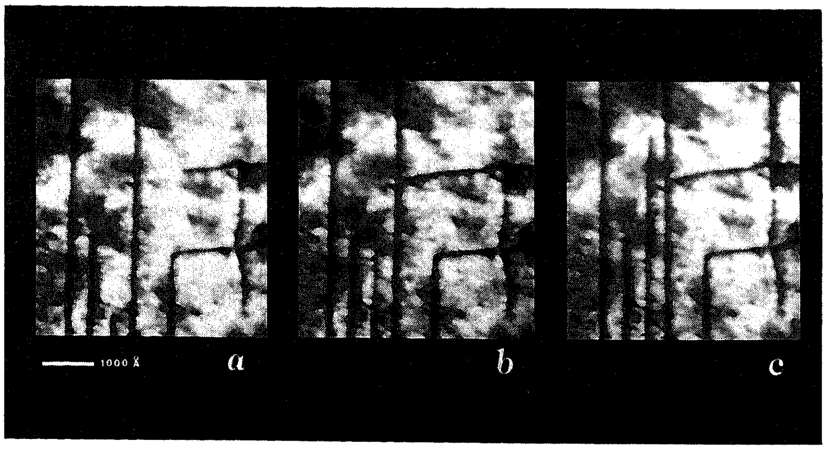

Fig. 4. Lenthwise growth of dislocation walls in a (100) Cu/Ni bicrystal at 550°C after 35 minutes. Consecutive photographs (video tape) were taken with time lapses of a few seconds. The sides of the photographs are along the <110> direction parallel to the original interface.

lattices accommodated about 11% of the misfit*.

Vermaak and van der Merwe[10] theoretically showed that during diffusion a climb force arises from the difference in atomic volume, which promotes distribution of the misfit dislocations in the diffusion zone†. They[9,10] suggested that the misfit dislocations may rearrange themselves into vertical alignment thus forming dislocation walls, a process which eventually should result in a three-dimensional dislocation cell structure. In interdiffused thin Pd/Au couples fragments of dislocation walls were observed only locally[12]. In our (100) Cu/Ni bicrystals we believe to have observed dislocation wall formation over the entire area investigated (c.f. Fig. 3b). Application of the $\underline{g}.\underline{b} = 0$ invisibility criterion confirmed that the dislocations in the wall were of edge character with Burgers vectors of type $\frac{1}{2}\underline{a}\langle 110\rangle$ parallel to the original interface. The dislocations in the wall could not be observed separately owing to their small separation (see below) and the ferromagnetism of the nickel substrate.

Video-recordings made during interdiffusion revealed that lengthwise growth of the dislocation walls occurred with shocks (see Fig. 4). This indicates that the dislocations lying parallel but at different depths in the diffusion zone aligned vertically part by part.

---

* As expected (c.f. ref. 13), with increasing thickness of the copper layer the coherency strain and hence the misfit dislocation spacing diminishes: z_{Cu} = 201 Å, S = 120 Å; z_{Cu} = 485 Å, S = 110 Å and z_{Cu} = 776 Å, S = 102 Å (corresponding to M_o values 172.2 ± 5.9 Å; 157.2 ± 0.4 Å and 147.1 ± 6.7 Å respectively).

† It should be noted that the literature is not conclusive in ascribing misfit dislocation behaviour during interdiffusion to a specific force (c.f. ref. 11).

Using the diffusion coefficient D as calculated from the increase of the average moiré spacing (see section 3), it was found that dislocation wall formation started when $\sqrt{2Dt} = (40-50)\mathrm{\AA}$ irrespective of temperature. This result is understood in the following way.

Let us consider the energy difference $\Delta E = E_w - E_d$ where E_w and E_d are respectively the elastic strain energies (per unit length edge dislocation) of the finite dislocation walls and of a quasi-continuous distribution of the misfit dislocations in the diffusion zone of magnitude $\sqrt{2Dt}$. An improved version of Li's approximation[14] for E_w has been derived elsewhere[3]. E_d can be approximated in the usual way[9,15]. For $\Delta E = 0$ it follows that

$$\frac{\Delta}{2} A(k, \Delta, R_w) + \ln \frac{e\Delta}{2\pi} = \ln R_d \qquad (2)$$

with
$$A = \frac{1}{\Delta^2} \left(2L \ln \frac{1+R_w^2/4L^2}{1+1/k^2} + \frac{R_w^2}{2L} \ln \frac{R_w^2+4L^2}{R_w^2}\right) - \frac{1}{k\Delta} \ln (1+k^2)$$

where k and Δ are respectively the number and spacing of the dislocations in the wall, $2L = k\Delta$ and R_w and R_d are the radii of the stress fields of the wall and of a dislocation in the quasi-continuous distribution respectively. From an energy point of view ($\Delta E \leq 0$) dislocation wall formation may start to occur when $\sqrt{2Dt} \geq \Delta_c$, where Δ_c is the root of transcendental eq.(2). For the formation of a dislocation wall from two misfit dislocations (k=2) it appears reasonable to estimate R_d by S/2 and accordingly R_w by S. For our (100) Cu/Ni bicrystals with S = 110 Å follows $\Delta_c = 46$ Å. Hence when $\sqrt{2Dt}$ exceeds this value dislocation wall formation may start. This calculated value agrees surprisingly well with the experimental results: only a rough estimate is expected from the model used.

Acknowledgements

We are indebted to Professor B. Okkerse and Dr. F.W. Schapink for critically reading the manuscript.

Financial support of the Stichting voor Fundamenteel Onderzoek der Materie (F.O.M.) is gratefully acknowledged.

References

1. Balluffi, R W and Blakely J M 1975 Thin Solid Films 25 363.
2. van Dijk T and Mittemeijer E J 1977 Thin Solid Films 41 173.
3. Beers A M and Mittemeijer E J Thin Solid Films in the press.
4. Freund J E Mathematical Statistics 1962 Prentice Hall.
5. E.g. the compilations in 1968 Diffusion Data 2 271 and 1970 4 440.
6. Lloyd J R and Nakahara S 1977 J.Vac.Sci.Technol. 14 655
7. Houska C R, Dietrich F and Subbaraman G 1977 Thin Solid Films 44 217.
8. Matthews J W 1961 Phil.Mag. 6 1347.
9. Vermaak J S and van der Merwe J H 1964 Phil.Mag. 10 785.
10. Vermaak J S and van der Merwe J H 1965 Phil.Mag. 12 453.
11. Beers A M and Mittemeijer E J 1978 Thin Solid Films 50 in the press.
12. Matthews J W and Crawford J L 1965 Phil.Mag. 11 977.
13. Kuntze R, Chambers A and Prutton M 1969 Thin Solid Films 4 47.
14. Li J C M 1960 Acta Met. 8 563.
15. Hirth J P and Lothe J 1968 Theory of Dislocations McGraw-Hill Book Company New York p. 78.

MODIFICATION OF INTERFACES IN THIN EPITAXIAL BIMETALLIC FILMS DURING INTERDIFFUSION

by

A.M. Beers and E.J. Mittemeijer

Laboratory of Metallurgy, Delft University of Technology
Rotterdamseweg 137, Delft, The Netherlands.

Accepted for publication in Thin Solid Films.

III.18

Abstract

With regard to the research on diffusion-modified interfaces in thin epitaxial bimetallic films some unsolved problems are identified and possible future directions of research are indicated.

1. Introduction

The many applications of thin metal films (e.g. electronic devices, metal coatings) enhance the interest in the diffusion-induced changes in these specimens: understanding of interdiffusion and diffusion related effects[1] is essential to product improvement.

Only a relatively small number of papers[2-13] is concerned with the theoretical and experimental aspects of diffusion-modified interfaces in thin bimetallic films, whereas "there is an urgent need for high resolution experiments which will yield detailed information regarding the fine structure and composition of the diffusion zone"[1].

The purpose of this communication is to identify some unsolved problems and to contribute to a discussion of the kind of work needed to attain future achievements.

2. Some unsolved problems

(i) Interface at the start of interdiffusion. Models set up for the description of the original interface deviate from practical situations in various respects[14]. In particular it is uncertain whether the assumption of an abrupt transition at the interface before the interdiffusion intended occurs, is correct:a pre-alloyed layer, a few atomic distances thick, might be present[15,16].

(ii) Misfit dislocations during interdiffusion. It is well known that arrays of misfit dislocations can be found in the interface of epitaxial bicrystals[17]. From the literature the following forces exerted on these misfit dislocations during interdiffusion canbe distinguished:

(a) the homogeneous force resulting from the difference in atomic volume[5,7];

(b) the force due to coherency strain (i.e. the strain associated with the misfit not accommodated by the misfit dislocations)[10].

(c) the osmotic force related with non-equilibrium concentrations of vacancies generated during diffusion (Kirkendall effect)[3,8];

(d) The image forces corresponding with the specimen surface boundary conditions[8];

(e) the dislocation interaction forces[5,7,8].

The different authors do not agree in ascribing the misfit dislocation behaviour to one (or more) of the forces mentioned and no treatment on the simultaneous operation of all these forces has been performed. Further, the total experimental evidence appears to be conflicting.

As diffusion proceeds, according to the theoretical work of Vermaak and van der Merwe[4,5] a climb force exists promoting distribution of the misfit dislocations in the diffusion zone. This has been experimentally confirmed[2,6,11]. On the other hand Shinohara and Hirth[8] state that such a dispersion of the dislocations in the alloyed volume is prevented by the interwoven nature of the dislocation network and by the attracting, restoring forces which come into play if a dislocation is slightly displaced from the network. Experimentally they indeed found the original misfit dislocation network to move as a whole[9]. Matthews[10], however, attributed the movement of misfit dislocation arrays as a whole to the force caused by the coherency strain.

(iii) Formation of dislocation walls. Vermaak and van der Merwe[5] suggested that at a certain stage of interdiffusion it may become energetically favourable for the original misfit dislocations, remaining parallel to the interface plane, to align vertically (i.e. parallel to the diffusion direction). Fragments of such dislocation walls were observed locally in interdiffused thin Au/Pd bicrystals[6]. Recent experiments[12,13] showed dislocation wall formation, resulting in a three-dimensional cell structure, to occur over large areas in interdiffused thin Cu/Ni bicrystals.

Various criteria for the start of wall formation have been proposed:

(a) It has been argued[6,11] that if the line joining adjacent parallel misfit dislocationsof edge character makes an angle of more than 45° to the interface plane, a glide force may cause the dislocations to arrange vertically above one another. This implies that the diffusion zone should at least be as large as the original misfit dislocation spacing S.

(b) According to van der Merwe[18] a separation of approximately S/4 (measured perpendicular to the original interface) would suffice.

(c) Comparing the strain energies of a quasi-continuous distribution of the misfit dislocations and an arrangement in walls, an energy criterion for dislocation wall formation was formulated[13]. For $S \approx 100$ Å it followed that wall formation may start to occur when the diffusion zone is approximately S/2.

(iv) Recrystallization phenomena. On annealing the growth of new grains was observed[6,11]. No misfit dislocations were found in the new-formed grains; to accommodate the misfit still present the grains were curved. Matthews and Crawford[6] considered the grain boundaries of the new grains to be made up of the original misfit dislocations; it was assumed that such new grains developed by lateral boundary displacements from dislocation cells as mentioned before. Recent *in situ* experiments[13] showed boundary motion to occur by leaps and bounds, and also the orientation of the matrix was not conserved, which is unlikely to agree with the above model for grain growth.

As compared to "normal" recrystallization behaviour, the formation of these new grains at later stages of homogenization suggests that interdiffusion stimulates the nucleation and growth of new grains. However, stresses arising from the experimetal set-up (e.g. specimen mounting) may influence nucleation and growth of these grains too.

3. Future directions of research

(i) Instrumental techniques. Transmission electron microscopy is one of the most powerful techniques for obtaining experimental data on the structure of the diffusion zone[19]. It is expected that micro-diffraction (for example to determine orientation changes caused by misfit dislocation wall formation) and video-recording or similar continuous techniques(to study the misfit dislocation behaviour on annealing *in situ*) will still intensify the application of TEM in this field of research.

X-ray topography may become more important, although the determination of Burgers vectors can be difficult[20]. With the advantage of thehigh intensity of synchrotron radiation this technique may especially become more attractive for *in situ* experiments.

X-ray diffraction line profile analysis does not provide a detailed structure of the diffusion zone, but the mosaic structure can be revealed, as has been done recently[21,22].

(ii) Specimen preparation. To test theoretical predictionsthe specimens used in experiments should be compatible with the requirements imposed by the models proposed. Usually this condition is not satisfied. Most specimens were prepared by vapour depositing both components. This technique is known to bring along many lattice defects which influence the structure of the diffusion zone obtained as well as the diffusion velocity. To reduce the number of lattice defects the following techniques are considered to be promising:

(a) Thin bicrystals can be obtained by vapour depositing one component onto a thin jet-electropolished substrate of the other component.

Using Cu/Ni bicrystals prepared in this way, more regular dislocation walls were formed during interdiffusion[13] and smaller diffusion coefficients were found[23,12] as compared to other results[6,9].

(b) Thin bicrystals may be obtained (c.f. ref. 24) from the constituting single crystals as grown in a gel by chemical reduction[25].

Until now the specimens investigated in the electron microscope all possessed an original interface perpendicular to the electron beam. This implies that the events in the diffusion zone are registered in projection onto a plane parallel to the original interface. Fruitful information may be obtained from experiments with specimens where the original interface is parallel to the electron beam (also micro-diffraction along the concentration profile will then be possible).

(iii) Theory. From section 2 it is evident that it is necessary to obtain a theory covering all phenomena in such a way that the results of diffusion anneals can be adequately predicted. Until now theories were developed fitting the experimental data obtained in a single study. In particular the theory should include the diffusion-induced behaviour of inefficient misfit dislocations (i.e. no pure edge character) as well as of coincidence misfit dislocations[26,27] occurring in interfaces with large misfit.

Two other points deserve special interest.

(a) Li[28-30] already performed calculations on the stress field of a finite edge dislocation wall and its interactions with separate dislocations. These calculations seem especially appropriate for dislocation interactions in the misfit dislocation configurations obtained on annealing, but in this field of research they did not get the attention deserved. It is expected that the complicated dislocation configurations present in the diffusion zone can only fully be handled numerically by employing elaborate computer modeling techniques, in contrast with theprevious analytical approaches.

(b) One way of model testing consists of comparing the image contrast observed in the electron microscope with that predicted by numerically solving the Howie-Whelan equations of dynamical diffraction theory[31]. Such calculations were carried out to predict the image contrast of misfit dislocations in the original interface of bicrystals[32]. Application of this technique to interdiffused thin bicrystals may be fruitful.

(iv) Relation with diffusion coefficient determinations. With regard to the study of the structure of the diffusion zone the development of non-destructive *in situ* methods for determination of diffusion coefficients at low temperatures is very important. Using a highly simplified model of electron diffraction it was possible to obtain an average diffusion coefficient from the broadening of the moiré spacing on annealing[23,12]. According to a suggestion of Shinohara and Hirth[9] it may even be possible to measure interdiffusivity by mathematical analysis of the intensity across a moiré fringe. Otherwise, analysis of the intensity profile of electron diffraction "spots" of both components involved may be possible and become as powerful as X-ray line profile analysis[21] in obtaining concentration-distance curves. As far as such techniques enable to obtain information on the concentration profile in the specimen, an alternative approach will be available to study the structure of the diffusion zone.

Acknowledgements

We are indebted to Professor B. Okkerse, Dr. F.W. Schapink and Ir. R. Delhez for critically reading the manuscript.

Financial support of the Stichting voor Fundamenteel Onderzoek der Materie (F.O.M.) is gratefully acknowledged.

References

1. R.W. Balluffi and J.M. Blakely, Thin Solid Films, 25 (1975) 363.
2. J.W. Matthews, in M.H. Francombe and H. Sato (eds.), Single Crystal Films, Pergamon Press, New York, 1964, p. 165.
3. J.P. Hirth, op. cit., p. 173.
4. J.S. Vermaak and J.H. van der Merwe, Philos. Mag., 10 (1964) 785.
5. J.S. Vermaak and J.H. van der Merwe, Philos. Mag., 12 (1965) 453.
6. J.W. Matthews and J.L. Crawford, Philos. Mag., 11 (1965) 977.
7. P.G. Winchell, J. Boah and P.S. Ayres, J. Appl. Phys., 42 (1971) 2612.
8. K. Shinohara and J.P. Hirth, Philos. Mag. 27, (1973) 883.
9. K. Shinohara and J.P. Hirth, Thin Solid Films, 16 (1973) 345.
10. J.W. Matthews, Scripta Met., 8 (1974) 505.
11. J.W. Matthews, Thin Solid Films, 25 (1975) 199.
12. A.M. Beers, E.J. Mittemeijer and R. Delhez, Proceedings of the International Conference on the Occasion of 50th Anniversary of the Discovery of Electron Diffraction, London, 19-21 September 1977, in the press.
13. A.M. Beers and E.J. Mittemeijer, Thin Solid Films, in the press.
14. J.W. Matthews (ed.), Epitaxial Growth, part A & B, Academic Press, New York, 1975.
15. D.W. Pashley, Adv. in Phys., 14 (1965) 327.
16. H. Mayer, in H.G. Schneider and V. Ruth (eds.), Advances in Epitaxy and Endotaxy, VEB Deutscher Verlag für Grundstoffindustrie, Leipzig, 1971, p. 63.
17. J.W. Matthews, in J.W. Matthews (ed.), Epitaxial Growth, part B. Academic Press, New York, 1975, p. 559.
18. J.H. van der Merwe, in H. Herman (ed.), Treatise on Materials Science and Technology, Academic Press, New York, 1973, p. 1.

19. C. Goux, J. of Microscopy, 102 (1974) 241.

20. S. Mader, A.E. Blakeslee and J. Angilello, J. Appl. Phys., 45 (1974) 4730.

21. J.A. Carpenter, D.R. Tenney and C.R. Houska, J. Appl. Phys., 42 (1971) 4305.

22. J. Unnam, J.A. Carpenter and C.R. Houska, J. Appl. Phys., 44 (1973) 1957.

23. T. van Dijk and E.J. Mittemeijer, Thin Solid Films, 41 (1977) 173.

24. J.G. Erlings and F.W. Schapink, Scripta Met., 11 (1977) 427.

25. P. Kratochvil, B. Sprusil and M. Heyrovskey, J. Cryst. Growth, 3 (1968) 360.

26. J.W. Matthews, IBM Res. Rep. R.C. 4266 (1973) No. 19084.

27. R.W. Vook and C.T. Horng, Philos. Mag., 33 (1976) 843.

28. J.C.M. Li, Acta Met. 8 (1960) 296.

29. J.C.M. Li, Acta Met. 8 (1960) 563.

30. J.C.M. Li, in G. Thomas and J. Washburn (eds.), Electron Microscopy and Strength of Crystals, Interscience Publishers, New York, 1963, p. 713.

31. P.B. Hirsch, A. Howie, R.B. Nicholson, D.W. Pashley and M.J. Whelan, Electron Microscopy of Thin Crystals, Butterworths, London, 1971.

32. G.C. Weatherly and T.D. Mok, Surf. Sci. 31 (1972) 355.

IV

Epitaxial Growth of Copper Layers onto a Nickel Single Crystal Substrate

With a view on the preparation of specimens suitable for the diffraction studies the morphology, epitaxy and twinning are investigated for copper layers either electrocrystallized or vapour deposited onto a 111 nickel substrate.

THE INITIAL STAGES OF ELECTROCRYSTALLIZED COPPER LAYERS ON A 111 NICKEL SURFACE

by

R. Delhez, E.J. Mittemeijer and W. Smid
Laboratory of Metallurgy, Delft University of Technology
Rotterdamseweg 137, Delft, The Netherlands

Acta Cryst., A31 (1975) Part S3, S212.

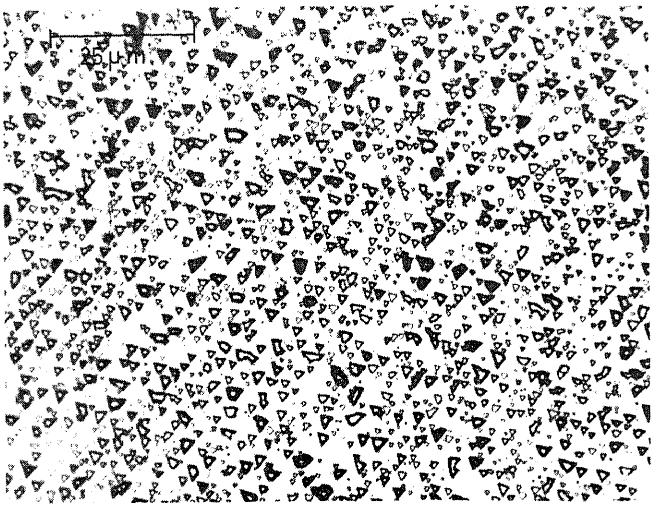

Fig. 1. Optical micrograph. Mean thickness: about 0.5 μm; current density: about 0.5 mA/cm^2.

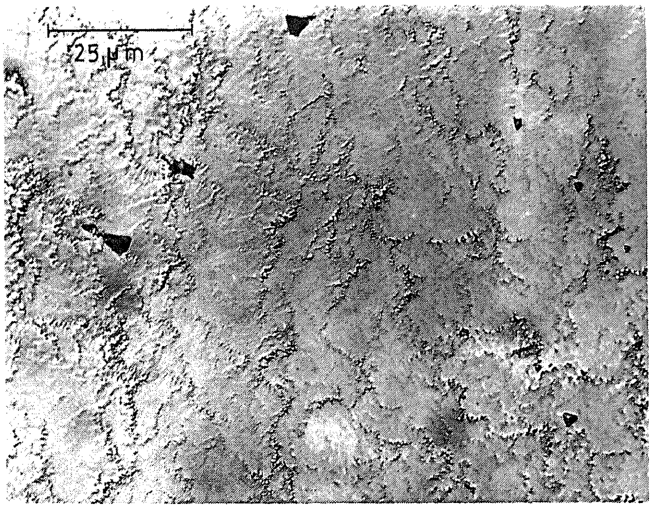

Fig. 2. Optical micrograph. Mean thickness: about 14.8 μm; current density: about 0.5 mA/cm^2.

After mechanical polishing nickel monocrystals were electropolished until no deformation was detectable. The copper bath was prepared and purified according to Schultze (Schultze, W.A. (1970). Thesis Delft University of Technology, p. 44, p. 58). The morphology and epitaxy of the copper layers (less than 10 μm thick) were investigated by optical and scanning electron microscopy and X-ray diffraction. The thickness of the deposit was determined using an X-ray fluorescence technique.

At current densities of about 0.5 mA/cm^2 the nuclei were truncated trilateral pyramids with the edges of the base plane parallel to 110 directions *(Fig. 1)*. These nuclei appeared to coalesce as has been observed with vapour deposition (Pashley, D.W. (1965). Adv. in Phys. 14, 327). The closed layers (after ≈ 1μm) were mirror-like *(Fig. 2)*. Oscillation photographs showed that the deposit was perfectly epitaxial, even for a layer of 5.3 μm. Rocking curves showed that the mosaic structure of the substrate was preserved by the deposit. Schultze studied layers 20-1000 μm thick and did not observe this phenomenon.

At current densities of about 1 mA/cm^2 nuclei of the type mentioned were still observed although frequently with truncated corners *(Fig. 3)*. As the current density increased, the tendency for coalescence became less and the growth of isolated nuclei became more dominant. The resulting layer was dull and non-epitaxial growth could be observed as thickness increased *(Fig. 4)*. At a thickness of 1.1 μm a reasonable fraction of the deposit was epitaxial, but at a thickness of 5.5 μm this fraction had decreased considerably, indicating that the fraction of epitaxial material is determined by nucleation and growth.

At current densities of about 1.5 mA/cm^2 two shapes of nuclei were dominant: (i) rods with mainly 110 directions *(Fig. 5)* and (ii) crystallites with fivefold symmetry *(Fig. 6)*. The scanning electron micrograph *(Fig. 7)* shows an icosahedron with carved edges, which has not been observed before. This phenomenon may be explained as follows. Initially the misfit in crystallites

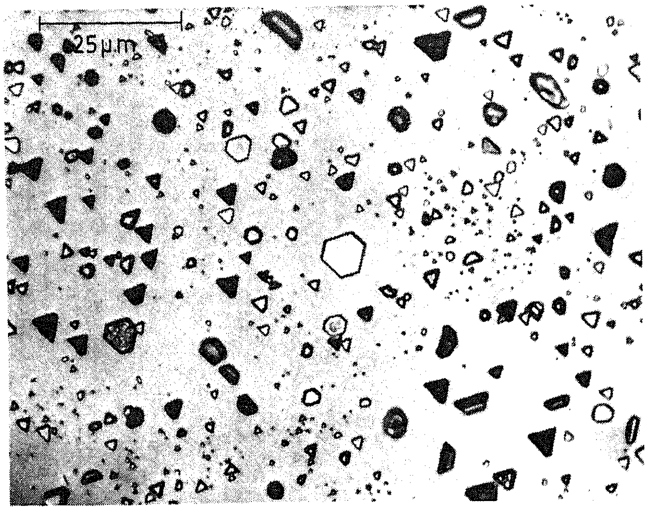

Fig. 3. Optical micrograph. Mean thickness: about 0.5 μm; current density: about 1 mA/cm^2.

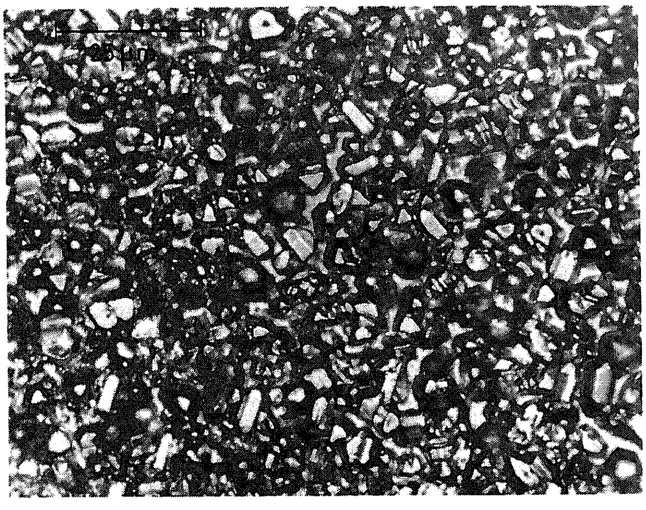

Fig. 4. Optical micrograph. Mean thickness: about 8 μm; current density: about 1 mA/cm^2.

with fivefold symmetry produces lattice strain (Allpress, J.G. & Sanders, J.V. (1970). Aust. J. Phys. 23, 23). The misfit is distributed throughout the particles by a relaxation of the f.c.c. structure of every tetrahedral building unit. We suppose that the carves on the edges of the icosahedra are formed while the crystal grows as a consequence of the relaxation of the lattice strain. An icosahedron becomes more and more a conglomerate of unstrained tetrahedra with the f.c.c. copper structure. The epitaxy was very imperfect for all thicknesses.Nevertheless there was still a tendency to fit the substrate.

Fig. 5. Optical micrograph. Mean thickness: about 1 μm; current density: about 1.5 mA/cm^2.

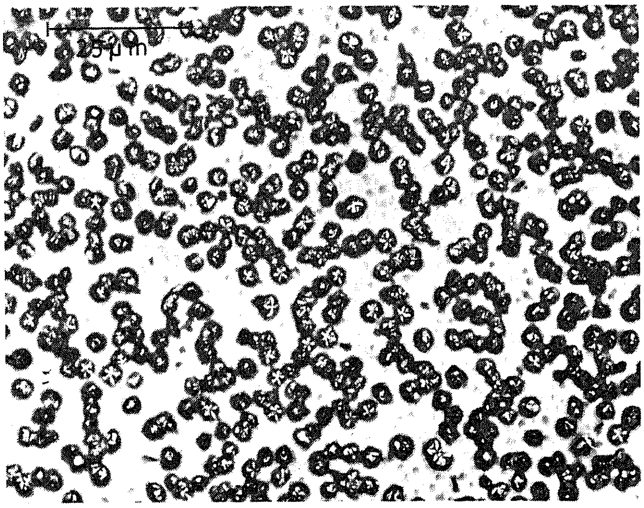

Fig. 6. Optical micrograph. Mean thickness: about 1 µm; current density: about 1.5 mA/cm^2.

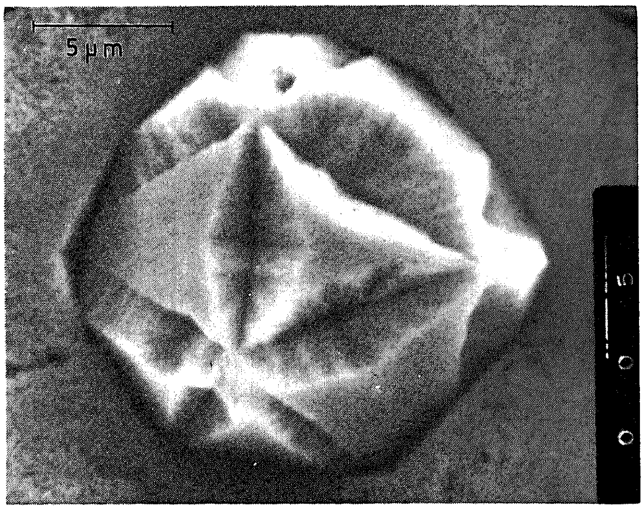

Fig. 7. Scanning electron micrograph showing icosahedron with carved edges. Current density: about 1.5 mA/cm^2.

Journal of Crystal Growth 36 (1976) 249–254
© North-Holland Publishing Company

ON TWINNING IN CRYSTALLIZED COPPER LAYERS ON A 111 NICKEL SURFACE

E.J. MITTEMEIJER, R. DELHEZ, R. VAN ROOIJEN and W. HOYER
Laboratory of Metallurgy, Delft University of Technology, Rotterdamseweg 137, Delft, The Netherlands

Received 19 July 1976; revised manuscript received 23 August 1976

The occurrence of twinning in the formation of copper layers on a 111 nickel surface has been investigated quantitatively both for electrodeposition and for crystallization from the vapour phase. The orientation relationships between deposit and substrate were determined from 200 pole figures. At current densities of ~0.5 mA/cm^2 nucleation copied the substrate or occurred in twin position with respect to the substrate 111 plane. At current densities of about 1.5 mA/cm^2 (repeated) twinning occurred at 111 planes not parallel to the substrate 111 plane. It was found that (repeated) twinning occurred only if the twin planes made an angle >45° with the surface of the substrate. This result was supported by a computer simulation of the 200 pole figures. Crystallization from the vapour phase showed the same features. However, in spite of a lower deposition rate, vapour deposition produced less perfect copper layers as compared to electrocrystallization. In addition it was found for both deposition techniques that a small fraction of the copper crystallized with a 100 plane parallel to the substrate 111 plane.

1. Introduction

The role of twinning on the formation of texture during the electrodeposition of metals has often been underestimated [1]. Recently Schultze [2,3] – investigating the electrodeposition of copper onto copper monocrystal substrates – stressed the dominance of twinning in the formation of textured deposits. However, no quantitative description of the process could be given, because only optical microscopy and an X-ray back reflection technique were used.

This paper reports preliminary results on the experimental quantitative determination of the orientation relationships between a copper deposit and a 111 nickel substrate. The results of Schultze will be related to the present results. Also the deposition of copper onto 111 nickel from the vapour phase is investigated.

2. Experimental procedure

After mechanical polishing nickel monocrystals with a 111 surface were electropolished until they were microscopically flat and no deformation was detectable.

The copper plating bath was prepared and purified according to Schultze [2]. All electroplating was done under a plastic hood to prevent dust contamination. Current densities applied were in the range 0.5–1.5 mA/cm^2 (100–300 Å/min). The thickness of the deposited layers (less than 10 μm thick) was determined using an X-ray fluorescence technique [4].

The vapour deposition experiments were performed in a bell jar in a vacuum of about 10^{-5} Torr. The thickness of the deposited film was measured by the Deposition Control Master Omni II (Sloan). The temperature of the substrate was 250°C; the deposition rate was 40 Å/min.

To obtain the orientation relationships between deposit and substrate pole figures were determined according to the Schulz reflection technique [5] applying CuKα radiation. To exclude coincidence of poles of different types of twins 200 pole figures were used. Special attention has been paid to the slit arrangement of the Siemens texture goniometer used to obtain the best resolution possible in the pole figure [6]. The measured intensities were corrected for background radiation, defocussing effects and absorption in the deposited layer by a computer program. Finally the pole figure was plotted according to the method of Love [9].

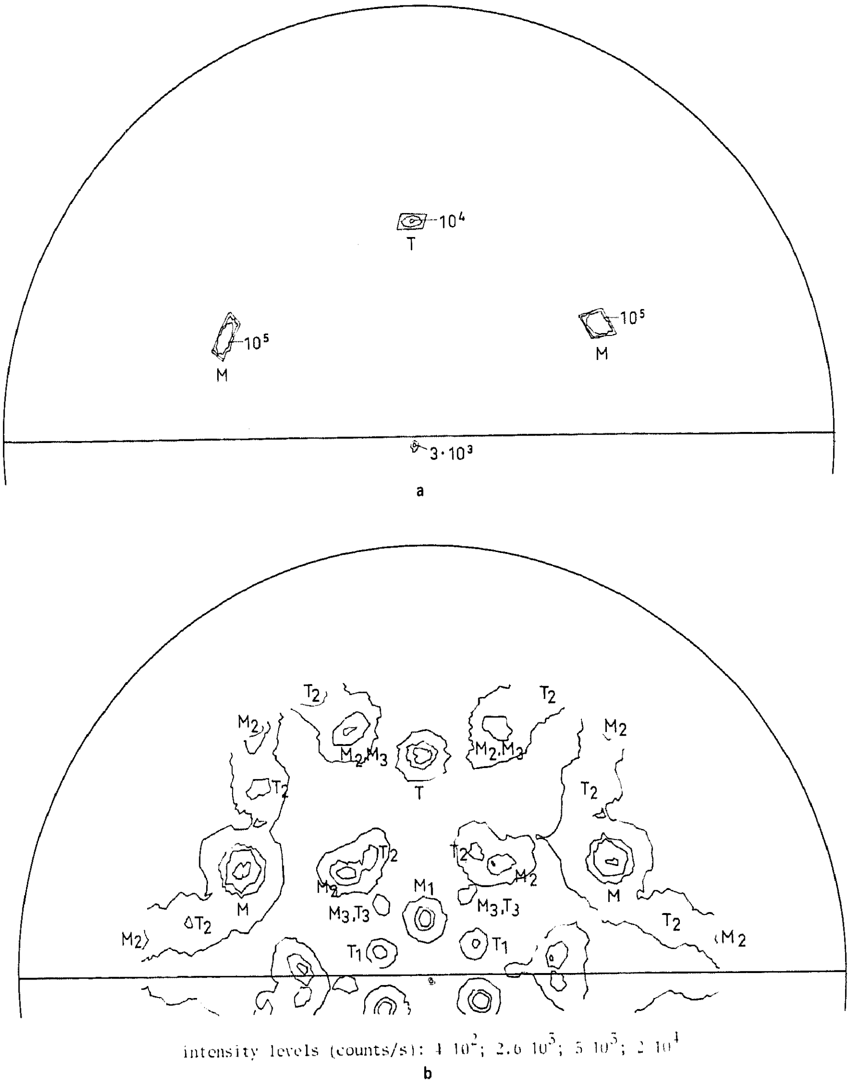

Fig. 1. The 200 pole figures of copper layers of 5 μm electrodeposited onto a 111 nickel surface at 0.5 mA/cm^2 (~100 Å/min) (a) and at 1.5 mA/cm^2 (~300 Å/min) (b). For symbols M and T, see text. A subscript *i* implies an *i*th order twin. Measurements were made up to 70° from centre.

3. Results and discussion

Recently Delhez, Mittemeijer and Smid [8] classified the deposits of copper on a 111 nickel crystal face according to the morphology. They distinguished three types occurring at current densities of ~0.5, ~1, and ~1.5 mA/cm^2.

The 200 pole figures of a member of the first type – a specimen with a layer of 5 μm thickness prepared at 0.5 mA/cm^2 – and of a member of the third type – a specimen with a layer of 5 μm thickness prepared at 1.5 mA/cm^2 – are shown in figs. 1a and b respectively.

In fig. 2, M denotes the positions of the 200 poles when the copper crystals copy the 111 nickel substrate. T denotes the positions of the 200 poles of the copper crystals in twin position with respect to the 111 nickel surface.

Comparing figs. 1a and 2 it can be seen that

Table 1
In this table the percentages of crystal types M and T and of their primary twins – M$_1$ and T$_1$ respectively – are given; the relative quantities in this table were derived from integrated intensities of the respective regions in the pole figures according to Jetter, McHarque and Williams [7]; the presence of higher twins is neglected, but this does not influence the volume ratios

Specimen	M (%)	T (%)	M$_1$ (%)	T$_1$ (%)	100 nuclei (%)
Electrocrystallized at 0.5 mA/cm^2; 5 μm	90	9	0	0	0.6
Electrocrystallized at 1.5 mA/cm^2; 5 μm	41	11	37	11	0.2
Vapour deposited at 40 Å/min; 1 μm	30	8	46	15	0.2

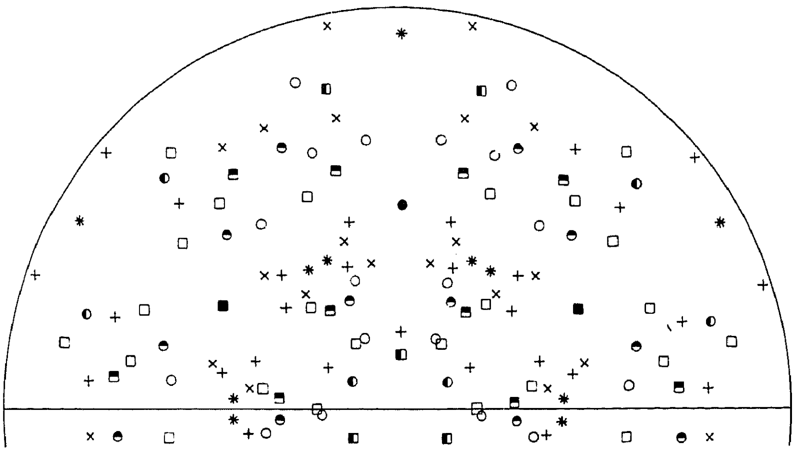

■ M	◨ M$_1$	⊟ M$_2$	□ M$_3$	These symbols denote 200-poles found for crystal types M and T (see text) and their i-th order twins for twin planes making an angle > 45° with substrate surface.
● T	◐ T$_1$	⊖ T$_2$	○ T$_3$	
		+	×	These symbols denote all other twin poles for i = 1, 2, 3 of crystal types M and T respectively.

Fig. 2. The positions of the 200-poles of crystal types M and T and their primary, secondary and tertiary twins.

apparently even at a low current density such as 0.5 mA/cm^2 a reasonable fraction of the copper crystallizes in twin position (cf. table 1). This fraction may be initially present in the deposit (analogous to vapour deposition, e.g. ref. [10]). This is supported by the lack of twins of crystal types M and T in fig. 1a and by nuclei in twin position on the 111 nickel surface in the initial stage of the deposition process shown in fig. 3. After nucleation crystals of type T and M are assumed to grow without further twinning. Schultze [2,3], depositing copper onto a 111 copper substrate, also observed crystals of type T, but at a current density of 10 mA/cm^2.

The pole figure of fig. 1a shows some intensity in the center. From Bragg's law and pulse height spectra recorded it was concluded that the occurrence of coherent scattering of white radiation and background radiation can be disregarded. The only possible explanation is that some copper crystallizes with an 100 plane parallel to the substrate 111 plane. The number of these crystals is very small (cf. table 1) which may be the reason that previous qualitative investigations did not account for this phenomenon.

The 200 pole figure of the specimen prepared at 1.5 mA/cm^2 (fig. 1b) shows the same features discussed in connection with fig. 1a. Besides intensity is also found at a number of other orientations. We explain this result as follows: As the thickness of the deposit increases twinning may occur at 111 planes not parallel to the 111 nickel surface, provided that the local current density is large enough. Furthermore repeated twinning is possible. In fig. 2 the positions of all the 200 poles of the primary, secondary and tertiary twins of the crystals of type M have been plotted together with the corresponding poles of the crystals of type T. A comparison of fig. 1b and fig. 2 shows that the experimentally determined pole figure contains only a part of all plotted poles: only those 200 poles due to (repeated) twinning at 111 planes making an angle with the surface of the substrate >45°, are present in fig. 1b. These poles are indicated in fig. 2. This result is made plausible by the following computer simulation:

Firstly the (repeated) twin orientations and the positions of their *hkl* poles are computed. Then a gaussian shape for the intensity distribution around

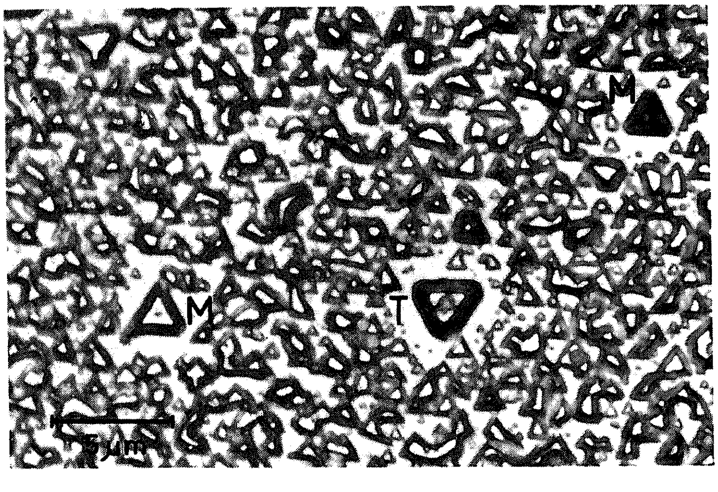

Fig. 3. An optical micrograph of an initial stage of a copper deposit prepared by electrocrystallization (1 mA/cm^2; mean thickness 0.5 µm). Three larger nuclei, two of crystal type M and one of crystal type T, are indicated. Note the coalescence-like character of the deposit.

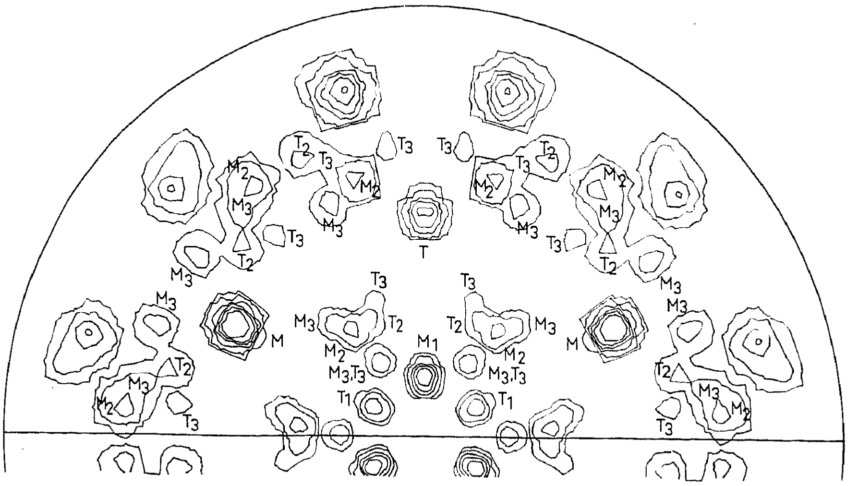

intensity levels (arbitrary units): 0.25; 1; 4; 8; 16; 32

Fig. 4. A computer simulated 200 pole figure showing the orientation distribution of crystal types M and T and their primary, secondary and tertiary twins due to (repeated) twinning at 111 planes making an angle with the surface of the substrate >45°.

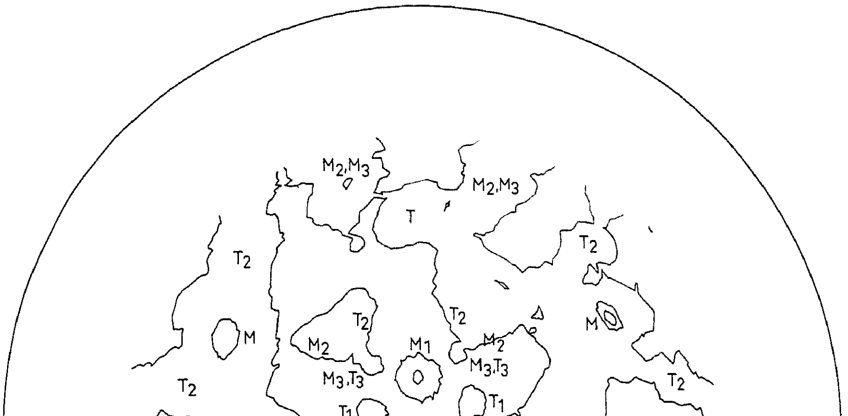

intensity levels (counts/s): 3 10^2; 3 10^3; 10^4; 10^5

Fig. 5. The 200 pole figure of a copper layer of 1 μm vapour deposited at 40 Å/min on a 111 nickel surface. Measurements were made up to 70° from centre.

each pole is assumed, the weight of each gaussian being the relative volume of the crystal type or twin type concerned, as determined from the pole figure measured. The resulting pole figure is plotted.

In this way the 200 pole figure – shown in fig. 4 – of a deposit containing crystals of type M and T and their primary, secondary and tertiary twins, *subject to the 45° criterion*, was computed. It can be seen that figs. 1b and 4 are in good agreement.

Schultze [2] – electrocrystallizing copper onto copper – earlier arrived at the 45° criterion using light microscopical evidence. He presumed that a twin with the twin plane making a small angle with the substrate surface will not grow easily because the "subcrystals" [3] at both sides of the twin plane tend to grow perpendicularly and tend to be bounded by close packed planes. Our determination of the orientation relationship between nickel substrate and copper deposit appears to give the finding of Schultze a more general and quantitative basis.

In fig. 5 the 200 pole figure of a specimen consisting of 1 μm copper vapour deposited onto a 111 nickel surface is shown. All the features discussed above can be found in this figure. This implies that the conclusions made above are not restricted to the process of electrocrystallization but concern more generally twinning processes in epitaxial crystal growth. However, under the conditions applied the vapour deposition process produces less perfect copper deposits (cf. fig. 5 and table 1) in spite of the low deposition rate of 40 Å/min.

Acknowledgement

We are indebted to Professor B. Okkerse, Dr. W.A. Schultze and Dr. F.W. Schapink for critically reading the manuscript.

Financial support of the Stichting voor Fundamenteel Onderzoek der Materie (F.O.M.) is gratefully acknowledged.

References

[1] J.O'M. Bockris and G.A. Razumney, Fundamental Aspects of Electrocrystallization (Plenum, New York, 1967).
[2] W.A. Schultze, Thesis, Delft University of Technology (1970).
[3] W.A. Schultze, J. Crystal Growth 13/14 (1972) 421.
[4] H.A. Liebhafsky and P.D. Zemany, Anal. Chem. 28 (1956) 455.
[5] L.G. Schulz, J. Appl. Phys. 20 (1949) 1030.
[6] G.J.A. Heideman and R. van Rooijen, in preparation.
[7] L. Jetter, C. McHarque and R. Williams, J. Appl. Phys. 27 (1956) 368.
[8] R. Delhez, E.J. Mittemeijer and W. Smid, Acta Cryst. A31, Part S3 (1975) S212.
[9] G.R. Love, Oak Ridge Technical Memorandum, ORNL-TM-2018, Oak Ridge National Laboratory, Oak Ridge, USA.
[10] D.W. Pashley, Advan. Phys. 14 (1965) 327.

Note added:

In the preceeding paper it was mentioned in passing that a very small number of the copper nuclei were oriented with a 100 plane parallel to the 111 nickel substrate plane. This was deduced from a very small intensity maximum found in the center of the pole figure. However, recent measurements with a Si(Li)-detector, which was not available during the course of the experiments reported in the preceeding paper, revealed that diffraction of white radiation is responsible for this effect.

V

Notes on phenomenological Diffusion Theory

V.21

Scripta METALLURGICA Vol. 10, pp. 941-943, 1976 Pergamon Press, Inc.
Printed in the United States

A RAPID METHOD FOR NUMERICAL SOLUTION OF FICK'S SECOND LAW WHERE THE DIFFUSION COEFFICIENT IS CONCENTRATION DEPENDENT

E.J. Mittemeijer and H.C.F. Rozendaal

Laboratory of Metallurgy, Delft University of Technology,
Rotterdamseweg 137, Delft, The Netherlands

(Received August 18, 1976)

1. Introduction

Fick's second law for linear diffusion reads:

$$\frac{\partial c}{\partial t} = \frac{\partial}{\partial x} \left(D \frac{\partial c}{\partial x}\right) \tag{1.1}$$

where c = concentration, t = time, x = distance and D = interdiffusion coefficient. Analytical solutions of (1.1) have been obtained in cases where D is independent of concentration (1). For some special functions D(c) analytical solutions have been found too (1, 2). In general however only numerical methods to solve (1.1) can be used if D is a function of concentration. A well known numerical method is given by Crank and Henry (3, 4). Because of the numerical integrations involved this method may be subject to lengthy computation times.

In 1955 in a paper (5) Philip mentioned a possible solution to the problem based on an idea of Neumann (6). Here D is assumed to be a n-step function of the concentration. Hence the method is applicable to any functional dependence of D on c. To our knowledge this idea has never been tested. The purpose of this paper is to apply the step solution to find the concentration profile and to develop the iterative procedure to solve the equations involved. The results will be compared with the method of Crank and Henry.

2. The method

a. The set of equations

Most of the diffusion experiments are subject to boundary conditions of the infinite or semi-infinite case. Then it is convenient to describe the concentration profile in terms of $z = x/t^{\frac{1}{2}}$ [e.g. the Boltzmann substitution (7)].

The diffusion coefficient is thought to be approximated by a n-step function. In the region $c_i < c < c_{i+1}$ the diffusion coefficient is assumed constant. Bearing in mind the boundary conditions, the concentration profile in this region then is given by:

$$c = A_{i+\frac{1}{2}} + B_{i+\frac{1}{2}} \operatorname{erfc} (z/2D^{\frac{1}{2}}_{i+\frac{1}{2}})$$

where $z_i < z < z_{i+1}$. The constants $A_{i+\frac{1}{2}}$ and $B_{i+\frac{1}{2}}$ follow from the boundary conditions.

At the interface of two regions the two solutions should match:

$$c_i = A_{i-\frac{1}{2}} + B_{i-\frac{1}{2}} \operatorname{erfc} (z_i/2D^{\frac{1}{2}}_{i-\frac{1}{2}}) \tag{2.1a}$$

$$c_i = A_{i+\frac{1}{2}} + B_{i+\frac{1}{2}} \operatorname{erfc} (z_i/2D^{\frac{1}{2}}_{i+\frac{1}{2}}) \tag{2.1b}$$

where i = 2, 3, ... n-1.

Equalizing the flux ($J = -D\frac{\partial c}{\partial x}$) at both sides of the interface results in:

$$B_{i-\frac{1}{2}}D^{\frac{1}{2}}_{i-\frac{1}{2}} \exp\left(-z_i^2/4D_{i-\frac{1}{2}}\right) = B_{i+\frac{1}{2}}D^{\frac{1}{2}}_{i+\frac{1}{2}} \exp\left(-z_i^2/4D_{i+\frac{1}{2}}\right) \qquad (2.2)$$

where $i = 2,3 \ldots\ldots n-1$.

Finally we have the boundary conditions which for example for the infinite case yield:

$$c_1 = A_{1\frac{1}{2}} + 2B_{1\frac{1}{2}} \qquad (2.3a)$$

$$c_n = A_{n-\frac{1}{2}} \qquad (2.3b)$$

The set equations (2.1a and b), (2.2) and (2.3a and b) can only be solved numerically.

b. The iterative procedure.

It was found that the following iteration scheme can be succesfully applied in practice:

(i) The concentration profile which can be calculated analytically if the diffusion coefficient is assumed constant, is taken as a first approximation.

(ii) The region $0 < c < 1$ is divided into a number of intervals (see below).

(iii) The z-values belonging to the interfaces are computed by the Newton-Raphson method.

(iv) The diffusion coefficient belonging to the midst of each concentration interval is calculated from the known functional relation $D(c)$ [$D(c)$ may be given in a numerical form].

(v) $B_{1\frac{1}{2}}$ is obtained from $B_{1\frac{1}{2}} = (c_1 - c_2)/\{2\text{-erfc}\,(z_2/2D^{\frac{1}{2}}_{1\frac{1}{2}})\}$.

(vi) All $B_{i+\frac{1}{2}}$'s ($i = 2,3 \ldots\ldots n-1$) are calculated from (2.2).

(vii) Using the values of $B_{i+\frac{1}{2}}$ and $D_{i+\frac{1}{2}}$ calculated in step (iv), (v) and (vi), values of $A_{i-\frac{1}{2}}$ ($i = 2,3 \ldots\ldots n-1$) are calculated from (2.1a). But also values of $A_{i+\frac{1}{2}}$ ($i = 2,3 \ldots\ldots n-1$) are calculated from (2.1b). Thus, including the boundary conditions, there are two values for $A_{i+\frac{1}{2}}$ ($i = 1,2 \ldots\ldots n-1$). The mean value of these two values for $A_{i+\frac{1}{2}}$ is taken as the new one.

(viii) Applying the values of $A_{i+\frac{1}{2}}$, $B_{i+\frac{1}{2}}$ and $D_{i+\frac{1}{2}}$ thus determined, new values for c_i are computed from (2.1a).

(ix) The procedure from (iv) to (viii) is repeated until the difference between the c_i-values of successive iterations is less than the desired limit.

Hence the basis of the iterative procedure is that after determining a set of z-values, the c-values are recalculated until - within the desired limit of accuracy - they fulfil the set of equations (2.1a and b), (2.2) and (2.3a and b).

It was found convenient to start with a very rough frame of z-values (a few z-values with large specings). If for these z-values a limit in accuracy for the c-values was reached by applying the above iteration scheme, a new set of z-values with smaller spacings was generated and the scheme (iv)-(ix) was repeated. This entire procedure was repeatedly performed until the concentration profile was accurately calculated with a sufficient density of points.

3. Results and discussion

The method was tested for a linear, parabolic and exponential dependence of D on c. We applied the boundary conditions of the infinite case ($c = 1$ at $z = -\infty$; $c = 0$ at $z = +\infty$). However the semi-infinite case proceeds analogously. The difference between c_i-values of the last two iterations should be < 0.001 ($0 < c < 1$). During the iterative procedure 4 sets of z-values were used: 3, 6, 10, 20 and 100 intervals.

In all cases convergence was establlished. The results are gathered in Tabel 1.

To check the stability of the solution found a small change in the boundary conditions was applied ($c = 0.95$ at $z = -\infty$; $c = 0.05$ at $z = +\infty$). As shown in Fig. 1

for the linear case (D = 1 + 10.c) the change in the concentration profile is not drastic. Therefore the solution found may be considered as a stable one.

Comparing the present method with the well known method of Crank and Henry (c.f. Table 1) it can be said that the method of Crank and Henry needs less iterations. However the present method is two orders of magnitude faster and should therefore be preferred in practice.

Acknowledgements

The authors are indebted to Professor B. Okkerse and Dr. F.W. Schapink for critically reading of the manuscript.

Financial support of the Stichting voor Fundamenteel-Onderzoek der Materie (F.O.M.) is gratefully acknowledged.

References

1. J. Crank, The Mathematics of Diffusion, Clarendon Press, Oxford (1956).
2. A.D. Pelton and T.H. Etsell, Acta Met. 20,1269 (1972).
3. J. Crank and M.E. Henry, Trans. Faraday Soc. 45, 636 (1949).
4. J. Crank and M.E. Henry, Trans. Faraday Soc. 45, 1119 (1949).
5. J.R. Philip, Trans. Faraday Soc. 51, 885 (1955).
6. H.S. Carslaw and J.C. Jaeger,Conduction of Heat in Solids, p. 72. Clarendon Press, Oxford (1947).
7. L. Boltzmann, Ann. Physik, Leipzig 53, 959 (1894).

TABLE I

Results for the Present Method and the Crank and Henry Method

	present method			Crank and Henry method		
D(c)	number of intervals	number of iterations	total c.p.u.-time(s)	number of intervals	number of iterations	total c.p.u.time(s)
1+10.c	3,6,10,20,100	5,3,2,2,1	0.40	100	5	39.53
1+10.c(1-c)	3,6,10,20,100	5,3,11,5,13	0.86	100	5	90.39
exp(5.c)	3,6,10,20,100	8,4,3,3,5	1.49	100	11	37.57

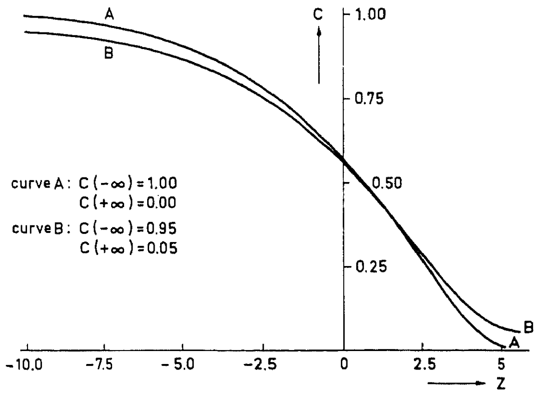

FIG. 1.

The concentration profile calculated for the linear dependence of D on c (D = 1 + 10.c).

V.22

Scripta METALLURGICA Vol. 11, pp. 113-115, 1977 Pergamon Press, Inc.
Printed in the United States

THE DETERMINATION OF CONCENTRATION DEPENDENT DIFFUSION COEFFICIENTS IN SEMI-INFINITE MEDIA

E.J. Mittemeijer and Th.H. de Keijser

Laboratory of Metallurgy, Delft University of Technology,
Rotterdamseweg 137, Delft, The Netherlands

(Received November 1, 1976)

1. Introduction

This paper deals with the diffusion of component A into a semi-infinite medium of a binary solid solution of components A and B, subject to the boundary condition that the concentration of component A at the interface is maintained constant during diffusion. An example is the diffusion in bimetallic vapor-solid couples (1).

Even in the case that the partial specific or molar volumes of components A and B, V_A and V_B respectively, are constant the total volume of the specimen will increase as a result of the inward diffusion of component A. If V_A and V_B are constant a frame of reference is usually chosen such that there is no net transfer of volume through a cross section of the sample (5). However in the case considered this frame of reference is inconvenient for the following reason.

For non-zero diffusion times the origin of the space coordinate which is confined to the original interface, will not coincide with the (moving) interface because of the expansion of the specimen. This difficulty cannot be eliminated by confining the origin ($x = o$) to the interface for all diffusion times. Then Fick's second law is no longer valid in its usual form. Fara (1, 2) arrived at this conclusion, and therefore in his analysis a shift of origin was eventually applied to confine $x = o$ to the original interface.

The necessary experimental location of the original interface after each diffusion run can be considered as a serious drawback of such a method. On the other hand the application of Fick's second law in its usual form is desirable, because this standard form has frequently been used as the starting point in calculations of diffusion behaviour.

It is the purpose of this paper to show that the determination of the position of the original interface is superfluous. A physically significant diffusion coefficient can be defined with a known relation to the intrinsic diffusion coefficients. It will also be shown that a Matano-like analysis (3) can be applied to determine concentration dependent diffusion coefficients in a semi-infinite medium.

2. The frame of reference

Hartley and Crank (4, 5) generally discussed several frames of reference which may be used in describing diffusion behaviour. In the present case the most convenient frame of reference is the one defined such that there is no net transfer of component B through a cross section of the sample (4, 5). In order to apply Fick's second law in its standard form in this frame of reference a modified spatial coordinate ξ_B is introduced such that equal increments of ξ_B imply equal increments in the amount of B. Furthermore the concentrations, denoted by a superscript B, are expressed as the amount of A per unit amount of B. Accordingly, concentrations in the frame of reference with volume-fixed cross sections are expressed as the amount of A per unit volume and will be denoted by a superscript V.

Obviously in the frame of reference with B-fixed cross sections the diffusion coefficient D_B^B of component B, equals zero. Therefore a single diffusion coefficient can be used to describe the diffusion behaviour: i.e. the diffusion coefficient D_A^B of component A.

During diffusion overall, non-diffusional mass-flows occur (giving rise to the Kirkendall-effect). In the present case an additional non-diffusional mass-flow arises from the absorption of component A. We wish to distinguish the "true" diffusion and these mass-flows. Therefore the intrinsic diffusion coefficients D_A^i en D_B^i are defined. These diffusion coefficients are confined to a cross section defined such that no mass-flows as mentioned above occur through it. If the volume transfers related to both above mentioned mass-flows are defined in the B-fixed reference system by Φ and Φ_A, it follows from the definition of a B-fixed cross section:

$$-D_B^i \frac{\partial C_B^V}{\partial x} - C_B^V (\Phi + \Phi_A) = 0$$

Hence:

$$(\Phi + \Phi_A) = - \frac{D_B^i}{C_B^V} \frac{\partial C_B^V}{\partial x} \tag{2.1}$$

The rate of transfer of component A across a B-fixed cross section by the mass-flows mentioned equals $C_A^V (\Phi + \Phi_A)$. Thus combining this rate of transfer with the one due to true diffusion we arrive at

$$-D_A^B \frac{\partial C_A^B}{\partial \xi_B} = - D_A^i \frac{\partial C_A^V}{\partial x} + \frac{C_A^V}{C_B^V} D_B^i \frac{\partial C_B^V}{\partial x} \tag{2.2}$$

Hereafter the same treatment as given by Hartley and Crank (4, 5) can be followed. If furthermore the Gibbs-Duhem rule is applied one obtains

$$D_A^B = (V_B^0 C_B^V)^2 (C_B^V V_B D_A^i + C_A^V V_A D_B^i) \tag{2.3}$$

where V_B^0 is an arbitrary specific volume used to define D_A^B in normal units [cm^2/s]. The next paragraph deals with the experimental determination of D_A^B.

3. Determination of the diffusion coefficient D_A^B

In the frame of reference with B-fixed cross sections ξ_B and C_A^B are defined such (see §2) that Fick's second law holds in the standard form:

$$\frac{\partial C}{\partial t} = \frac{\partial}{\partial \xi} (D \frac{\partial C}{\partial \xi}) \tag{3.1}$$

For reasons of clarity of presentation super- und subscripts have been omitted.

Because of the boundary conditions of the semi-infinite case the Boltzmann-substitution (6) can be used:

$$\eta = (\xi - \xi_0)/2t^{\frac{1}{2}} \tag{3.2}$$

Substitution of (3.2) in (3.1) yields the well-known result:

$$-2\eta \frac{dC}{d\eta} = \frac{d}{d\eta} (D \frac{dC}{d\eta}) \tag{3.3}$$

For the infinite case Matano (3) showed that D(C) can be determined from (3.3). For the semi-infinite case D(C) can be evaluated in the following way.

After integration of (3.3) with respect to η, rearranging of terms results in:

$$D(C) = -2 \left[\frac{d\eta}{dC}\right]_C \left\{ \int_{C_o}^{C} \eta dC - \tfrac{1}{2} \left[D \frac{dC}{d\eta}\right]_{C_o} \right\} \tag{3.4}$$

where C_0 denotes the concentration at the interface. The second term at the right hand side of (3.4) can be dealt with as follows. If C_∞ denotes the concentration at $\eta = +\infty$ and using $dC/d\eta$ (at C_∞) = 0 one obtains

$$\int_{C_0}^{C_\infty} -2\eta dC = -\left[D\frac{dC}{d\eta}\right]_{C_0} \qquad (3.5)$$

Combination of (3.2), (3.4) and (3.5) yields:

$$D(C) = -\frac{1}{2t}\left[\frac{d\xi}{dC}\right]_C \int_{C_\infty}^{C} (\xi - \xi_0)dC \qquad (3.6)$$

Applying a graphical analysis D(C) can be evaluated from (3.6) provided ξ_0 has been located. From (3.6) it follows for the flux j(C):

$$j(C) = -D(C)\left[\frac{dC}{d\xi}\right]_C = \frac{1}{2t}\int_{C_\infty}^{C} (\xi - \xi_0)dC \qquad (3.7)$$

From an inspection of (3.7) for t approaching zero it follows that ξ_0 should be confined to the (moving) interface. It can be concluded that for the determination of a physically significant diffusion coefficient the position (in cm) of the original interface need not be known.

The treatment given in this paper may be applied in studies of ternary diffusion where two solutes diffuse from the vapour phase into a ternary solid solution (7, 8).

Acknowledgements

The authors are indebted to Professor B. Okkerse, Dr. F.W. Schapink and Ir. R. Delhez for critically reading of the manuscript.

Financial support of the Stichting voor Fundamenteel Onderzoek der Materie (F.O.M.) is gratefully acknowledged.

References

1. R.W. Balluffi and L.L. Seigle, J.Appl.Phys. 25, 607 (1954).
2. H. Fara and R.W. Balluffi, J.Appl.Phys. 27, 964 (1956).
3. C. Matano, Jap.J.Phys. 8, 109 (1933).
4. G.S. Hartley and J. Crank, Trans.Far.Soc. 45, 801 (1949).
5. J. Crank, The Mathematics of Diffusion, pp. 219-228, Clarendon Press, Oxford (1956).
6. L. Boltzmann, Ann. Physik, Leipzig 53, 959 (1894).
7. M.A. Dayananda and R.E. Grace, Trans.Am.Soc.Metals 233, 1287 (1965).
8. M.A. Dayananda, P.F. Kirsch and R.E. Grace, Trans.Am.Soc.Metals 242, 885 (1968).

EPILOGUE*

In recent years the need became urgent for quantitative investigations of solid state kinetics. To this end it was decided in the Laboratory of Metallurgy to develop quantitative diffraction methods, building on the existing experience on diffraction phenomena from the imperfect solid state.

In the field of X-ray diffraction the tendency to quantitative investigations has been enhanced by the developments in electronic measuring equipment and by the availability of fast computers.

Looking at chapter I, in which methods for the quantitative analysis of the X-ray diffraction line broadening are outlined, one may find it rather astonishing that new aspects can still be originated, since the technique itself is several decades old. This may be due to an underestimation of the potential power of X-ray powder diffraction, to the relatively high cost of the equipment, to the "fear" for automatization and computer handling of data and - in contrast with the X-ray determination of "ideal" crystal structures - to a lack of international coordination and stimulation.

Applying the methods for line profile analysis considered in chapter I, the X-ray diffraction technique has been applied to specimens with concentration variations in Chapter II.

Up to the present attention was scarcely paid to X-ray investigations of long-range displacements, in contrast to X-ray investigations of non-systematical displacements, which are usually studied by application of the Warren-Averbach analysis for size and strain. The analysis we developed for studying long-range displacements [II.11] employs the sine Fourier coefficients

---

* The numbers in square brackets refer to the respective papers of this thesis (c.f. Table of Contents).

of the line profile, whereas the Warren-Averbach analysis is based on the cosine Fourier coefficients. Indeed, surveying both analyses one notices that the respective Fourier coefficients can be used most efficiently for the respective purposes. Our analysis, which was only applied to alloy catalyst particles, may also be profitably used to investigate spinodal decomposition, clustering phenomena, and mechanical deformation and interdiffusion in thin solid films, which are transparent for X-rays.

A method was developed for studying the homogenization process in a powder blend during annealing [II.12]. By tracing the position of an X-ray diffraction maximum it was found possible to determine the diffusion mechanisms(via the activation energies obtained). The model of interdiffusion adopted could be tested from a comparison of the peak position mentioned above and the "degree of interdiffusion", which is deduced from the same line profile. In view of the accuracy achieved in measuring and purifying the intensity distributions, appreciable more information from the line profiles recorded may be obtained by a further development of the analyses mentioned. Primarily a quantification of the surface diffusion effects observed in the early stages and the related sintering phenomena may be attained.

The powder diffractometer technique applied to single crystals [II.14] opens perspectives not only to investigations of interdiffusion (or evaporation or depletion of a component from an alloy) but also to the investigation of mechanical deformation (e.g. by rolling, or H_2 enclosure accompanying the electrocrystallization of metals) as a function of the distance to the surface.

In the field of electron diffraction it should be remarked that the advantage of a much higher resolution than obtained by X-ray diffraction is accompanied by serious drawbacks: (i) the specimens required are very thin and consequently the surface plays a significant role; and (ii) no analysis of the intensity profile of electron diffraction "spots" is available and hence no procedures analogous to line profile analysis methods employed in the X-ray diffraction technique can be applied. Furthermore, in many cases no "local" information is required but data averaged over much larger regions are desired. For most practical situations the X-ray diffraction methods presented in chapter II are much more powerful than the electron diffraction methods. Nevertheless, for special purposes and for investigation of the structure of the diffusion zone, the electron diffraction technique is highly attractive. This is especially true for the electron diffraction papers collected in chapter III.

The moiré-method developed [III.15] is very well suited for studying interdiffusion at very low temperatures, since diffusion zones of the order of 10 Å have a measurable effect on the increase of the moiré-spacing. The study of the structure of the diffusion zone [III.16] revealed dislocation wall formation, resulting in a dislocation cell structure of the diffusion zone.

It may be expected that eventually a model will emerge which relates the extent of the coherently diffracting domain (as mentioned in the X-ray diffraction experiments), the concentration variation concerned and the dislocation structure of the diffusion zone.

SUMMARY*

This thesis consists of twenty-two recent papers, which represent the contribution of the authors to the interpretation of X-ray and electron diffraction phenomena from specimens with concentration variations.

I. Methods for the purification of X-ray diffraction line profiles

To correct for the angle dependence of the polarization of the X-rays and the geometrical (Lorentz) and structure factors rules are suggested, which prescribe when and how to perform these corrections [I.2]. Formulae for the Lorentz-polarization factor for an assembly of line intensities and for integrated intensities are indicated.

An experimental approach was chosen for the description of the broadening of X-ray diffraction line profiles by instrumental factors and of the mutual importance of these and spectral factors, since no satisfactory theoretical description exists [I.3]. This approach is especially suited for size-strain analysis using Fourier transformation. Under common experimental conditions a set of line profiles were measured from an NBS standard silicon sample in the range 30 - 160° 2θ. It was found that for $2\theta > 50^{\circ}$ spectral broadening dominates. The Fourier coefficients corresponding to the broadening caused by the instrumental conditions become independent of 2θ provided that 2θ is sufficiently large and the harmonic number sufficiently small. If in size-strain analysis the standard specimen diffracts in a 2θ range different from the specimen to be investigated, only corrections for the difference in spectral broadening have to be made. Since the most important difference in spectral

---

* The numbers in square brackets refer to the respective papers of this thesis (c.f. Table of Contents).

broadening is the difference in doublet separation an α_2 elimination should be performed.

The most critical step in an α_2 elimination is not the method of the elimination itself, but the calculation of the doublet separation for which two formulae are proposed [I.4]. In both formulae the doublet separation is taken angle dependent within a given profile. The first one depends on the spacing of the reflecting lattice planes, whereas the other one does not and hence can be used as a "computerized monochromator", which is of special interest for specimens with varying lattice spacing (e.g. diffusion couples). Two methods for the α_2 elimination are compared: the Fourier correction and the substitution correction (Rachinger correction)[I.6]. It is shown that the latter should be preferred in practice although the methods are mathematically equivalent.

Because in size-strain analysis usually Fourier coefficients are used (Warren-Averbach analysis) and an α_2 elimination may be necessary, the errors in the Fourier coefficients of a calculated α_1 profile were analysed [I.5]. The error caused by counting statistics is a periodic function of the harmonic number. Errors in the doublet separation and in the ratio of the α_1 and α_2 intensities of the Kα radiation used mainly affect the Fourier coefficients with a small harmonic number. A method is proposed to determine the actual value of the ratio of the maxima of the α_1 and α_2 components [I.3].

Size-strain analysis is usually performed according to Warren and Averbach. The formula used in practice is based on power series expansions for the logarithm and for the cosine. The first one was shown to be superfluous, which is very important because the truncation of the power series concerned yields the largest errors [I.7].

Non-ideal standard specimens are used frequently in line profile analysis. This non-ideality may consist of remaining structural broadening and/or different spectral broadening in case the standard specimen diffracts in a 2θ range different from the specimen under investigation. Easily applicable correction formulae are derived [I.9]. It is shown that errors in the order of 50% in the mean square strain calculated may arise, if these corrections are ignored [I.8].

A method is suggested to correct for the "hook"-effect in line profile analysis [II.11].

II. Analysis of X-ray diffraction line broadening of specimens with concentration variations

The broadening of X-ray diffraction line profiles was analysed for three types of specimens containing concentration variations:

(a) powder samples where the concentration variation occurs within the individual crystallites (Au/Pt);

(b) powder blends where the concentration variations occur across the contact places of the particles (each particle consists of a number of crystallites or domains) (Cu/Ni and RbCl/KCl).

(c) monocrystals where the concentration variation extends over many coherently diffracting domains (Cu/Ni).

X-ray diffraction by a coherently diffracting domain, as present in the specimens mentioned, was investigated theoretically. Applying the kinematical diffraction theory it was deduced, that the shape of the intensity profile is entirely characterized by a single parameter for a domain (or crystallite) where the lattice spacing (concentration) varies linearly [II.10]. This parameter contains the lattice spacing gradient, the square of the number of diffracting lattice planes and the order of the reflection.

For the first type of specimens a method was developed to obtain the concentration profile from the sine Fourier coefficients of a single line profile [II.11]. This analysis appears to be especially suited for the investigation of concentration inhomogeneities occurring within the crystallites of alloy catalysts. The method was applied to sintered and unsintered AuPt alloys catalysts. In the interior of the crystallites of the sintered specimens the concentration remained constant, whereas the surface region was enriched by gold, which agrees with other experimental results and with theoretical predictions. The crystallites of the unsintered specimens consisted of a platinum-rich nucleus and a gold-rich shell, as was expected from the preparation method.

To describe homogenization in a powder blend - the second type of specimens - a method was developed on the basis of simulation of line profiles [II.12]. This fast and simple procedure utilizes the position of the maximum of an intensity band. It allows a severe test of the model of interdiffusion applied. Experimental results were obtained from a metal system (Cu/Ni [II.12]) and a non-metal system (RbCl/KCl [II.13]). For both systems it was found that surface diffusion dominated at the start of homogenization. At later stages grain boundary diffusion prevailed in Cu/Ni and volume diffusion in RbCl/KCl. It was found that the concentric sphere geometry (the minor component in the nucleus and the major component in the shell) afforded the best - although not quite satisfactory - description of the homogenization process.

For the third type of specimens a direct method is presented to determine the concentration profile from a single intensity band of a binary diffusion couple [II.14]. Previous methods employed iterative or trial and error procedures. It was shown that the background is dominated by thermal diffuse scattering (TDS) and that - as a consequence - a linear background profile is a poor approximation to the real background. An iterative calculation of the TDS intensity is proposed. The direct method for the determination of the concentration profile as well as the calculation and the subsequent elimination of the TDS intensity are illustrated by experiments with CuNi bicrystals.

III. Electron diffraction investigations of diffusion-annealed specimens

Transmission electron microscopical investigations of small diffusion zones yielded information

(i) on the diffusion process from the change of the moiré spacing;

(ii) on the microstructure of the diffusion zone.

A distinct increase in moiré spacing was observed during diffusion-annealing (450 - 600°C) of epitaxial bicrystals consisting of a copper layer of a few hunderd Ångstrom on a nickel substrate of about thousand Ångstrom [III.15]. It was found that the relative increase of the moiré spacing varies linearly with the square root of the annealing time. On the basis of a highly simplified model of electron diffraction the diffusion coefficient can be determined from the proportionality constant of this relation. Activation energies and frequency factors obtained from these diffusion coefficients are in good agreement with published data on volume diffusion in the Cu/Ni system, although at lower temperatures (450 - 475°C) the activation energy tends to become smaller and the frequency factor larger [III.17].

Misfit dislocations originally observed as a network in the Cu/Ni interface were redistributed throughout the alloyed volume during diffusion-annealing and formed dislocation walls [III.16]. This process eventuated in a cell structure. An energy criterion for dislocation wall formation was formulated by comparing the elastic strain energies of a quasi continuous distribution of misfit dislocation in the diffusion zone and an arrangement in walls. The onset of dislocation wall formation predicted from this criterion agreed very well with the experimental finding.

With regard to the research on diffusion-modified interfaces in thin epitaxial bimetallic films some unsolved problems are identified and possible future directions of research are indicated [III.18].

IV. Epitaxial growth of copper layers onto a nickel single crystal substrate

With a view on the preparation of specimens for the diffraction investigations, a study of the morphology, epitaxy and twinning of copper layers either electrocrystallized or vapour deposited onto a 111 nickel surface was made with optical microscopy, scanning electron microscopy and X-ray diffraction. It was found that the shape of the nuclei and the amounts of fully epitaxial nuclei and of twins depended on the current density applied. An interesting "nucleus" found was an icosahedron (five fold symmetry) with carved edges [IV.19].

The twinning process was studied quantitatively for electrocrystallization and vapour deposition [IV.20]. Only if the twin planes make an angle > 45° with the surface of the substrate (repeated) twinning occurs. As compared to electrocrystallization vapour deposition produced less perfectly epitaxial copper layers.

V. Notes on phenomenological diffusion theory

Fick's second law is solved numerically for the case of one-dimensional diffusion with a diffusion coefficient with known concentration dependence [V.21]. The iterative method proposed is based on an idea of Neumann and can be used for infinite and semi-infinite media. Computation time needed is about two orders of magnitude smaller than for the well known method of Crank and Henry.

A discussion is given on the determination of concentration dependent diffusion coefficients in a semi-infinite medium of a binary solid solution subject to the boundary condition that the surface concentration of one component is constant [V.22]. It is shown that (i) the position of the original surface need not be known, that (ii) a physically significant diffusion coefficient can be defined with a known relation to the intrinsic diffusion coefficients and that (iii) a Matano-like analysis can be applied.

SAMENVATTING *

Dit proefschrift bestaat uit twee en twintig recente publicaties. Deze vormen tezamen de bijdrage van de auteurs tot de interpretatie van röntgen- en electronendiffractieverschijnselen aan preparaten met concentratievariaties.

I. Methoden voor het zuiveren van röntgendiffractielijnprofielen

Er worden regels voorgesteld, die voorschrijven wanneer en hoe er gecorrigeerd moet worden voor de hoekafhankelijkheid van de polarisatie van de röntgenstraling en de geometrische (Lorentz)- en structuurfactoren [I.2]. Formules voor de Lorentz-polarisatiefactor voor een verzameling lijnintensiteiten en voor geïntegreerde intensiteiten worden aangegeven.

Er werd een experimentele benadering gevolgd voor de beschrijving van de verbreding van röntgendiffractielijnprofielen door instrumentele factoren en voor het wederzijds belang van deze en spectrale factoren, daar er geen bevredigende theoretische beschrijving voorhanden is [I.3]. Deze benaderingswijze is in het bijzonder geschikt voor de bepaling van deeltjesgrootte en roostervervorming indien er gebruik gemaakt wordt van Fouriertransformaties. Van een NBS-standaard silicium poeder werd een reeks lijnprofielen opgenomen in het gebied van 30-160 $^{o}2\theta$ onder normale experimentele omstandigheden. Voor $2\theta > 50^{o}$ domineert de spectrale verbreding. De Fouriercoëfficiënten die behoren bij de verbreding ten gevolge van de instrumentele omstandigheden, worden onafhankelijk van 2θ mits 2θ voldoende groot is en tevens het harmonisch getal klein is. Als bij het bepalen van deeltjesgrootte en roostervervorming een standaardpreparaat wordt gebruikt dat in een ander gebied diffracteert dan het te onderzoeken preparaat behoeven

---

* De getallen in vierkante haken verwijzen naar de betrokken publicaties in dit proefschrift (zie "Table of Contents").

er alleen maar correcties voor het verschil in spectrale verbreding te worden uitgevoerd. Daar het belangrijkste verschil in spectrale verbreding het verschil in doubletscheiding is, moet dan een α_2-eliminatie worden uitgevoerd.

Het kritiekste deel van een α_2-eliminatie is niet de keuze van de methode, maar de berekening van de doubletscheiding, waarvoor twee formules worden voorgesteld [I.4]. In beide formules wordt de doubletscheiding hoekafhankelijk verondersteld binnen het betreffende profiel. De eerste formule bevat de netvlaksafstand van de reflecterende vlakkenschaar, terwijl de tweede daarvan onafhankelijk is en daarom gebruikt kan worden als een "computermonochromator", hetgeen speciaal van belang is voor preparaten met een veranderende roosterconstante (bijv. diffusiekoppels). Twee methoden voor α_2-eliminatie worden vergeleken: de Fouriercorrectie en de substitutiecorrectie (Rachingercorrectie) en er wordt aangetoond dat de laatste in de praktijk te verkiezen is, hoewel de methoden mathematisch gelijkwaardig zijn [I.6].

Omdat bij de bepaling van deeltjesgrootte en roostervervorming gewoonlijk gebruik gemaakt wordt van Fouriercöefficiënten en een α_2-eliminatie noodzakelijk kan zijn, worden de fouten in de Fouriercoëfficiënten van een berekend α_1-profiel onderzocht [I.5]. De telstatistiek veroorzaakt een fout, die een periodieke functie van het harmonisch getal is. Fouten in de doubletscheiding en in de verhouding van de α_1- en α_2-intensiteiten van het gebruikte Kα-doublet beïnvloeden hoofdzakelijk de Fouriercoëfficiënten met een laag harmonisch nummer. Er wordt een methode voorgesteld om de actuele waarde van de verhouding van de maxima van de α_1- en α_2-componenten van een lijnprofiel te bepalen [I.3].

De bepaling van deeltjesgrootte en roostervervorming wordt meestal volgens de methode van Warren en Averbach uitgevoerd. De daarbij in de praktijk gebruikte formule is afgeleid door gebruik te maken van twee ontwikkelingen in machtreeksen: een voor een logarithme en een voor een cosinus. Aangetoond werd, dat de eerste reeksontwikkeling overbodig is, hetgeen van groot belang is, omdat het afbreken van die machtreeks de grootste fouten introduceert [I.7].

Bij lijnprofielanalyse worden vaak niet-ideale standaardpreparaten gebruikt. Niet-ideaal impliceert of restant structurele verbreding en/of verschil in spectrale verbreding indien het standaard preparaat in een ander gebied diffracteert dan het te onderzoeken preparaat. Voor deze gevallen zijn eenvoudig toepasbare correctieformules afgeleid [I.9]. Indien deze correcties niet worden toegepast, kan dat fouten in de orde van 50% in het berekende gemiddelde kwadraat van de rek ten gevolge hebben [I.8].

Er is een methode gesuggereerd om voor het "hook"-effect te corrigeren bij lijnprofielanalyse [II.11].

II. Analyse van de röntgendiffractielijnverbreding van preparaten met concentratievariaties

De verbreding van röntgendiffractielijnprofielen werd geanalyseerd voor drie typen preparaten die concentratievariaties bevatten:

(a) poederpreparaten waarbij de concentratievariatie geheel binnen ieder afzonderlijk kristalliet valt (Au/Pt);

(b) poedermengsels waar de concentratievariaties juist plaatsvinden over de kontaktplaatsen van de deeltjes heen (ieder deeltje bestaat uit een aantal kristallieten of domeinen) (Cu/Ni en RbCl/KCl);

(c) eenkristallen waarbij de concentratievariatie zich over vele coherent diffracterende domeinen uitstrekt (Cu/Ni).

De diffractie van röntgenstraling door een coherent verstrooïend gebied zoals dat in bovengenoemde preparaten voorkomt, werd theoretisch bestudeerd. Door de kinematische diffractietheorie toe te passen, werd afgeleid, dat de vorm van het intensiteitsprofiel volledig bepaald wordt door één parameter voor een domein (of kristalliet) waarin de netvlaksafstand (concentratie) lineair verandert [II.10]. Die parameter bevat de gradiënt van de netvlaksafstand, het kwadraat van het aantal diffracterende netvlakken en de orde van de reflectie.

Voor het eerstgenoemde type preparaten werd een methode ontwikkeld om het concentratieprofiel uit de sinus Fouriercoëfficiënten van één lijnprofiel te bepalen [II.11]. Deze analyse blijkt in het bijzonder geschikt te zijn voor het onderzoeken van veranderingen in de concentratie zoals die in de kristallieten van legeringskatalysatoren voorkomen. De methode werd toegepast op gesinterde en ongesinterde AuPt-legeringskatalysatoren. In het inwendige van de deeltjes van de gesinterde preparaten bleek de concentratie constant te zijn, maar de oppervlaktelaag was goudrijker, hetgeen overeenstemt met andere experimentele resultaten en met theoretische voorspellingen. De kristallietjes van de ongesinterde preparaten bestonden uit een platinarijke kern en een goudrijke mantel, zoals verwacht mocht worden op grond van de bereidingswijze.

Om de homogenisatie in een poedermengsel - het tweede type preparaten - te beschrijven, werd een methode ontwikkeld die berust op lijnprofielsimulaties [II.12]. Deze snelle, eenvoudige methode maakt gebruik van het maximum van een intensiteitsprofiel en staat een scherpe test van het (geometrische) model van de interdiffusie toe. Een metaalsysteem (Cu/Ni [II.12]) en een niet-metaalsysteem (RbCl/KCl [II.13])werden onderzocht. Bij beide systemen bleek oppervlaktediffusie te overheersen tijdens de aanvang van de homogenisatie. In latere stadia overheerste grensvlakdiffusie bij Cu/Ni en volumediffusie bij RbCl/KCl. Als beschrijving van de geometrie gedurende de homogenisatie voldeed het concentrisch bolmodel (de minst voorkomende component in de kern en de meest voorkomende component in de mantel)het best - hoewel niet geheel bevredigend.

Voor het derde type preparaten wordt een methode voorgesteld, waarbij uit één intensiteitsprofiel behorend bij een binair diffusiekoppel rechtstreeks het concentratieverloop berekend wordt [II.14]. De bestaande methoden gebruikten iteratieve of proefondervindelijke ("trial and error") procedures. Aangetoond werd dat de waargenomen ondergrond hoofdzakelijk bepaald wordt door thermisch diffuse verstrooiing (TDS) en dat daarom een rechte ondergrond een slechte benadering van de werkelijke is. Voor de berekening van de intensiteit van de TDS wordt een iteratieve procedure voorgesteld. Zowel de genoemde methode om het concentratieprofiel rechtstreeks te bepalen, als de berekening en eliminatie van de TDS-intensiteit worden geïllustreerd door experimenten aan Cu/Ni-eenkristallen.

III. Electronendiffractieonderzoek van gediffundeerde preparaten

Onderzoekingen van kleine diffusiezones met transmissie electronenmicroscopie leverde informatie
(i) over het diffusieproces, namelijk uit de verandering van de moiré-spatie;
(ii) over de microstructuur van de diffusiezone.

Er werd een duidelijke toename van de moiré-spatie geconstateerd tijdens het verhitten (450-600°C) van epitactische bikristallen bestaande uit een koperlaagje van een paar honderd Ångstrom op een nikkelsubstraat van ongeveer duizend Ångstrom [III.15]. De relatieve toename van de moiré-spatie bleek recht evenredig met de wortel van de diffusieduur. Op basis van een sterk vereenvoudigde beschrijving van de electronendiffractie in die preparaten kan de diffusiecoëfficiënt worden bepaald uit de evenredigheidsconstante van dat verband. Activeringsenergieën en frequentiefactoren verkregen uit deze diffusiecoëfficiënten stemmen goed overeen met gepubliceerde waarden voor volumediffusie in het systeem Cu/Ni, hoewel bij lagere temperaturen (450-475°C) de activeringsenergie naar lagere en de frequentiefactor naar hogere waarde nijgt [III.17].

Misfit-dislocaties, die aanvankelijk een netwerk in het Cu/Ni-scheidingsvlak vormden, werden in het gelegeerde deel van het preparaat verspreid tijdens de verhitting en vormden dislocatiemuren [III.16]. Dit proces mondt tenslotte uit in een celstructuur. Er werd een energiecriterium voor dislocatiemuurvorming opgesteld door de energie van de elastische vervormingen van een quasi-continue verdeling van dislocaties in de diffusiezone te vergelijken met die van een rangschikking van dislocaties in muren. Het begin van de dislocatiemuurvorming, zoals daaruit voorspeld wordt, klopte wonderwel met het experimenteel waargenomen begin.

Met betrekking tot het onderzoek van scheidingsvlakken in dunne bimetallische lagen die door diffusie veranderd zijn, worden een aantal onopgeloste problemen belicht, waarbij mogelijke toekomstige richtingen in het onderzoek worden aangegeven [III.18].

IV. Epitactische groei van koperlagen op een nikkel eenkristalsubstraat

Met het oog op het maken van preparaten voor het diffractieonderzoek werden de morfologie, epitaxie en tweelingvorming van koperlagen, bereid door electrokristallisatie of opdampen, bestudeerd met de optische en de scannende elektronenmicroscoop en met röntgendiffractie. Gevonden werd, dat de vorm van de kiemen en de hoeveelheden tweelingen en volledig epitactische kiemen afhingen van de toegepaste stroomdichtheid. Een interessante "kiem" die aangetroffen werd, was een regelmatig twintigvlak (vijfvoudige symmetrie!) open gespleten langs de ribben [IV.19].

De vertweelinging werd kwantitatief bestudeerd aan geëlektrokristalliseerde en aan opgedampte lagen [IV.20]. Alleen indien de tweelingvlakken een hoek > 45° maken met het substraatoppervlak, treedt (herhaalde) vertweelinging op. Opdampen leverde minder perfect epitactische lagen op dan elektrokristallisatie.

V. Kanttekeningen bij de fenomenologische diffusietheorie

De tweede wet van Fick wordt numeriek opgelost voor diffusie in één richting met een diffusiecoëfficiënt met een bekende concentratieafhankelijkheid [V.21]. De voorgestelde iteratieve methode is gebaseerd op een idee van Neumann en kan worden toegepast op oneindige en half-oneindige media. De benodigde rekentijd is ongeveer twee orden van grootte kleiner dan voor de bekende methode van Crank en Henry.

Er wordt een discussie gegeven van de bepaling van concentratieafhankelijke diffusiecoëfficiënten in een half-oneindige medium gevormd door een binaire vaste oplossing met als randvoorwaarde, dat de oppervlakteconcentratie van één component constant is [V.22]. Er wordt aangetoond, dat (i) de positie van het oorspronkelijke oppervlak niet bekend behoeft te zijn, dat (ii) een diffusiecoëfficiënt met fysische betekenis kan worden gedefinieerd die een bekende relatie met de intrinsieke diffusiecoëfficiënten heeft en dat (iii) een Matano-achtige analyse kan worden toegepast.

Assistentie Röntgendiffractiemetingen: N.M. van der Pers

Assistentie Preparaatbereiding : L.A.J. van Velzen, H. Weerheijm,
A.W.J. Gommers

Assistentie Optische Mikroskopie : P.F. Colijn

Scannende Elektronenmikroskopie : Emma van der Zwaag-Venema

COLOFON

Omslagidee : Paula Delhez-de Kok

Omslagrealisering: Leo Bolt

Typewerk : Anke Kerklaan-Koene, Agaath van Elsas

Fotografisch werk: J.C.M. Jacobse

Lijntekeningen : G. van Slingerland

STELLINGEN VAN R. DELHEZ

1. Een aantal röntgendiffractiemethoden voor de bepaling van een concentratieverloop hebben ruime toepassingsmogelijkheden:
   - de methode toegepast op kristallieten van legeringskatalysatoren voor het onderzoek van spinodale ontmenging, klontering en mechanische deformatie en interdiffusie in dunne lagen;
   - de methode toegepast op een epitactisch binair diffusiekoppel voor het onderzoek van mechanische deformatie als functie van de afstand tot het aangestraalde oppervlak.

   Dit proefschrift.

2. In de Warren-Averbach analyse voor de bepaling van deeltjesgrootte en roostervervorming wordt veelal ten onrechte een machtreeksontwikkeling voor een logarithme toegepast.

   B.E. Warren & B.L. Averbach, J.Appl.Phys. 21, 595(1950); & 23, 497(1952).
   R. Delhez & E.J. Mittemeijer, J.Appl.Cryst. 9, 233(1976).

3. Het is zeer waarschijnlijk, dat het model van de "effectieve deeltjesgrootte" met vrucht gebruikt kan worden bij de beschrijving van sinterprocessen in poedermengsels.

   R.W. Heckel, Trans. ASM 57, 443(1964).

4. Met de grote vlucht die de Lang-methode genomen heeft, worden ten onrechte eenvoudige röntgen(topografische) methoden meer naar de achtergrond gedrongen.

   o.a. J.Cryst.Growth 1965 - heden.

5. Bij kristalgroeionderzoek zou meer aandacht moeten worden besteed aan het in situ toepassen van röntgentopografische methoden.

6. Gezien de omvang van de literatuur betreffende kwantitatieve analysetechnieken van de profielen van röntgendiffractiemaxima, de diversiteit van deze technieken en de uiteenlopende meningen daarover, lijkt het zeer nuttig dat de "Commission on Crystallographic Apparatus" van de "International Union of Crystallography" een subcommissie of project voor bovenbedoeld gebied instelt.

7. Dat slechts een klein deel van de tarieven van de nederlandse posterijen op rationele, economische gronden is gebaseerd, heeft bezwaren. Er zijn mogelijkheden hierin verbetering te brengen.

   Nederlandse Staatswetten, Editie Schuurman en Jordens, deel 22, Wetten betreffende de posterijen, 6^e *druk (Tjeenk Willink, Zwolle, 1976).*

8. Een trouwring is niet alleen een pand van trouw, maar ook een uitwendig teken, dat trouw oplegt door zijn herkenbaarheid.

   Oosthoeks Encyclopedie, deel 7 (Oosthoek Uitgeversmaatschappij, Utrecht, 1968), p. 378.
   W. Jones, "Finger-ring lore" (Chatto and Windus, London, 1877).

9. Zij die een poging tot zelfdoding doen, willen leven: zij onderzoeken één mogelijkheid tot oplossing van hun problemen.

   H.A. Kuyt e.a., Maandblad Geestelijke Volksgezondheid, 28, 537(1973).

10. In het algemeen is het goed, dat er maatschappelijke conventies zijn rond trouwen en kinderen krijgen. Het is echter niet goed, dat dezelfde conventies het uitgangspunt vormen voor kritiek op ongehuwden en kinderloze echtparen.

    R. Veenhoven, Vrij Nederland 34, 13(1973), d.d. 28 april.
    J.E. Veevers, Intermediair 11, 17(1975), d.d. 25 februari.

11. Voor het promoveren van twee promovendi op één gezamenlijk proefschrift vertoont het Promotiereglement van de Technische Hogeschool Delft de volgende onvolkomenheden:
    - Artikel 1 lid 1 staat toe, dat de twee promovendi volstaan met zes gezamenlijke stellingen;
    - Artikel 2 lid 1 en lid 2 en Artikel 9 lid 1 houden in, dat de referent eer hij is aangewezen, zijn verklaring als referent dient af te leggen.

    College van dekanen, Promotiereglement, Technische Hogeschool Delft, vastgesteld bij besluit van het college van dekanen d.d. 6 juni 1977.

12. Uit milieutechnisch en uit energie- en tijdbesparend oogpunt verdient het aanbeveling het Hobbitse begrip MATHOM in te voeren en het Hobbitse gebruik daarvan in onze maatschappij te bevorderen.

    "...alles dat niet van direct nut voor de Hobbits was, maar dat zij niet wilden wegdoen, noemden zij een MATHOM. ...en vele van de geschenken die van hand tot hand gingen, waren van dat soort".

    Uit "In de ban van de ring", deel 1 (Spectrum Utrecht, 1971) pag. 17 in de vertaling van M. Schuchart van J.R.R. Tolkien, "The Lord of the Rings", part 1 (George Allen & Unwin Ltd, London, 1955).

R. Delhez,
Delft, 22 februari 1978.

STELLINGEN VAN E.J. MITTEMEIJER

1. Ten onrechte draagt een bekende rekenmethode om de α_2-component uit gemeten Kα-doubletten te verwijderen de naam van Rachinger.

   W.A. Rachinger, J.Sci.Instrum. 25, *254(1948).*

2. Voor de bepaling van de deeltjesgrootte en roostervervorming uit de verbreding van profielen van röntgendiffractiemaxima is de "profile fitting" methode van Huang en Parrish minder geschikt.

   T.C. Huang en W. Parrish, Appl.Phys. Letters 27, *123(1975).*

3. Omdat de berekening van de lijnverbreding door de instrumentele condities van een diffractometer slecht met het experiment overeenstemt, verdient een experimentele beschrijving van de instrumentele lijnverbreding de voorkeur.

   H.P. Klug en L.E. Alexander, X-ray Diffraction Procedures, (New York: John Wiley and Sons), p. 297 (1974).

4. Het effect van de door McLaren en MacKenzie onderkende "ruimtelijke coherentie" van röntgenstraling op röntgendiffractiepatronen valt geheel onder de noemer "instrumentele verbreding".

   A.C. McLaren en W.S. MacKenzie, Phys.Stat.Sol. (a) 33, *491(1976).*

5. De ontwikkeling van methoden voor het bestuderen van de vorm der elektronendiffractiestippen, analoog aan de procedures voor lijnprofielanalyse van röntgendiffractiepatronen, dient met kracht ter hand genomen te worden.

6. Voor het onderzoek van de structuur van diffusiezônes is elektronenmikroskopie geschikter dan röntgendiffractie.

   Y.G. Nakagawa en J.G. Greenfield, Acta Met. 21, *335(1973).*
   J.A. Carpenter, D.R. Tenney en C.R. Houska, J.Appl.Phys. 42, *4305 (1971).*

7. De door Ives, Edington en Rothwell waargenomen én berekende spaties van (200) parallel moiré-patronen van Ni/Cu bikristallen van 115 Å en 120 Å respectievelijk, dienen als uiterst onwaarschijnlijk beschouwd te worden.

   A.G. Ives, J.W. Edington en G.P. Rothwell, Electrochem. Acta 15, *1979 (1970).*

8. De stellingname dat tussen het twintigste en dertigste levensjaar van een onderzoeker de wetenschappelijk productiefste periode ligt, is gebaseerd op een vooroordeel.

9. Die geestdrift onder wetenschappers die nogal eens met "vakidiotisme" betiteld wordt, heet op andere plaatsen in de samenleving "bezieling".

10. Op basis van de huidige kennis is het mogelijk te concluderen dat de verdeling van de diverse aspecten van de intelligentie, voor zover erfelijk bepaald, voor mannen en vrouwen verschilt.

11. Voor het promoveren van twee promovendi op één gezamenlijk proefschrift vertoont het Promotiereglement van de Technische Hogeschool Delft de volgende onvolkomenheden:
    - Artikel 1 lid 1 staat toe, dat de twee promovendi volstaan met zes gezamenlijke stellingen;
    - Artikel 2 lid 1 en lid 2 en Artikel 9 lid 1 houden in, dat de referent eer hij is aangewezen, zijn verklaring als referent dient af te leggen.

    College van Dekanen, Promotiereglement, Technische Hogeschool Delft, vastgesteld bij besluit van het college van dekanen d.d. 6 juni 1977.

12. Het vreedzaam en waarachtig gebruik van de taal in woord en geschrift wordt in de weg gestaan door de zucht naar sensatie in de menselijke natuur.

    L. Tiger en R. Fox, The Imperial Animal (Secker and Warburg, London, 1972).
    R. Ardrey, The Social Contract (Atheneum Publishers, New York, 1970).
    G. Wallraff, Der Aufmacher. Der Mann der bei "Bild" Hans Esser war (Kiepenheuer und Witsch, 1977).

E.J. Mittemeijer,
Delft, 22 februari 1978.

The analysis of X-ray diffraction line broadening and electron diffraction contrast originating from specimens with concentration variations

Systems studied:

Copper - Nickel
Gold - Platinum and
Rubidiumchloride - Potassiumchloride

Delft University Press